UCGE Reports
Number 20285

Department of Geomatics Engineering

Multi-frequency GPS and Galileo Kinematic Positioning with Partial Ambiguity Fixing

(URL: http://www.geomatics.ucalgary.ca/research/publications)

by

Wei Cao

February 2009

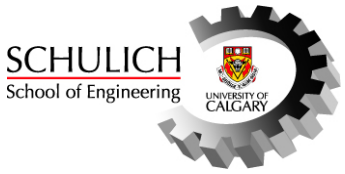

UNIVERSITY OF CALGARY

Multi-frequency GPS and Galileo Kinematic Positioning with Partial Ambiguity Fixing

by

Wei Cao

A THESIS

SUBMITTED TO THE FACULTY OF GRADUATE STUDIES

IN PARTIAL FULFILMENT OF THE REQUIREMENTS FOR THE

DEGREE OF MASTER SCIENCE

DEPARTMENT OF GEOMATICS ENGINEERING

CALGARY, ALBERTA

FEBRUARY, 2009

Abstract

With the modernization of GPS and deployment of Galileo, observations on multiple carrier frequencies will be available to global users from both systems. For GPS, three carrier frequencies, L1, L2 and L5 will be available; for Galileo, the three frequencies for civil users are E1, E5a and E5b. The availability of multi-frequency GNSS observations provides various combinations for the frequency selection of a future GNSS receiver for high precision applications and also brings up the problem of increased computational burden, huge ambiguity search volume due to a large number of ambiguities to be fixed to obtain a fixed position solution.

A carrier phase processor is developed with the single-difference (SD) GNSS carrier phase and pseudorange observations. Performance evaluations of GPS/Galileo kinematic positioning using observations on different subsets of frequencies are carried out and the strategy of partially fixing a subset of float ambiguities is investigated as well. A covariance simulation analysis based on the geometry of observed GPS/Galileo satellites is conducted first and it is followed by processing simulated data from a software GNSS simulator. Included in this thesis are the numerical results and analyses of simulations in different scenarios. It is shown that the performance of combined dual-frequency GPS/Galileo is better than that of a triple-frequency GPS in terms of time to fix ambiguities (TTTF). The ambiguity partial fixing reduces the TTTF at the expense of decreased position accuracies. Recommendations for future work on GPS/Galileo kinematic positioning are also addressed.

Acknowledgements

The work in this thesis would be impossible with the kind and generous help from many people with whom I have been working for more than two years.

I express my great gratitude to my supervisors, Drs. Elizabeth Cannon and Kyle O'Keefe, for their continuous support, guidance and encouragement of my studies and research. They not only offered me the study opportunities and research environment, but also set vivid examples of researchers. Beyond research, they also shed the light of their impressive personalities on my professional career and life.

I would like to thank friends throughout my graduate studies: Glenn MacGougan, David Chiu, Debo Sun, Changsheng Cai, Fang Wang, Hang Liu, Tao Lin, Man Feng, Tao Li, Fatemeh Ghafoori, Ossama Al-Fanek, Mohammed Zafer Sadeque and many others. Special thanks are due to Mr. Glenn MacGougan for his kind help on the software development in this thesis, unselfish knowledge sharing, beneficial discussions and suggestive comments, and Mr. Junjie Liu for fruitful discussions on ambiguity resolution.

Dr. Susan Skone and Dr. John Nielsen agreed to serve on my oral examine committee. I thank them for their thoughtful questions and valuable suggestions to improve this thesis.

Finally and most importantly, my thanks would be given to my parents and sisters for their unconditional and everlasting love, support and patience for all the years.

Table of Contents

List of Tables

List of Figures

List of Symbols, Abbreviations

List of Symbols

Δ	Single-difference (SD) operator between receivers
$\Delta\nabla$	Double-difference (DD) operator
ϕ_{LC}	Phase linear combination
ϕ_i	Phase measurement on the i^{th} frequency in units of cycles (i=1 ~ 3)
Φ_i	Phase measurement on the i^{th} frequency in units of metres
Φ_{LC}	Phase measurement of ϕ_{LC} in units of metres
ε_{Φ_i}	Phase measurement noise in units of metres
B	Transformation matrix from SD to DD ambiguities
H	Design matrix
K	Kalman Gain matrix
I_i	Ionospheric delay on the i^{th} frequency
T_i	Ionospheric delay on the i^{th} frequency
N_i	Carrier phase ambiguity on the i^{th} frequency
N_{LC}	Carrier phase ambiguity corresponding to phase observation ϕ_{LC}
N_{EWL}	Carrier phase ambiguity of the EWL linear combination
N_{WL}	Carrier phase ambiguity of the WL linear combination
$\hat{N}$	Float-valued DD phase ambiguity (cycle)
$\breve{N}$	Integer-valued DD phase ambiguity (cycle)

$\Delta\nabla N_{12}$	DD ambiguity of the linear combination using 1st and 2nd frequencies
$\Delta\nabla N_{23}$	DD ambiguity of the linear combination using 2nd and 3rd frequencies
$\Delta\nabla T_1$	DD tropospheric error in the measurement on the 1st frequency
$\Delta\nabla I_1$	DD ionospheric error in the measurement on the 1st frequency
f	Carrier frequency
f_{L1}	L1 carrier frequency
f_{L2}	L2 carrier frequency
λ_i	Wavelength of the i-th frequency
λ_{LC}	Wavelength of specified phase linear combination
P	Variance-covariance matrix of state estimates
Q	Noise variance-covariance matrix
sp	Spectral density of state estimates
r	True geometric range (m)
Δr	Satellite orbital error (m)
T_0	Time constant of a first-order Gauss-Markov process
u	Number of unknowns
w	System driving noise
z	Observation vector

List of Abbreviations

AltBOC	Alternative Binary Offset Carrier
AR	Ambiguity Resolution

ARNS	Aeronautical Radio Navigation Service
AS	Authorized Service
BOC	Binary Offset Carrier
BPSK	Binary Phase Shift Keying
CAR	Cascading Ambiguity Resolution
CBOC	Composite Binary Offset Carrier
CDMA	Code Division Multiple Access
CIR	Cascading Integer Resolution
CODE	Center for Orbit Determination in Europe
CS	Commercial Service
CSPNC	China Satellite Navigation Project Centre
DD	Double-Difference
DGNSS	Differential GNSS
DLL	Delay Lock Loop
EC	European Commission
ESA	European Space Agency
EU	European Union
EWL	Extra Wide Lane
FAMCAR	Factorized Multi-Carrier Ambiguity Resolution
FDMA	Frequency Division Multiple Access
FOC	Full Operational Capability
IAC	Information Analytical Centre
IF	Ionosphere-Free

IGS	International GNSS Station
ILS	Integer Least Squares
IOV	In-Orbit Validation
ITCAR	Integrated Triple Frequency Cascading Ambiguity Resolution
ITRF	International Terrestrial Reference Frame
ITRS	International Terrestrial Reference System
GB	Geometry-based
GF	Geometry-free
GGSP	Galileo Geodetic Service Provider
GGTO	GPS to Galileo Time Offset
GIM	Global Ionosphere Map
GLONASS	GLObal NAvigation Satellite System
GNSS	Global Navigation Satellite System
GPS	Global Positioning System
GPST	Global Positioning System Time
GSA	GNSS Supervisory Authority
GST	Galileo System Time
GTRF	Galileo Terrestrial Reference Frame
LAMBDA	Least-squares Ambiguity Decorrelation Adjustment
LC	Linear Combination
LSQ	Least-squares
MBOC	Multiplexed Binary Offset Carrier
MEO	Medium Earth Orbit
MEDLL	Multipath Estimation Delay Lock Loop

MET	Multipath Estimation Technique
ML	Medium Lane
MTTFFA	Mean Time To First Fix Ambiguities
OCS	Operation Control Segment
OCX	Next Generation Operational Control Segment
OS	Open Service
PCF	Probability of Correct Fix
PCFA	Percent of Correct Fix Ambiguities
PIF	Probability of Incorrect Fix
PIFA	Percent of Incorrect Fix Ambiguities
PNFA	Percent of No Fix Ambiguities
PPM	Part Per Million
PPP	Public-Private Partnership
PCV	Phase Centre Variations
PLL	Phase Lock Loop
PRN	Pseudo Random Noise
PRS	Public Regulated Service
PPM	Part Per Million
PVT	Position, Velocity and Time information
QPSK	Quadrature Phase Shift Keying
QZSS	Quasi-Zenith Satellites System
RMS	Root Mean Square
RNSS	Radio Navigation Satellite Service
RTK	Real Time Kinematic

SA	Selective Availability
SD	Single-Difference
SNR	Signal to Noise Ratio
SPHA	Spherical Harmonics
SPF	Scoreboard Partial Fixing
SPS	Standard Positioning Service
TAI	International Atomic Time
TCAR	Triple Frequency Cascading Ambiguity Resolution
TEC	Total Electron Content
TMBOC	Time-Multiplexed Binary Offset Carrier
TTCFA	Time To Correctly Fix Ambiguities
UD	Un-Differenced
UERE	User Equivalent Range Error
USNO	U.S. Naval Observatory
UT	Universal Time
UTC	Universal Time Coordinated
VC	Variance-Covariance
VTEC	Vertical Total Electron Content
WAAS	Wide Area Augmentation System
WL	Wide-lane
WGS 84	World Geodetic System 84

Chapter One: Introduction

1.1 Background

With more than three decades since the launch of the first satellite in 1978, the Global Positioning System (GPS) has been applied in a wide range of application areas on land, sea, air and space. It has evolved from an enabling technology to a ubiquitous technology (Kaplan 2005) and its applications are only limited by imagination.

The GPS Standard Positioning Service (SPS) provides positioning accuracies of approximately 3 m in horizontal and 5 m in vertical at a 95% probability level to civil users world-wide (Department of Defence 2008). To meet applications with higher accuracy requirements, differential GPS (DGPS) which involves positioning between two or more receivers has been developed. The differencing operation can effectively reduce or eliminate most of the errors in GPS measurements thus significantly improving the positioning accuracy. According to the type of measurements used, DGPS methods can be divided into two groups: code-based DGPS and phase-based DGPS. Code-based DGPS is straightforward and can deliver a sub-metre positioning accuracy, whereas phase-based DGPS can achieve centimetre or even millimetre accuracies in most cases when the unknown number of integer cycles in the phase measurements are correctly determined. The process to determine these unknown cycles is called ambiguity resolution (AR), which remains a significant area of research in the GNSS community (Teunissen and Verhagen 2007a).

Motivated by further improving the integrity, availability, reliability and accuracy of GPS positioning and navigation, a GPS modernization program began in the late 1990s to improve GPS performance for both civilian and military applications (Kaplan et al. 2005). For military users, new signals, called M-codes have been added on the L1 and L2 frequencies of the Block IIR-M satellites and will replace the P-code for military services. For civil users, the modernization includes the following steps: the first one was to discontinue the Selective Availability (SA) on the L1 C/A signal, which occurred on May 1, 2000 and will not be implemented in future GPS (U.S. PNT National Executive Committee 2007). The subsequent steps consist of adding a second civil signal on the L2 frequency (L2C) from Block IIR-M satellites, and broadcasting new civil signals on a third frequency (L5) from Block IIF satellites. In addition, a new civil signal (L1C) will also be transmitted on the L1 frequency from Block IIIA satellites. Thus civil users will be authorized to receive signals on three frequency bands in the future instead of only one civil signal from current GPS, which will significantly improve the system integrity and reliability. At present, the GPS modernization program is moving forward: the first Block IIR-M satellite was launched on September 25, 2005 and six are now in space. The first Block IIF satellite will be launched in early 2009 and the launch of the first Block III satellite was scheduled around 2014 (Madden 2008).

In parallel with GPS modernization, other Global Navigation Satellite Systems (GNSS), e.g., GLONASS, Galileo and Compass, are also under development by other countries and organizations around the globe. Galileo is being jointly developed by the European

Commission (EC) and the European Space Agency (ESA). The system will consist of 30 satellites, which will be distributed in three circular Medium Earth Orbit planes at a nominal average semi-major orbit axis of 29601 km, and at an inclination angle of 56 degrees with respect to the equatorial plane, and will transmit signals on four frequency bands, namely E1, E6, E5a and E5b (ESA/European GSA 2008).

1.2 Related Research

The implications of GPS modernization and the deployment of Galileo are substantial for users employing GNSS positioning and navigation technologies. A number of studies have been carried out to analyse the performance of modernized GPS, Galileo and combined GPS/Galileo in terms of availability, accuracy, reliability and integrity (Ochieng et al. 2001, Sheridan et al. 2001, O'Keefe 2001, O'Donnell 2002, Ochieng et al. 2002, Verhagen 2002, Ji 2007). When the nominal constellations of 24 and 30 satellites were assumed for GPS and Galileo, studies have demonstrated that Galileo has a slightly improved availability than GPS, especially at high latitudes; better positioning accuracy and integrity can also be obtained with Galileo compared to those of GPS. However, the combination of two systems offers tremendous improvements in terms of the above figures of merit.

Besides the improvement brought by GPS modernization and Galileo to standalone positioning users, they can also benefit precise positioning applications, e.g., surveying, geodynamics and other scientific applications with high precision requirements, where

carrier phase observations are generally used. Ambiguity resolution using three or more carriers for modernized GPS or Galileo has been an active research topic in the GNSS community for more than a decade.

GPS ambiguity resolution involving three frequencies can be dated back to Hatch (1996), which introduced the wide-laning technique in the case of modernized GPS, and analysed the benefits of triple-frequency on GPS carrier phase ambiguity resolution. This topic was furthered thorough investigation by Jung (1999) and Jung et al. (2000), in which a geometry-free cascading integer resolution (CIR) method was proposed. With respect to Galileo ambiguity resolution, early studies were conducted in the stage of system conceptual design, results can be found in Forssell et al. (1997), Vollath et al. (1998) and Bonillo-Martínez et al. (1999), in which similar cascading ambiguity resolution methods to CIR for GPS, named Three Carrier Ambiguity Resolution (TCAR) was proposed and evaluated for Galileo. Besides the effort on cascading integer resolution, most of the recent research has focused on optimization of three or four frequency combinations for GPS or Galileo. A distance-independent ambiguity resolution method can be found in Han and Rizos (1999). Feng (2004, 2005 and 2006) and Feng and Rizos (2008) also proposed a geometry-free, distance-independent three carrier ambiguity resolution method. A systematic search of optimal carrier-phase combinations of triple-frequency GPS (also applicable to three or four frequencies Galileo) was conducted by Cocard et al. (2008), which aimed to find the best combinations in every cascading step of CIR. Efforts on applying the Least-square Ambiguity Decorrelation Adjustment (LAMBDA) (Teunissen 1993 & 1994) to three carrier ambiguity resolution have also been carried out

by researchers (Tiberius et al. 2002a & 2002b). Ambiguity resolution performance with applying LAMBDA and the cascading scheme (CIR and TCAR) was tested and compared, and it was shown that LAMBDA has better performance than CIR and TCAR in terms of ambiguity resolution (Teunissen et al. 2002, Ji et al. 2007, O'Keefe et al. 2008). With the co-existence of two systems, it is important to investigate the ambiguity resolution of combined GPS and Galileo. Alves (2001) studied ambiguity resolution involving two common frequencies of GPS and Galileo. Real-time kinematic (RTK) positioning performance of combined GPS/Galileo was investigated by Eissfeller et al. (2001) and Tiberius et al. (2002a & 2002b). In Julien et al. (2003), a so-called tightly coupled GPS/Galileo combination ambiguity resolution was proposed and tested based on simulated observations. To tightly couple the two systems, extra measurements on two common frequencies (L1 vs E1 and L5 vs E5a) were used between the two base satellites of two systems. In studies of Zhang et al. (2003) and Zhang (2005), a geometry-based cascading approach was proposed and tested to overcome the limitations of geometry-free cascading method. The network RTK positioning using combined GPS/Galileo was investigated by Schüler (2007) and Schüler et al. (2007), and it showed that a dual-frequency combined GPS/Galileo has better performance than independent triple-frequency GPS or Galileo in terms of ambiguity resolution and positioning accuracy. With the existence of multiple systems, the number of ambiguities and other nuisance parameters to be estimated in the filter will be significantly increased compared to those of the current dual-frequency GPS. To efficiently use observations from all systems and reduce the high computational burden due to the large number of estimated parameters, a Factorized Multi-Carrier Ambiguity Resolution (FAMCAR) (Vollath 2005 & 2008,

Sauer et al. 2004) method was proposed for future GNSS. This method has already been used for the current GPS and GLONASS integrated carrier phase positioning and has shown superior performance (Vollath & Doucet 2007).

The concept of partial ambiguity fixing was first proposed in Teunissen et al. (1999), where partial fixing was evaluated for three-frequency GPS single-epoch AR based on least-squares covariance simulation. This was further carried out to evaluate different subsets of frequencies from combined GPS/Galileo based on Kalman filter covariance propagation in Cao et al. (2007). In Dai et al. (2007 & 2008), a partial search strategy for current dual-frequency GPS was developed to improve long range RTK reliability and availability. In Vollath and Doucet (2008), a so-called scoreboard partial fixing (SPF) method was proposed for GPS/GLONASS carrier phase AR and it could also be used for future GNSS including Galileo. The partial fixing of a subset of ambiguities in scenarios of GPS, GPS/QZSS (Quasi-Zenith Satellites System, the Japanese Satellite Navigation System) and GPS/Galileo was investigated; however, the partial fixing was only implemented in the original float ambiguity domain based on the signal to noise ratio (SNR) and satellite elevation angle of observation satellites and it was essentially equivalent to just use a subset of GNSS observations for ambiguity resolution. In Lawrence (2009), a new method of partial ambiguity resolution was developed, which makes a position error cost function minimized subject to a minimum probability of correct fix (PCF).

1.3 Statement of Problem

Several limitations have been identified in the research described above. Firstly, the proposed CIR and TCAR use observation combinations with predefined transformations, which are not optimal in the sense of LAMBDA decorrelation (Teunissen et al. 2002). Secondly, these combinations are specifically defined for observations on particular frequencies and not generally applicable to observations on other frequencies. For example, extra wide lane (EWL) and wide lane (WL) measurements can be formed when three-frequency GPS observations are available, however this is not the case when only observations on two of the three frequencies are available or for another three-frequency GNSS, e.g., Galileo. Therefore, these combinations are not sufficiently flexible.

For all previous studies, it was only shown that better results, like reduced time to fix ambiguities and capability to extend separations between the rover and reference receivers, would be obtained if GNSS observations on more frequencies or from another system are available. However, investigations have not been conducted with respect to comparisons of kinematic positioning performance, e.g., AR and positioning accuracy using different sets of GNSS signals, such as a triple-frequency single system GPS receiver comparing to a dual-frequency GPS/Galileo receiver. The answers to these questions are important for future GNSS RTK receiver design. Using observations on more frequencies of existing GNSS or from another GNSS means more carrier phase ambiguities to be fixed during the ambiguity resolution process, which significantly increases the computational burden of the filtering and ambiguity search space volume.

However, it should be easier to just fix a subset of the ambiguities instead of fixing them all. An ambiguity partial fixing strategy in the decorrelated ambiguity domain is proposed and investigated in this thesis.

1.4 Objectives

The overall objective of this research is to assess the performance of kinematic positioning and ambiguity resolution using a multi-system GNSS (GPS and Galileo in this study). The specific objectives of this research are defined as follows:

1) To develop a GNSS carrier phase processor focused on algorithm development (not software development) to process GPS and Galileo code and phase observations for single baseline RTK (post-mission processing is adopted here instead of real-time processing) surveying applications.
2) To evaluate ambiguity resolution performance in terms of time to first fix ambiguities and reliability of ambiguity fixing when using observations on subsets of GPS and Galileo frequencies.
3) To assess the results from fixing subsets of decorrelated float ambiguities in terms of time to first fix, probability of correct fix and fixed position accuracy.
4) To provide recommendations for future GNSS RTK receiver design in terms of frequency use, channel allocation and processing strategies.

1.5 Thesis Outline

This thesis begins with a review of state-of-the-art ambiguity resolution strategies for modernized GPS, Galileo and combined GPS/Galileo. The background information in Chapter 1 provided the foundation for the remainder of this thesis.

Chapter 2 gives an overview of GNSS systems: those that are currently available and those that are under development, and special attention is paid to modernized GPS and Galileo. Issues on the compatibility and interoperability of different GNSS systems are also addressed. The GNSS observation equations are introduced with the single and double differencing schemes being described with their pros and cons for precise positioning discussed. Various error sources in GNSS observations are then briefly described.

Chapter 3 discusses the concept of differential GNSS positioning using carrier phase observations. The development of a float filter is described in detail. Methods for GNSS multi-carrier ambiguity resolution are reviewed and compared. Methods for ambiguity validation are also introduced in this chapter.

Chapter 4 shows the results of evaluating ambiguity resolution performance in terms of probability of correct fix, which is conducted through Kalman filter covariance propagation based on the geometry of observed GNSS satellites.

Chapter 5 uses the phase processor described in Chapter 3 to process simulated GNSS observations from an in-house software simulator and provides quantitative results for ambiguity resolution with different subsets of GPS and Galileo observations. Results for partial fixing ambiguities are also presented and explained in this chapter.

Chapter 6 draws conclusions from the preceding chapters and summarizes the findings of the research. Ideas for future investigation are also recommended.

Chapter Two: Global Navigation Satellite Systems

This chapter will have an overview of current and future GNSS, discuss issues on compatibility and interoperability of different GNSS. GNSS observations and different differencing schemes of them will be studied. The advantages and disadvantages of using different kinds of observations will be compared. Some of the important GNSS error sources will be discussed at the end of this chapter.

2.1 Overview of GNSS Systems

2.1.1 GPS and its modernization

GPS has shown excellent performance in a broad range of applications since its initial development three decades ago. A combination of Block IIA, IIR and IIR-M satellites makes up the current constellation, which currently consists of 31 active satellites broadcasting signals in space (Madden 2008). They are distributed in six orbital planes with inclination angles of approximately 56 degrees and are separated by 60 degrees right ascension of the ascending node. They are orbiting at an altitude of approximate 20,200 km, with each satellite making two complete orbits every sidereal day (ARINC 2004).

However, improvements are still needed to satisfy both civil and military GPS users. The first effort was to turn off selective availability (SA) on May 1st, 2000 and this policy was confirmed by the U.S. Government in 2007 (U.S. PNT National Executive Committee

2007). To enhance both civil and military services, a new civil signal on the L2 band (L2C) and new military signals (M-Code) on L1 and L2 bands were broadcast on the Block II-R satellites. The new military signals can be directly accessed by authorized users without dependence on the L1 C/A signal for obtaining timing information to acquire P(Y) signals (McDonald 2005). The L2C signal will enable robust L2 signal tracking and has great advantages over the current semi-codeless or codeless technologies implemented in civilian dual-frequency GPS receivers for high precision applications (Michael & Hegarty 2003). This will also enable civil users to directly correct ionospheric error, which is the most prominent error source in satellite positioning and navigation, thus significantly improving the positioning accuracy. In addition, the longer code length will significantly mitigate the error due to signal cross-correlation, thus making it appropriate for applications in weak signal environments, such as indoors, under forest canopies and in urban canyons (ibid). To benefit users in the civil aviation community, a third frequency - L5, which is located in the Aeronautical Radio Navigation Service (ARNS) band, will be transmitted on the Block IIF satellites since the L2 frequency is not located in the protected ARNS band (McDonald 2005). The third frequency will further improve performance for high precision applications using carrier phase measurements (Hatch 1996). To achieve interoperability with other GNSS, e.g., Galileo, a fourth civil signal - L1C will be added on the Block IIIA satellites, which will have increased power levels, increased security and integrity and also have better anti-jamming capabilities (Madden 2008). An overview of the legacy and modernized GPS signals is presented in Table 2.1. Besides the modernization of GPS spacecraft in the space segment, a series of upgrades in the control segment have also been carried out.

The first one was to update the existing Operation Control Segment (OCS) in 2007 (Taylor et al. 2008) which is being followed by building a Next Generation Operational Control Segment (OCX) to accommodate GPS III satellites (Gower 2008). Table 2.2 gives a summary of GPS modernization activities.

Table 2.1: Summary of GPS Signal Characteristics (after Ward et al. 2005)

Signal	Centre Frequency (MHz)	Modulation Type	Band-width (MHz)	Chip Rate (MHz)	Spreading Codes	Code Length	Signal Component	Service Name
L1 C/A	1,575.42	BPSK(1)	2.046	1.023	Gold Codes	1023	N/A	Civil
L1 P(Y)	1,575.42	BPSK(10)	20.46	10.23	M-Sequences	Encrypted	N/A	Military
L2 P(Y)	1,227.60	BPSK(10)	20.46	10.23	M-Sequences	Encrypted	N/A	Military
L2CM	1,227.60	BPSK(1)	2.046	0.5115	M-Sequences	10,230	Data	Civil
L2CL	1,227.60	BPSK(1)	2.046	0.5115	M-Sequences	767,250	Pilot	Civil
L5-I	1,176.45	BPSK(10)	20.46	10.23	M-Sequences	10,230	Data	Civil
L5-Q	1,176.45	BPSK(10)	20.46	10.23	M-Sequences	10,230	Pilot	Civil
L1-M	1,575.42	BOC(10,5)	30.69	10.23	N/A	N/A	N/A	Military
L2-M	1,227.60	BOC(10,5)	30.69	10.23	N/A	N/A	N/A	Military
L1C	1,575.42	TMBOC(6, 1,1/11)	4.092	1.023	Weil Codes	10230	N/A	Civil

Table 2.2: GPS Modernization Activities (after Madden 2008)

Activity	Implementation Date
Second civil signal: L2C (begin from Block IIR-M satellite)	First satellite launched in Sept 2005 Six satellites now in space 24 satellites full capability around 2016
Third civil signal: L5 (begin from Block IIF satellite)	First launch scheduled to be in early 2009 24 satellites full capability around 2018
Forth civil signal: L1C (begin from Block IIIA satellite)	First launch in 2014 24 satellites full capability around 2021
Control Segment Upgrades	OCS switch over in Sept 2007 OCX is underway

2.1.2 Galileo

The establishment of Galileo was conceived by the European Union (EU) in 1990s and it was finally approved in a meeting of the EU Transport Council in 2004. The first test-bed satellite system, GIOVE-A was launched in December, 2005 and the second one, GIOVE-B was launched in April, 2008. A series of in-space signal validations have been carried out and the ground control segment has been under development since that time. With the break-down of the Public-Private Partnership (PPP) funding strategy for Galileo development, a new strategy with funding from EU public sectors was established in the EU Finance Ministers and Transport Ministers meetings in 2007 (Inside GNSS 2007). The four Galileo In Orbit Validation (IOV) satellites will be launched in the following

two years and Galileo is expected to achieve its Full Operational Capability (FOC) in 2013 (Falcone 2008).

An initial version of the Galileo signal and frequency plan (Hein et al. 2002) was published in 2002. It claimed that Galileo would provide five types of services on ten signals to worldwide users. It also established the foundation for later signal refinement. A few important changes were made on the E1 and E6 signal waveforms based on agreements between the U.S. and E.U. to resolve issues surrounding system compatibility and interoperability of GPS and Galileo (Avila-Rodriguez et al. 2008). To achieve interoperability of the two systems, a common signal wave form - Multiplexed Binary Offset Carrier (MBOC) - will be used for Galileo E1 and GPS L1C signal modulations, and this task was finalized in September 2007 (Avila-Rodriguez et al. 2007). GPS/Galileo cooperation on a wide range of areas was reaffirmed in a U.S.-European meeting in October 2008 (U.S. PNT National Executive Committee 2008). However, the optimization of Galileo E1 open service (OS) spreading codes is still under way (Wallner et al. 2008). A summary of Galileo signal characteristics is listed in Table 2.3 and the corresponding Galileo frequency plan (with respect to that of GPS) are shown in Figure 2.1.

Table 2.3: Galileo Signal Characteristics (after ESA Galileo Project Office 2008)

Signal	Centre Frequency	Modulation Type	Bandwidth (MHz)	Chip Rate (MHz)	Spreading Codes	Code Length	Signal Component	Service Name
E1A	1,575.42	BOC(15,2.5)	15.345	2.5575	N/A	N/A	N/A	PRS
E1B	1,575.42	CBOC(6,1,1/11)	1.023	1.023	Random Codes	4092	Data	OS
E1C	1,575.42	CBOC(6,1,1/11)	1.023	1.023	Random Codes	4092	Pilot	OS
E6A	1278.75	BOC(15,2.5)	10.230	5.115	N/A	N/A	N/A	PRS
E6B	1278.75	BPSK(5)	10.230	5.115	Random Codes	5115	Data	CS
E6C	1278.75	BPSK(5)	10.230	5.115	Random Codes	5115	Pilot	CS
E5a-I	1176.45	AltBOC(15,10)	15.345	10.23	M-Sequence	10230	Data	OS
E5a-Q	1176.45	AltBOC(15,10)	15.345	10.23	M-Sequence	10230	Pilot	OS
E5b-I	1207.14	AltBOC(15,10)	15.345	10.23	M-Sequence	10230	Data	OS
E5b-Q	1207.14	AltBOC(15,10)	15.345	10.23	M-Sequence	10230	Pilot	OS

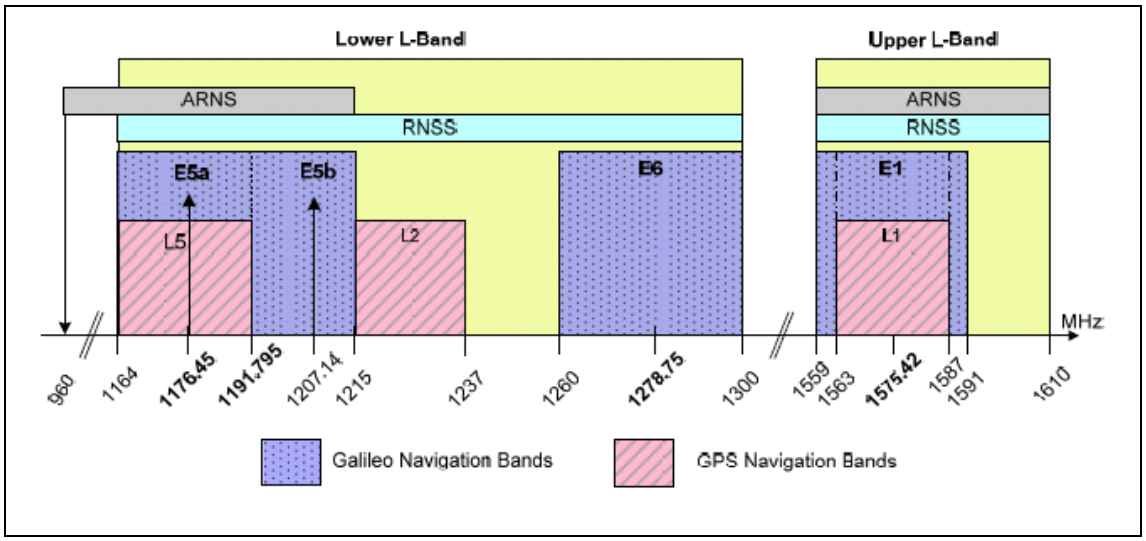

Figure 2.1: Galileo Frequency Plan (from Galileo SIS ICD 2008)

2.1.3 Other GNSS

Though this thesis focused on precise kinematic positioning of Galileo and modernized GPS, it is still worthwhile to review other GNSS, which are currently under development in the world and can be incorporated into the performance evaluation in the future.

One of them is Russia's counterpart to GPS, namely GLONASS, which was developed in parallel with GPS and achieved FOC in 1996. However, it broke down due to insufficient funding (Feairheller & Clark 2005). A GLONASS modernization program was started in 2001 to replenish the system (Polischuk et al. 2002). It is expected that GLONASS will regain its FOC in 2010 with launches of GLONASS-M satellites (Revnivykh 2008). A new block GLONASS-K satellites will be launched in 2011, and they will broadcast a third civil signal – L3 and CDMA (Code Division Multiple Access) type signals at the L1 and L5 frequency bands to realize interoperability with other GNSS (ibid). In addition, efforts have been made to refine the geodetic and time reference frames. The GLONASS reference system has been updated to PZ-90.02 and will continue to be improved to be compatible with the International Terrestrial Reference Frame (ITRF) within a discrepancy of less than 5 cm (Revnivykh 2007). The time reference system will be improved to a level of 12 ns relative to UTC (Coordinated Universal Time) and to have less than a 120 ns discrepancy with respect to UTC (ibid). As of October 2008, there are 19 operational GLONASS satellites transmitting FDMA (Frequency Division Multiple Access) signals on L1 and L2 (Information Analytical Centre 2008).

China is also building its own GNSS - Compass (or Beidou-II), which will be the world's fourth GNSS and is considered as a successor of China's first generation satellite navigation system - Beidou-I. The system will consist of 30 MEO satellites placed in three orbital planes in an altitude of 21,500 km with an inclination angle of 55 degrees and five satellites in geostationary orbits (China Satellite Navigation Project Centre (CSNPC) 2008). Compass will provide two types of service - a free-of-charge open service for global users and an authorized service (AS) for restricted users (CSNPC 2008). Ten signals will be broadcast on five frequency bands: B1, B1-2, B2, B3 and L5 (B is a national notation for Beidou). These frequencies will partially overlap those of GPS and Galileo thus providing good compatibility and interoperability among different GNSS.

Table 2.4: Compass Signal Characteristics (after CSNPC 2008)

Signal	Centre Frequency	Modulation Type	Bandwidth (MHz)	Chip Rate (MHz)	Signal Component	Service Name
B1-I	1,561.098	QPSK	4.092	2.046	Data	OS
B1-Q	1,561.098	QPSK	4.092	2.046	Data	AS
B1-2	1,589.742	QPSK	4.092	2.046	Data	AS
B2-I	1207.14	QPSK	24	10.23	Data	OS
B2-Q	1207.14	QPSK	24	10.23	Data	AS
B3	1268.52	QPSK	24	10.23	Data	AS
B1-BOC	1575.42	CBOC(6,1,1/11)	16.368	1.023	Data	OS
B2-BOC	1207.14	BOC(10,5)	30.69	5.115	Data	OS
B3-BOC	1268.52	BOC(15,2.5)	35.805	2.5575	Data	AS
L5	1176.45	QPSK	24	10.23	Data	OS

A general overview of the above four GNSS and a summary of their frequency allocations and signal structures can be found in Hein (2007) and Hein et al. (2007).

2.1.4 System compatibility and interoperability

With the co-existence of multiple GNSS, compatibility and interoperability among different systems are important. Compatibility refers to the capability of two or more systems to operate simultaneously without interference causing performance degradation to each other (Dellago et al. 2003). Interoperability, which is defined as the performance of two or more systems will be significantly improved when they are combined (Dellago et al. 2003). There are a number of factors having influence on system compatibility and interoperability, with three primary concerns being: the signal in space, the geodetic reference frame and the time reference frame (Hein et al. 2002). Since this thesis is

concentrated on GPS and Galileo precise kinematic positioning, only compatibility and interoperability between GPS and Galileo are addressed herein.

Signal in Space

The interoperability of GPS and Galileo is achieved by overlapping carrier frequencies over L1/E1 and L5/E5a (Hein et al. 2002). A further improvement will be realized by using the MBOC on the L1/E1 frequency band to benefit mass market users (Avila-Rodriguez et al. 2008). However, potential problems like mutual interference arise when broadcasting navigation signals on common frequency bands between two systems. This topic has been investigated in past years, and fortunately, results show that the mutual interference between GPS and Galileo will be marginal thus there will be no significant influences on the user side (Avila-Rodriguez et al. 2008, Fyfe et al. 2002, Ganguly 2004).

Geodetic Reference Frame

As a practical realization of the ITRF, the World Geodetic System (WGS) 84 has been used for GPS as the geodetic coordinate reference frame. Discrepancies between the three components of ITRF and WGS84 are very small, i.e., at centimetre level (one sigma) (Merrigan et al. 2002). To allow the system to be independent of GPS, Galileo will use the Galileo Terrestrial Reference Frame (GTRF), which is another version of the realization of ITRF (Hein et al. 2002). Thus the difference between WGS84 and GTRF should be very small and is expected to be within a few centimetres, which is sufficient

for navigation and most user requirements. For very high precision applications, e.g., tectonics and geodynamics, transformation parameters can be provided by an external Galileo Geodetic Service Provider (GGSP) (Hein et al. 2005). For simplification of simulated data generation in this thesis, the difference between the GPS and Galileo geodetic reference frames is neglected and the WGS84 is used for both systems.

Time Reference Frame

The GPS time is established by the U.S. Naval Observatory (USNO) and it is steered to UTC and is not adjusted for leap seconds. It has been maintained to within ± 25 ns with respect to UTC in the past years (Hein et al. 2005). The Galileo System Time (GST) will be a continuous time scale steered towards the International Atomic Time (TAI) with an offset of 33 ns (Hein et al. 2002). To achieve the interoperability of GPS and Galileo, the difference between the GPS and Galileo system times should be resolved and the two time systems should be synchronized with an accuracy of less than 5 ns with a two-sigma confidence interval over any 24-hour period (Hahn et al. 2004). Generally, there are two approaches to resolving this problem. One is to determine the GPS to Galileo Time Offset (GGTO) and transmit it to users via the GPS and Galileo navigation messages (Hahn et al. 2004). The other one is to estimate the GGTO (or estimate receiver clock errors for GPS and Galileo separately) in the navigation solution by users. It has been shown the two approaches provide similar stand-alone positioning results based on simulation studies (Bonhoure 2008). In this study, the GPS system time is used for both systems to simplify the generation of simulated data.

2.2 GNSS Observations

2.2.1 Un-differenced (UD) observations

A modern GNSS receiver can record measurements from the line-of-sight (LOS) signal between satellites and receiver and report a number of types of observables, e.g., pseudorange, carrier phase, Doppler, which are called UD observations in this thesis. The UD carrier phase and pseudorange observation on an L1 channel can be described in following equations which closely follow the development of Teunissen & Kleusberg (1998),

$$\begin{aligned}\Phi_i^k(t_i) = {} & \rho_i^k(t_i - \tau_i^k, t_i) + c[\delta t_i(t_i) - \delta t^k(t_i - \tau_i^k)] + T_i^k(t_i) \\ & - I_i^k(t_i) + \delta m_i^k(t_i) + \lambda[\phi_i(t_0) - \phi^k(t_0)] + \lambda N_i^k + \varepsilon_i^k(t_i)\end{aligned} \tag{2.1}$$

$$\begin{aligned}P_i^k(t_i) = {} & \rho_i^k(t_i - \tau_i^k, t_i) + c[\delta t_i(t_i) - \delta t^k(t_i - \tau_i^k)] + T_i^k(t_i) \\ & + I_i^k(t_i) + dm_i^k(t_i) + e_i^k(t_i)\end{aligned} \tag{2.2}$$

where

$_i$, ^{j}	Receiver and satellite identification respectively
t_i	Time of reception of the signal at receiver i in GPS time
$\rho_i^k(t_i - \tau_i^k, t_i)$	Distance between receiver i at time t_i and satellite k at time $t_i - \tau_i^k$
τ_i^k	Travel time of signal, i.e., time needed for the signal to travel from signal generator in the satellite to the signal correlator in the GNSS receiver
$\delta t_i(t_i)$	GNSS receiver clock error at the time of reception t_i

$\delta t^k(t_i - \tau_i^k)$	Satellite clock error at the time of transmission $t_i - \tau_i^k$
c	The speed of light in vacuum (299, 792, 458.0 m/s)
$T_i^k(t_i)$	Delay due to tropospheric effect
$I_i^k(t_i)$	Delay due to ionospheric effect
$\delta m_i^k(t_i)$	Carrier phase multipath error
$dm_i^k(t_i)$	Pseudorange multipath error
λ	Wavelength of L1-carrier: $c/f \approx 0.19$ m
f	Frequency of L1-carrier: = 1575.42 MHz
$\phi_i(t_0)$	Non-zero initial phase of receiver i
$\phi^k(t_0)$	Non-zero initial phase of satellite k
N_i^k	Integer carrier phase ambiguity of carrier phase observation for receiver i and satellite k
$\varepsilon_i^k(t_i)$	Receiver noise and un-modeled effects for carrier phase observables
$e_i^k(t_i)$	Receiver noise and un-modeled effects for pseudorange observables

Observations on other GNSS frequency bands can be expressed in similar ways, and differences result from different levels of the various error sources.

2.2.2 Single-difference (SD) observations between receivers

The SD carrier phase observation between two receivers i and j for signals from the same satellite can be written as

$$\begin{aligned}\Phi_i^k(t_i)-\Phi_j^k(t_j)=&\rho_i^k(t_i-\tau_i^k,t_i)-\rho_j^k(t_j-\tau_j^k,t_j)\\&+c[\delta t_i(t_i)-\delta t^k(t_i-\tau_i^k)]-c[\delta t_j(t_j)-\delta t^k(t_j-\tau_j^k)]\\&+T_i^k(t_i)-T_j^k(t_j)-I_i^k(t_i)+I_j^k(t_j)+\delta m_i^k(t_i)-\delta m_j^k(t_j)\\&+\lambda[\phi_i(t_0)-\phi^k(t_0)]-\lambda[\phi_j(t_0)-\phi^k(t_0)]\\&+\lambda N_i^k-\lambda N_j^k+\varepsilon_i^k(t_i)-\varepsilon_j^k(t_j)\end{aligned}\tag{2.3}$$

Since the difference of travel time from the satellite to the two receivers is very small (less than 50 ms) and the atomic clocks on the satellite are very stable (frequency stability of $10^{-13}\sim10^{-15}$ /day), the satellite clock errors can be considered as approximately constant, then

$$\tau_i^k\approx\tau_j^k\tag{2.4}$$

Thus,

$$\delta t^k(t_i-\tau_i^k)\approx\delta t^k(t_j-\tau_j^k)\tag{2.5}$$

By omitting the explicit time variables and introducing the between-receiver SD operator Δ, the SD carrier phase observation in Equation (2.3) can be abbreviated as

$$\Delta\Phi_{ij}^k=\Delta\rho_{ij}^k+c\Delta\delta t_{ij}+\Delta T_{ij}^k-\Delta I_{ij}^k+\Delta\delta m_{ij}^k+\lambda\Delta\phi_{ij}(t_0)+\lambda\Delta N_{ij}^k+\Delta\varepsilon_{ij}^k\tag{2.6}$$

In the same way, the SD carrier phase observation for satellite l reads

$$\Delta\Phi_{ij}^l=\Delta\rho_i^l+c\Delta\delta t_{ij}+\Delta T_{ij}^l-\Delta I_{ij}^l+\Delta\delta m_{ij}^l+\lambda\Delta\phi_{ij}(t_0)+\lambda\Delta N_{ij}^l+\Delta\varepsilon_{ij}^l\tag{2.7}$$

The two SD observations can be computed from the matrix-vector relation, which reads

$$\Delta\Phi=C\Phi\tag{2.8}$$

where

$$\Delta\Phi = \begin{bmatrix} \Delta\Phi_{ij}^{k} \\ \Delta\Phi_{ij}^{l} \end{bmatrix} \tag{2.9}$$

$$C = \begin{bmatrix} -1 & 1 & 0 & 0 \\ 0 & 0 & -1 & 1 \end{bmatrix} \tag{2.10}$$

$$\Phi = \begin{bmatrix} \Phi_{i}^{k} \\ \Phi_{j}^{k} \\ \Phi_{i}^{l} \\ \Phi_{j}^{l} \end{bmatrix} \tag{2.11}$$

By substituting the above equations, the result is

$$\begin{bmatrix} \Delta\Phi_{ij}^{k} \\ \Delta\Phi_{ij}^{l} \end{bmatrix} = \begin{bmatrix} -1 & 1 & 0 & 0 \\ 0 & 0 & -1 & 1 \end{bmatrix} \begin{bmatrix} \Phi_{i}^{k} \\ \Phi_{j}^{k} \\ \Phi_{i}^{l} \\ \Phi_{j}^{l} \end{bmatrix} \tag{2.12}$$

By assuming that the UD carrier phase observations are linearly independent or un-correlated, the variance of the UD observation vector Φ is

$$Cov(\Phi) = \sigma^2 I \tag{2.13}$$

Applying the covariance propagation law, the covariance of SD observation reads

$$\begin{aligned} Cov(\Delta\Phi) &= C \cdot Cov(\Phi) \cdot C^T \\ &= C \cdot \sigma^2 I \cdot C^T \\ &= \sigma^2 C C^T \end{aligned} \tag{2.14}$$

Since

$$CC^T = 2\begin{bmatrix} 1 & 0 \\ 0 & 1 \end{bmatrix} = 2I \tag{2.15}$$

then

$$\begin{aligned} Cov(\Delta\Phi) &= \sigma^2 CC^T \\ &= 2\sigma^2 I \end{aligned} \tag{2.16}$$

Equation (2.6) shows that the between-receiver SD observations are mathematically un-correlated.

2.2.3 Double-difference (DD) observations between receivers and satellites

The DD carrier phase observation between two receivers and two satellites can be written as

$$\begin{aligned} \Delta\Phi_{ij}^{l} - \Delta\Phi_{ij}^{k} = {} & \Delta\rho_{ij}^{l} - \Delta\rho_{ij}^{k} + c\Delta\delta t_{ij} - c\Delta\delta t_{ij} + \Delta T_{ij}^{l} - \Delta T_{ij}^{k} \\ & - \Delta I_{ij}^{l} + \Delta I_{ij}^{k} + \Delta\delta m_{ij}^{l} - \Delta\delta m_{ij}^{k} + \lambda\Delta\phi_{ij}(t_0) \\ & - \lambda\Delta\phi_{ij}(t_0) + \lambda\Delta N_{ij}^{l} - \lambda\Delta N_{ij}^{k} + \Delta\varepsilon_{ij}^{l} - \Delta\varepsilon_{ij}^{k} \end{aligned} \tag{2.17}$$

By introducing the DD operator $\Delta\nabla$, the above equation can be abbreviated as

$$\Delta\nabla\Phi_{ij}^{kl} = \Delta\nabla\rho_{ij}^{kl} + \Delta\nabla T_{ij}^{kl} - \Delta\nabla I_{ij}^{kl} + \Delta\nabla\delta m_{ij}^{kl} + \lambda\Delta\nabla N_{ij}^{kl} + \Delta\nabla\varepsilon_{ij}^{kl} \tag{2.18}$$

In the same way, the DD carrier phase observation between satellites m and k reads

$$\Delta\nabla\Phi_{ij}^{km} = \Delta\nabla\rho_{ij}^{km} + \Delta\nabla T_{ij}^{km} - \Delta\nabla I_{ij}^{km} + \Delta\nabla\delta m_{ij}^{km} + \lambda\Delta\nabla N_{ij}^{km} + \Delta\nabla\varepsilon_{ij}^{km} \tag{2.19}$$

The two DD observations can be computed from the matrix-vector relation as

$$\Delta\nabla\Phi = C'\Delta\Phi \tag{2.20}$$

where

$$\nabla\Delta\Phi = \begin{bmatrix} \nabla\Delta\Phi_{ij}^{kl} \\ \nabla\Delta\Phi_{ij}^{km} \end{bmatrix} \tag{2.21}$$

$$C' = \begin{bmatrix} -1 & 1 & 0 \\ -1 & 0 & 1 \end{bmatrix} \tag{2.22}$$

$$\Delta\Phi = \begin{bmatrix} \Delta\Phi_{ij}^{k} \\ \Delta\Phi_{ij}^{l} \\ \Delta\Phi_{ij}^{m} \end{bmatrix} \tag{2.23}$$

By substituting equations, the result is

$$\begin{bmatrix} \nabla\Delta\Phi_{ij}^{kl} \\ \nabla\Delta\Phi_{ij}^{km} \end{bmatrix} = \begin{bmatrix} -1 & 1 & 0 \\ -1 & 0 & 1 \end{bmatrix} \begin{bmatrix} \Delta\Phi_{ij}^{k} \\ \Delta\Phi_{ij}^{l} \\ \Delta\Phi_{ij}^{m} \end{bmatrix} \tag{2.24}$$

The covariance matrix for the DD observations is given as

$$\begin{aligned} Cov(\nabla\Delta\Phi) &= C' \cdot Cov(\Delta\Phi) \cdot C'^{T} \\ &= 2\sigma^2 C' C'^{T} \\ &= 2\sigma^2 \begin{bmatrix} 2 & 1 \\ 1 & 2 \end{bmatrix} \end{aligned} \tag{2.25}$$

From Equation (2.25), it can be seen that DD observations between receivers and satellites are mathematically correlated.

2.2.4 Single-differencing versus double-differencing

There have been debates on using either SD or DD observations in GNSS data processing (Vollath 2008). It has been proved that the two approaches are equivalent (Schaffrin & Grafarend 1986, Shen & Xu 2008). The trade-off for choosing one method against the

other is mostly on software implementation issues. Here comparisons on using single-differencing versus double-differencing are listed in Table 2.5.

Table 2.5: Comparisons of single- and double-differencing schemes

	Single-differencing	Double-differencing
Advantages	• it is easier to form SD observations • SD observations are mathematically uncorrelated, they are appropriate for sequential processing in the filter	• It is easy to fix DD ambiguities since they are integers
Disadvantages	• SD ambiguities cannot be estimated separately from the common receiver clock offset, which is not an integer value, and thus must be differenced before being fixed	• it is more complicated to form DD observations • they are more book-keeping operations during implementation • DD observations are mathematically correlated, they are more complicated for sequential processing in the filter

It can be seen from the comparisons that it is advantageous to use SD over DD observations, the problem of non-integer SD ambiguities can be resolved with a transformation in the ambiguity domain, which will be discussed in Chapter 3.

2.2.5 Observation combinations

When multi-frequencies GNSS observations are available, linear combinations among observations on different frequencies can be performed to make observables with longer wavelength or reduced ionospheric errors. The general form of linear combinations of

GPS L1, L2 and L5 (or Galileo E1, E5b and E5b) phase observations (in cycles) can be expressed as follows (Cocard et al. 2008),

$$\phi_{LC} = i \cdot \phi_1 + j \cdot \phi_2 + k \cdot \phi_3 \tag{2.26}$$

The resulting integer ambiguity corresponding to ϕ_{LC} is

$$N_{LC} = i \cdot N_1 + j \cdot N_2 + k \cdot N_3 \tag{2.27}$$

and the frequency of this combined observation is

$$\lambda_{LC} = \frac{1}{\frac{i}{\lambda_1} + \frac{j}{\lambda_2} + \frac{k}{\lambda_3}} \tag{2.28}$$

Various combinations can be made for GPS and Galileo. A popular one among them is the so-called EWL-WL-L1/E1 combination as shown in Table 2.6.

Table 2.6: Observation combinations of GPS and Galileo

System	Combination	Coefficients			Wavelength (m)
		L1/E1	L2/E5b	L5/E5a	
GPS	EWL	0	1	-1	5.861
	WL	1	-1	0	0.862
	L1	1	0	0	0.193
Galileo	EWL	0	1	-1	9.765
	WL	1	-1	0	0.814
	E1	1	0	0	0.193

Assuming that the observations on each frequency are uncorrelated and writing the original and combined observations in vector forms gives,

$$\Phi = \begin{bmatrix} \Phi_1 \\ \Phi_2 \\ \Phi_3 \end{bmatrix} \tag{2.29}$$

$$\Phi_{LC} = \begin{bmatrix} \Phi_1 \\ \Phi_{WL} \\ \Phi_{EWL} \end{bmatrix} \tag{2.30}$$

The relationship between Equations (2.29) and (2.30) is:

$$\Phi_{LC} = B \cdot \Phi \tag{2.31}$$

where

$$B = \begin{bmatrix} 1 & 0 & 0 \\ 1 & -1 & 0 \\ 0 & 1 & -1 \end{bmatrix} \tag{2.32}$$

By applying the covariance propagation law, the corresponding variance-covariance matrix of Φ_{LC} is derived as

$$\begin{aligned} Cov(\Phi_{LC}) &= B \cdot Cov(\Phi) \cdot B^T \\ &= \begin{bmatrix} 1 & 0 & 0 \\ 1 & -1 & 0 \\ 0 & 1 & -1 \end{bmatrix} \cdot \begin{bmatrix} \sigma_{\Phi_1}^2 & 0 & 0 \\ 0 & \sigma_{\Phi_2}^2 & 0 \\ 0 & 0 & \sigma_{\Phi_3}^2 \end{bmatrix} \cdot \begin{bmatrix} 1 & 0 & 0 \\ 1 & -1 & 0 \\ 0 & 1 & -1 \end{bmatrix}^T \\ &= \begin{bmatrix} \sigma_{\Phi_1}^2 & \sigma_{\Phi_1}^2 & 0 \\ \sigma_{\Phi_1}^2 & \sigma_{\Phi_1}^2 + \sigma_{\Phi_2}^2 & -\sigma_{\Phi_2}^2 \\ 0 & -\sigma_{\Phi_2}^2 & \sigma_{\Phi_2}^2 + \sigma_{\Phi_3}^2 \end{bmatrix} \end{aligned} \tag{2.33}$$

From Equation (2.33), it is found that the combined observations are mathematically correlated. However, this has been generally ignored in previous studies and has led to optimistic results.

2.3 GNSS Measurement Errors

As shown in Equations (2.1) and (2.2), the GNSS code and phase observations contain a number of error sources, which are divided into three groups (Wübbena & Willgalis 2001):

1) Clock related errors, which include receiver and satellite clock errors and instrumental delays presented in the receiver and satellites. These errors can be eliminated through observation differencing or can be estimated as nuisance parameters.
2) Baseline dependent errors, including ionospheric, tropospheric and satellite orbital errors. The magnitude of these errors increases as a function of the physical separation of the reference and rover receivers.
3) Station dependent errors, which consist of receiver noise and multipath, phase centre variations (PCV) of receiver and satellite antennas.

Some of the important error sources are discussed in detail in the following subsections.

2.3.1 Satellite orbital error

GPS signals are broadcast from satellites in the navigation message which are used to compute satellite coordinates in real time. The orbital parameters are updated by the ground control facility in two-hour intervals. The influence of satellite orbital errors on differential positioning can be determined based on Equation (2.34) (Conley et al. 2005).

$$\Delta b = \frac{b}{\rho}\Delta r \tag{2.34}$$

where Δb is the baseline estimation error, b is the length of the baseline between two receivers, Δr is satellite orbital error and ρ is the mean distance between a satellite and a receiver.

Given the fact that the current satellite orbital error is around 1.6 m (IGS 2008) and will be further improved to 0.6 m (Madden 2008), the baseline estimation error is about 8 mm over a 100 km baseline and it is negligible over short baselines applications.

2.3.2 Tropospheric error

The troposphere is a non-dispersive medium for frequencies up to 15 GHz and it is located in lower part of the atmosphere extending to 40 km above the Earth's surface. The GNSS signal undergoes a path delay when it travels through the troposphere and the delay is dependent on the local temperature, pressure, and relative humidity (Conley et al., 2005).

The tropospheric delay is generally modeled as including both dry and wet components. The dry component arises from the dry air and contributes to about 90% of the total delay, and it can be predicted very accurately. The remaining wet component is induced from the water vapour in the troposphere, and it is difficult to predict because of the rapid variation of water vapour. Several models have been developed to correct tropospheric

delays, e.g., those proposed by Hopfield (1970) and Saastamoinen (1972) and the UNB3 model (Leandro et al. 2006), the last one having the merit of being free of meteorological parameter input. Both the dry and wet components of tropospheric delay are usually predicted in the zenith direction. In order to get slant tropospheric delays for other elevations, a specific function is used to map the zenith tropospheric delay. This task can be fulfilled by a number of mapping functions, such as the Neil mapping function (Neil 1996) for geodetic and surveying data processing and the Black and Eisner mapping function (Black & Eisner 1984) for real-time navigation applications (Guo & Langley 2003).

In differential GNSS (DGNSS) applications, the residual tropospheric delay after correction of the two receivers is generally very small. For example, it is on the order of 2 cm over a 100 km baseline in normal weather conditions (Cosentino et al. 2005), so this can be ignored for most applications. In extreme weather conditions, the troposphere is significantly decorrelated even over a baseline of several kilometres (Lawrence et al. 2006). It has been shown that decorrelated tropospheric errors amount to 0.23 m and 0.40 m for baselines over 5.4 km and 16 km, respectively (Huang & van Graas 2006). Since the work in this thesis focuses on short baseline kinematic positioning in normal weather conditions, the differential trosposheric delay is safely neglected.

2.3.3 Ionospheric error

The ionosphere is a dispersive medium located 70 km to 1,000 km above the Earth's surface. The ionosphere is a major error source for GNSS range and range-rate measurements (Conley et al. 2005). The rapid fluctuations of electrons in the ionosphere, called ionospheric scintillations, can even cause the receiver to lose satellite tracking (Kintner et al. 2007). The first order ionospheric effect on range measurements can be approximated as a function of the carrier frequency f as shown in Equation (2.35) (Klobuchar 1996) and the second and higher order effects are generally less than 10 cm (Hoque & Jakowski 2008) and are generally ignored even in high precision applications.

$$I = \frac{40.3}{f^2} TEC \tag{2.35}$$

where TEC is the total electron content along the signal path through the ionosphere over a $1\,m^2$ surface.

For single frequency GNSS users, the ionospheric error can be corrected in real time using broadcast models, such as the Klobuchar model (Klobuchar 1987, Feess & Stephens 1987) used for GPS and the NeQuick model (Belabbas et al. 2005) proposed for Galileo. The latter has better performance than the former in terms of ionospheric correction on a global scale (Aragón-Ángel & Amarillo-Fernández 2006). However, the broadcast models can only compensate about 50% of the ionospheric error; other state-of-the-art models, like International Reference Ionosphere (IRI) and Bent models can improve the correction to 75%; when an external ionospheric correction, like WAAS correction is used, the improvement goes to 90% (Klobuchar 2001). Recently, a tomography technique has been developed and used for single frequency GNSS

ionospheric correction, promising result has been obtained and it was shown that almost the first order ionospheric effect could be corrected (Allain & Mitchell 2008). However, these single frequency ionospheric models are not sufficiently for use in precise carrier phase applications.

For dual or multiple frequency GPS/Galileo users, the first order ionospheric error on the L1/E1 frequency can be completely estimated using code or phase measurements on two carrier frequencies as shown in Equations (2.36) and (2.37), respectively.

$$I_1 = \frac{f_i^2 f_j^2}{f_j^2 - f_i^2} \cdot \frac{1}{f_1^2} \cdot (\rho_i - \rho_j) \tag{2.36}$$

$$I_1 = \frac{f_i^2 f_j^2}{f_j^2 - f_i^2} \cdot \frac{1}{f_1^2} \cdot (\Phi_i + \mathrm{N}_i - \Phi_j - N_j) \tag{2.37}$$

where ρ_i and ρ_j are pseudorange observations on frequencies f_i and f_j, Φ_i, Φ_j, N_i and N_j are corresponding phase observations and their ambiguities.

In DGNSS positioning, ionospheric errors are significantly reduced by observation differencing between two receivers because of the correlation of the ionosphere effect. The remaining residual ionospheric error can be estimated as a nuisance parameter if dual or multiple frequency observations are available. This ionospheric residual will restrict the effective use of single frequency RTK to about 10 km since the ionospheric error is not observable in the estimation.

2.3.4 Receiver noise and multipath

Receiver noise is caused by tracking errors in the receiver delay lock loop (DLL) and phase lock loop (PLL). The C/A code receiver noise of a typical modern GNSS receiver is on the order of one decimetre or less (one sigma). For modernized GPS and Galileo signals, the magnitude of the code noise will be decreased to the centimetre levels (vila-Rodríguez et al. 2005). The receiver noise of the phase observations is generally independent of the signal modulation scheme and chipping rate for different signals and is generally on the order of 1 mm or less (Ward et al. 2005).

Multipath is induced from the interference of the line-of-sight GNSS signals and reflected signals received by the receiver. The magnitude of the multipath errors is closely related to the environment where the receiver is located, satellite elevation angle, antenna gain pattern and signal characteristics (Conley et al. 2005). To mitigate the code multipath, a number of advanced correlators have been developed and implemented in high-end GNSS receivers. To name a few, there is the narrow correlator, the MEDLL (Multipath Estimation Delay Lock Loop) correlator, and the MET (Multipath Elimination Technique) correlator (Ray 2006). The maximum carrier phase multipath error is generally less than a quarter of the wavelength of the carrier frequency (Conley et al. 2005). Reduction of carrier phase multipath errors is still a challenge in GNSS precise positioning, though some investigations can be found in Lau and Cross (2007) and Bilich et al. (2008).

Both receiver noise and multipath will be increased through observation differencing in DGNSS applications. To reduce the effects of multipath, the receiver sites should be carefully selected and multipath mitigation antennas, e.g., choke ring and ground plane antennas should be used (Hofmann-Wellenhof et al. 2001).

2.4 Summary

This chapter reviewed the current and developing GNSS, and special attention was paid to modernized GPS and Galileo, which will be studied in this thesis in terms of kinematic positioning performance. GNSS observations and different differencing schemes were studied and the advantages and disadvantages of using different kinds of observations were compared. Various error sources in GNSS observations were briefly described as they will be carefully considered in a covariance analysis in Chapter 4 and the creation of simulated data in Chapter 5.

Chapter Three: Differential GNSS Positioning

3.1 Introduction

Stand-alone positioning with pseudorange observations provides a few metres of accuracy. To achieve sub-metre or better positioning accuracy, a reference receiver is set up near the rover receiver to reduce or eliminate the common errors between two receivers. This method is called differential GNSS (DGNSS). DGNSS positioning with pseudorange observations is straightforward, while it is more complicated if using carrier phase observations, which contain the ambiguous cycles. There are four steps involved in DGNSS positioning using carrier phase observables (Teunissen & Verhagen 2007b).

1) Estimate the ambiguities and other parameters while ignoring the integer characteristic of ambiguities. As a result, the so called float ambiguity solution and the corresponding covariance matrix of the ambiguity estimates are obtained.
2) Adjust the float ambiguities to corresponding integer values. This step is called ambiguity resolution.
3) Decide whether or not to accept the computed integer values based on some statistical properties, e.g., the ratio test. This is called ambiguity validation.
4) Once the computed integer ambiguities are accepted, the fixed position solutions are calculated as the last step in carrier phase DGNSS positioning.

As mentioned in Section 2.2, either DD or SD observations can be used in carrier phase DGNSS float filtering. Using SD may have advantages in implementation but suffers from disadvantages in terms of ambiguity resolution. Figure 3.1 shows a flowchart for using SD carrier phase observables in GNSS positioning and the details of each step are discussed in following sections.

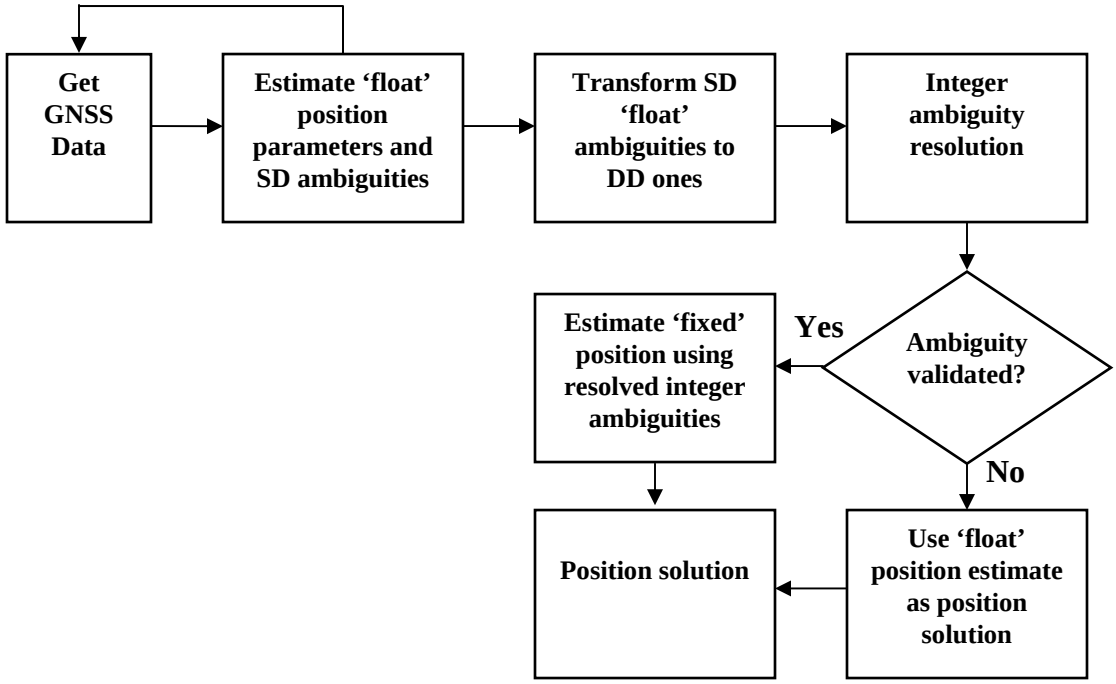

Figure 3.1: Flowchart of DGNSS positioning using SD carrier phase observations

3.2 Float Filter

Sequential estimation technique such as Kalman filtering is usually implemented in kinematic carrier phase DGNSS processing. Four steps are generally involved in a Kalman filter (shown in Figure 3.2): prediction, computation of Kalman gain, updating

estimate with observations and computation of covariance for updated estimate (Brown & Hwang 1997).

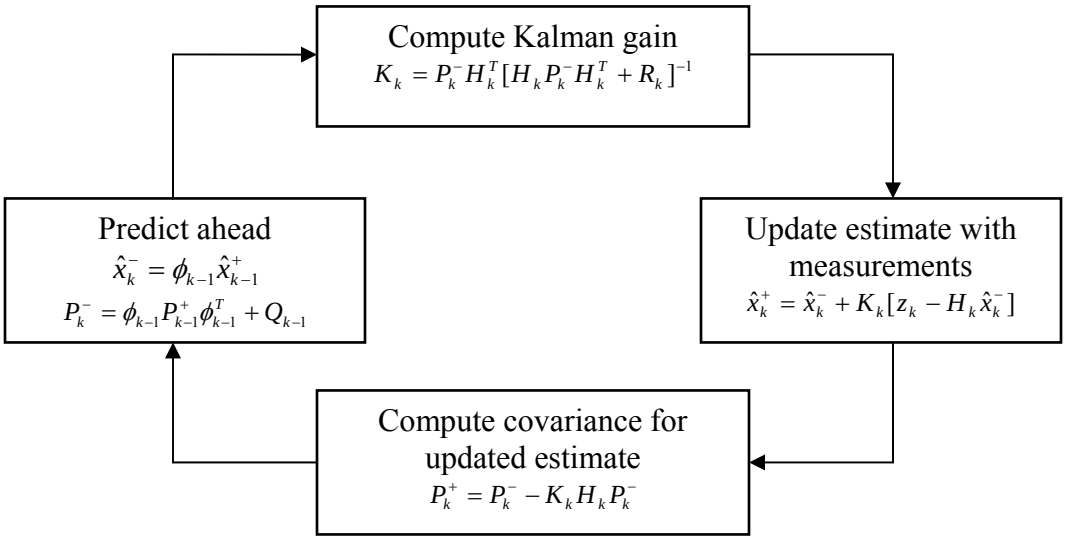

Figure 3.2: Kalman filter loop (after Brown & Hwang 1997)

In Figure 3.2, where

$\hat{x}_k$ is the state vector estimated at epoch k

z_k is the observation vector at epoch k

P_k is the variance-covariance matrix of state vector $\hat{x}_k$ at epoch k

ϕ_k is the state transition matrix

Q_k is the system process noise matrix at epoch k

K_k is the Kalman gain at epoch k

H_k is the design matrix at epoch k

R_k is the variance-covariance matrix of observation vector z_k at epoch k

$^-$ indicates the state estimate and its covariance before the "Update" step

$^+$ indicates the state estimate and its covariance after the "Update" step

3.2.1 Dynamic model

In the implementation of this work, the state vector $\hat{x}_k$ usually contains three position states - latitude, longitude and height $(\varphi, \quad \lambda, \quad h)$ and float ambiguities. Since the SD observations are used in the processing, the clock offsets for the two receivers can not be cancelled out and another state dt corresponding to the relative receiver clock offset has to be estimated in the filter. Assuming n common satellites are observed by the reference and rover receivers, there are n SD ambiguities to be estimated. The state vector reads

$$\hat{x}_k = (\varphi, \quad \lambda, \quad h, \quad dt, \quad \Delta N_1, \quad \Delta N_2, \quad \Delta N_3, \quad \cdots, \quad \Delta N_n) \tag{3.1}$$

In this study, a random walk is assumed for the position states since the rover receiver is static or in low dynamics for surveying applications. The values of the ambiguity will not change if there is no cycle slip, so a random constant model is used to describe the ambiguity states. The system transition matrix Φ is an identity matrix as per Equation (3.2).

$$\Phi = \begin{bmatrix} 1 & 0 & 0 & 0 & 0 & 0 & 0 & \cdots & 0 \\ 0 & 1 & 0 & 0 & 0 & 0 & 0 & \cdots & 0 \\ 0 & 0 & 1 & 0 & 0 & 0 & 0 & \cdots & 0 \\ 0 & 0 & 0 & 1 & 0 & 0 & 0 & \cdots & 0 \\ 0 & 0 & 0 & 0 & 1 & 0 & 0 & \cdots & 0 \\ 0 & 0 & 0 & 0 & 0 & 1 & 0 & \cdots & 0 \\ 0 & 0 & 0 & 0 & 0 & 0 & 1 & \cdots & 0 \\ 0 & 0 & 0 & 0 & 0 & 0 & 0 & \ddots & 0 \\ \underbrace{0 \quad 0 \quad 0}_{position} & & & \underbrace{0}_{clock} & \underbrace{0 \quad 0 \quad 0 \quad \cdots \quad 1}_{ambiguity} & & & & \end{bmatrix} \tag{3.2}$$

The spectral density values of the position states depend on the system dynamics. For the data sets used in this thesis, the rover receiver is practically static but processed in kinematic mode, so a small value, namely 0.05 m/s, is given as the spectral density of each position state. The clock error is not bounded and it can change quickly from epoch to epoch, a large value, e.g., 10000 m/s, is assigned to the spectral density of the clock state. The ambiguity states are modeled as constants and their process noise values are simply set to zero. The corresponding system noise matrix Q is shown in Equation (3.3).

$$Q = \begin{bmatrix} sp_{\varphi} & 0 & 0 & 0 & 0 & 0 & 0 & \cdots & 0 \\ 0 & sp_{\lambda} & 0 & 0 & 0 & 0 & 0 & \cdots & 0 \\ 0 & 0 & sp_{h} & 0 & 0 & 0 & 0 & \cdots & 0 \\ 0 & 0 & 0 & sp_{clock} & 0 & 0 & 0 & \cdots & 0 \\ 0 & 0 & 0 & 0 & 0 & 0 & 0 & \cdots & 0 \\ 0 & 0 & 0 & 0 & 0 & 0 & 0 & \cdots & 0 \\ 0 & 0 & 0 & 0 & 0 & 0 & 0 & \cdots & 0 \\ 0 & 0 & 0 & 0 & 0 & 0 & 0 & \ddots & 0 \\ \underbrace{0 \quad 0 \quad 0}_{position} & & & \underbrace{0}_{clock} & \underbrace{0 \quad 0 \quad 0 \quad \cdots \quad 0}_{ambiguity} & & & & \end{bmatrix} \tag{3.3}$$

3.2.2 Measurement model and sequential processing

The measurement model relates the state vector in the filter and the GNSS observations through the design matrix H (shown in Figure 3.2). Continuous updates in the filter are crucial to keep the system from diverging.

As discussed in Section 2.2, the SD observations are mathematically uncorrelated thus the measurement error variance-covariance matrix R is diagonal. This merit gives an advantage of processing the measurements in a sequential way. Then the equations in the update steps are adapted as follows (Grewal & Andrews 2001):

$$K_k^{[i]} = \frac{1}{h_i P_k^{[i-1]} h_i^T + r_i} P_k^{[i-1]} h_i^T \tag{3.4}$$

$$P_k^{[i]} = P_k^{[i-1]} - K_k^{[i]} h_i P_k^{[i-1]} \tag{3.5}$$

$$\hat{x}_k^{[i]} = \hat{x}_k^{[i-1]} + K_k^{[i]} [z_i - h_i \hat{x}_k^{[i-1]}] \tag{3.6}$$

where h_i is the i_{th} row in the design matrix H and r_i is the i_{th} diagonal element in matrix R, z_i is the i_{th} observation in the measurement vector and $[i]$ indicates the i_{th} update of the filter states. The other parameters are the same as those in Figure 3.1.

The implementation of sequential processing significantly reduces the computation burden of the filter since there is no inversion operation of large dimensional matrices, just the inversion of a scalar $\left(h_i P_k^{[i-1]} h_i^T + r \right)$ instead.

3.2.3 Transformation of ambiguities from SD to DD

As discussed in Section 2.2, SD float ambiguities are not easily fixed, so a transformation operator B (Equation (3.7)) is applied to get the DD float ambiguities and their

corresponding covariance matrix. The transformations are shown in Equations (3.8) and (3.9).

$$B = \underbrace{\begin{bmatrix} 1 & 0 & -1 & \cdots & 0 \\ 0 & 1 & -1 & \cdots & 0 \\ 0 & 0 & -1 & \cdots & 0 \\ \vdots & \vdots & \vdots & \vdots & 0 \\ 0 & 0 & -1 & \cdots & 1 \end{bmatrix}}_{(n-1)xn} \tag{3.7}$$

$$N_{DD} = B \cdot N_{SD} \tag{3.8}$$

$$C_{DD} = B \cdot C_{SD} \cdot B^T \tag{3.9}$$

The SD float ambiguities are biased by the between-receiver clock offset. However, this common clock error is the same for all float ambiguities. By choosing an ambiguity (one for each frequency band) as the reference one, the clock errors for the other float ambiguities are effectively cancelled by applying the above transformation. Thus the transformed DD float ambiguities should be identical to those using DD observations and they are essentially integers and can be more easily fixed.

3.3 GNSS Multi-Carrier Ambiguity Resolution

Before moving to the topic of ambiguity resolution, the differences between the models used in GNSS positioning are addressed to facilitate the further discussion on different AR methods.

Single-epoch and multi-epoch models: the difference between these two models resides in the number of observation epochs involved in estimation. For the single-epoch model, it only uses information from current epoch observations and its aim is to resolve ambiguities instantaneously. Least-squares is generally used in this model. For the multi-epoch model, information from previous epochs and the current one is used and the estimation technique employed can be a Kalman filter or Least-squares depending on the assumed user dynamics.

Geometry-free (GF) and Geometry-based (GB) models: the distinction between these two models is whether the three baseline components are estimated or not. In the GF model, the ranges (including tropospheric delays) between satellites and receiver are estimated. In application, once the ambiguities are resolved, the fixed values are used in a subsequent position estimation step. In the GB model, the three baseline components (or three position parameters of the rover receiver) are estimated at the same time as the ambiguities.

Given that there will be multiple-frequency observations available from both GPS and Galileo in the future, extensive research has been conducted on AR in multi-carrier (and multi-system) scenarios in the last decade. The proposed methods can be divided into two categories: one is resolving the ambiguities using a cascading approach according to different combinations of frequencies. The other is resolving all the ambiguities on all the

frequencies simultaneously following the procedures of the LAMBDA method. This section gives a comprehensive review of these methods and discusses their pros and cons.

3.3.1 Cascading ambiguity resolution (CAR)

The longer the wavelengths of the carrier phase observables, the easier it is to fix the ambiguities. The basic idea behind cascading ambiguity resolution is to resolve the ambiguities on optimized linear combinations of frequencies in several steps. This optimization is generally based on measurement noise, ionospheric refraction error and wavelength on different frequency bands (Zhang 2005). Within this approach, the ambiguities on each combined frequency are fixed in the order of decreasing wavelength (see Table 2.5), then ambiguities on each basic (or original) frequency, e.g., L1, L2 and L5, are determined accordingly.

An overview of multi-carrier GPS/Galileo AR has been given in Chapter 1. Extensive investigations have been conducted on optimized combinations of frequencies for Galileo and modernized GPS (Cocard et al. 2008, Ji et al. 2007, Zhang 2005). For example, a popular combination of GPS and Galileo frequencies is shown in Table 2.5, with the corresponding cascading step is given in Figure 3.3.

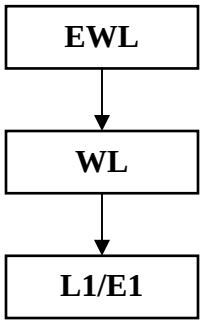

Figure 3.3: Scheme of Cascading Ambiguity Resolution (CAR)

The CAR methods can be further divided into two groups: three-filter and one-filter approaches. Details of each are described below along with their pros and cons.

Three filters

The approach of using three filters was adopted in Forssell et al. (1997) for Galileo, Jung (1999) and Jung et al. (2000) for GPS and Zhang et al. (2003) and Zhang (2005) for combined GPS/Galileo. This method is straightforward and is currently the most popular one for cascading ambiguity resolution.

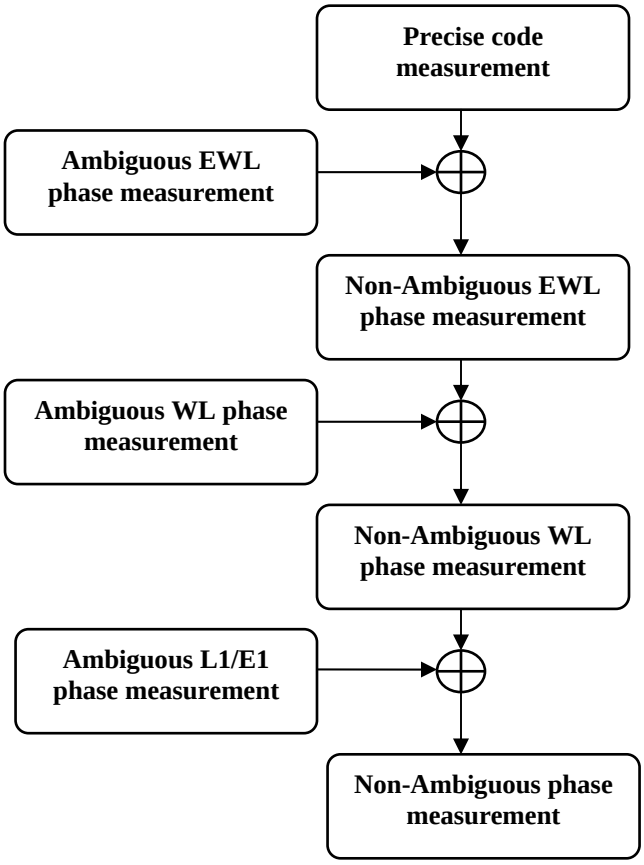

Figure 3.4: Flowchart of CAR (after Schlötzer & Martin 2005)

As shown in Figure 3.4, there are three steps in this approach: the first step is to use the precise code observations, such as GPS L5 and Galileo E5a, to directly resolve EWL ambiguities. Once the EWL ambiguities are fixed, they are used to resolve the WL ambiguities as the second step. The last step is to resolve the L1/E1 ambiguities with the fixed WL ambiguities. When the EWL, WL and L1/E1 ambiguities are fixed correctly, the corresponding ambiguities on the original frequencies (L1/E1, L2/E5b and L5/E5a) can be easily obtained. Details to implement each cascading step can be found in Zhang (2005).

Both CIR and TCAR are based on geometry-free models, which do not exploit the variation of geometric information between the satellites and receiver at different epochs and they are generally useful for instantaneous (or single-epoch) AR over short baselines. To avoid these limitations, a cascading ambiguity resolution method with a geometry-based model was proposed and tested in Zhang et al. (2003) and Zhang (2005), and it showed that the geometry-based model performed better than the geometry-free one.

One filter

As an improvement of the three-filter approach adopted in TCAR (Forssell et al. 1997), a one-filter approach was proposed by Vollath et al. (1998) and it was named the Integrated TCAR (ITCAR) by Schlötzer & Martin (2005). In contrary to only the most precise code measurement being used in TCAR, ITCAR uses code observations on all three frequencies. This one-filter approach is intuitively simpler than the three-filter one as the following models are used.

$$l = Ax \tag{3.10}$$

$$l = \begin{bmatrix} \rho_1 \\ \rho_2 \\ \rho_3 \\ \Phi_1 \\ \Phi_2 \\ \Phi_3 \end{bmatrix},\ A = \begin{bmatrix} 1 & 0 & 0 & 0 \\ 1 & 0 & 0 & 0 \\ 1 & 0 & 0 & 0 \\ 1 & 0 & \lambda_{EWL} & -\lambda_{EWL} \\ 1 & \lambda_{WL} & -\lambda_{WL} & 0 \\ 1 & \lambda_{L_1} & 0 & 0 \end{bmatrix},\ x = \begin{bmatrix} R \\ N_{EWL} \\ N_{WL} \\ N_{L_1} \end{bmatrix} \tag{3.11}$$

where

l is the observation vector

A	is the design matrix
x	is the state vector
R	is the range between receiver and satellite
ρ_1, ρ_2, ρ_3	are pseudorange observations on L1, L2 and L5 or E1, E5b and E5a frequencies
$\Phi_{EWL}, \Phi_{WL}, \Phi_{L_1}$	are EWL, WL and L1/E1 carrier phase observations
$\lambda_{EWL}, \lambda_{WL}, \lambda_{L_1}$	are wavelengths of $\Phi_{EWL}, \Phi_{WL}, \Phi_{L_1}$ observations
N_{EWL}, N_{WL}, N_{L_1}	are ambiguities of $\Phi_{EWL}, \Phi_{WL}, \Phi_{L_1}$ observations

In the one-filter approach, information on the code observations on three frequencies is used in the estimation. In addition, the ionospheric errors are estimated as states and are isolated from the observations thus the AR performance is improved (Vollath et al. 1998). The performances of TCAR and ITCAR were compared by Schlötzer & Martin (2005), who concluded that the performance of the latter was superior to that of the former.

Comparison of three-filter and one-filter approaches

Below are some remarks on the three-filter and one-filter approaches for cascading ambiguity resolution.

1) If the geometry-free model is used, the three-filter approach only uses the most precise code measurement, which leads to loss of information in estimation.

2) If the geometry-based model is used, in the last step of the three-filter approach, when new satellites come in, the observations from these satellites have to be discarded since the EWL and WL ambiguities of these satellites have not been estimated (Zhang 2005). This also leads to loss of information in estimation.
3) For the three-filter approach, if DD observations are used, when there is a base-satellite change in the EWL or WL cascading step, the corresponding ambiguities in subsequent steps are also needed to be switched, which makes the implementation inefficient.
4) Since all the code and phase measurements at each epoch are used in the one-filter approach, the computational load is significantly heavier than the three-filter approach. This may be the reason for investigating combinations of different frequencies and using a three-filter approach (Cocard et al. 2008).

3.3.2 LAMBDA for multi-carrier ambiguity resolution

The well-known LAMBDA method (Teunissen 1993 & 1994) has been applied to ambiguity resolution for three-frequency GPS and Galileo AR in Tiberius et al. (2002a & 2002b) and four-frequency Galileo in Ji et al. (2007). When using LAMBDA, no combinations between frequencies need to be formed and the original observations and ambiguities on each frequency are directly used and estimated, respectively. The basic mathematical model for the geometry-based float solution is described as follows,

$$l = Ax \tag{3.12}$$

$$l=\begin{bmatrix}\rho_1\\ \rho_2\\ \rho_3\\ \Phi_1\\ \Phi_2\\ \Phi_3\end{bmatrix},\ A=\begin{bmatrix}\frac{\partial R}{\partial X} & \frac{\partial R}{\partial Y} & \frac{\partial R}{\partial Z} & 0 & 0 & 0\\ \frac{\partial R}{\partial X} & \frac{\partial R}{\partial Y} & \frac{\partial R}{\partial Z} & 0 & 0 & 0\\ \frac{\partial R}{\partial X} & \frac{\partial R}{\partial Y} & \frac{\partial R}{\partial Z} & 0 & 0 & 0\\ \frac{\partial R}{\partial X} & \frac{\partial R}{\partial Y} & \frac{\partial R}{\partial Z} & \lambda_1 & 0 & 0\\ \frac{\partial R}{\partial X} & \frac{\partial R}{\partial Y} & \frac{\partial R}{\partial Z} & 0 & \lambda_2 & 0\\ \frac{\partial R}{\partial X} & \frac{\partial R}{\partial Y} & \frac{\partial R}{\partial Z} & 0 & 0 & \lambda_3\end{bmatrix},\ x=\begin{bmatrix}X\\ Y\\ Z\\ N_1\\ N_2\\ N_3\end{bmatrix} \tag{3.13}$$

where

l, A, x, R	are the same as those in Equation (3.11)
X, Y, Z	are three coordinate components of the rover receiver
ρ_1, ρ_2, ρ_3	are pseudorange observations on L1, L2 and L5 or E1, E5b and E5a frequencies
Φ_1, Φ_2, Φ_3	are carrier phase observations on L1, L2 and L5 or E1, E5b and E5a frequencies
$\lambda_1, \lambda_2, \lambda_3$	are wavelengths of Φ_1, Φ_2, Φ_3 observations
N_1, N_1, N_3	are ambiguities of Φ_1, Φ_2, Φ_3 observations

To reduce the computational burden of the float solution using multiple-frequency code and phase observations with LAMBDA, a factorized multi-carrier ambiguity resolution (FAMCAR) method was developed by Vollath (2005 & 2008). This method is independent of the number of carrier frequencies used and significantly reduces the computational load to speed up the float filter while the ambiguity resolution technique is essentially not changed since LAMBDA is used in the process of ambiguity fixing.

A comparison of multi-carrier AR using LAMBDA, TCAR and CIR was discussed in Teunissen et al. (2002), who showed that the one-filter TCAR and CIR were just special cases with predefined transformations of the decorrelation steps using LAMBDA and they were less optimal than LAMBDA. The decorrelations in LAMBDA use the variance-covariance matrix of ambiguities, which contains all the information inherited in the observations and float ambiguities while the selection of frequency combinations in TCAR and CIR is only based on criteria like frequency wavelength, measurement noise and ionospheric error reduction. Performance comparisons between the CAR and LAMBDA methods can be found in Ji et al. (2007) and O'Keefe et al. (2008), both of which showed that LAMBDA had better performance than the CAR methods.

In this thesis, the LAMBDA method was used for ambiguity resolution and the original carrier observations were used without any combination to make the filter flexible.

3.4 Ambiguity Validation

The last but important step of GNSS AR is ambiguity validation, which is to check the correctness of obtained integer ambiguities from the AR step described in the previous section. Two methods are implemented in this work, namely

1) Discrimination test
2) Probability of correct ambiguity resolution

Discrimination test

By applying ambiguity search techniques, a number of ambiguity candidate sets can be found. These candidate sets can be ordered based on the criterion in Equation (3.14).

$$r(\breve{N}) = (\hat{N} - \breve{N})^T Q_{\hat{N}} (\hat{N} - \breve{N}) \tag{3.14}$$

where $\hat{N}$ is the float ambiguity vector, $Q_{\hat{N}}$ is the variance-covariance of the float ambiguity solution and $\breve{N}$ is the vector of fixed ambiguities.

According to Equation (3.14), the best ambiguity set $\breve{N}_1$, which has the minimum value of $r(\breve{N}_1)$ and second best ambiguity set $\breve{N}_2$, which has second minimum value of $r(\breve{N}_2)$, can be easily obtained.

The usual method for ambiguity validation is to test the discrimination between the best and second best ambiguity sets. A number of statistical tests, e.g., R-ratio test, F-ratio test, difference test and projector test, have been proposed to validate the integer ambiguities. A comparison and evaluation of different test methods can be found in Verhagen (2004). However, the test methods are not optimal since they use fixed ratio values, which are experience-based. To overcome this limitation, a validation method based on fixed failure rate of AR was proposed by Teunissen & Verhagen (2008) and results showed this model-driven approach had better performance than the conventional ratio tests (Verhagen 2006 & 2007).

The popular ratio test of ambiguity residuals for the best and second best ambiguity sets can be expressed in Equation (3.15) and the threshold value *ratio* is set to 2, which is found to be an appropriate value for the data sets used in this thesis.

$$ratio < \frac{r(\breve{N}_2)}{r(\breve{N}_1)} = \frac{(\hat{N} - \breve{N}_2)^T Q_{\hat{N}} (\hat{N} - \breve{N}_2)}{(\hat{N} - \breve{N}_1)^T Q_{\hat{N}} (\hat{N} - \breve{N}_1)} \tag{3.15}$$

Probability of correct ambiguity resolution

Besides the discrimination test methods, a probabilistic description of the correctness of AR, called probability of correct fix (PCF) (O'Keefe et al. 2006) or success rate (Verhagen 2005), has been used for ambiguity validation. In order to fix ambiguities to their correct integer values, the PCF values should be high enough, i.e., close to one (Verhagen 2005). However, the PCF value is difficult to be evaluated if the integer least squares (ILS) (e.g., LAMBDA) estimator is applied in ambiguity resolution. Instead, a bootstrapped lower bound on the PCF of ILS can be easily obtained as a by-product of the LAMBDA decorrelation process, and it is as follows.

$$P(\breve{N}_B = N) = \prod_{i=1}^{n} (2\Phi(\frac{1}{2\sigma_{\breve{N}_{i|I}}}) - 1) \tag{3.16}$$

$$\Phi(x) = \frac{1}{\sqrt{2\pi}} \int_{-\infty}^{x} e^{-\frac{1}{2}n^2} dn \tag{3.17}$$

where $\breve{N}_B$ is the bootstrapped integer ambiguity vector, while $\sigma_{\breve{N}_{i|I}}$ is the conditional standard deviation of i_{th} ambiguity conditioned on the previous $I = (1,2,...,i-1)$ ambiguities having been successfully fixed, and $\Phi(x)$ describes the area under the normal distribution.

3.5 Fixed Solution

Once the ambiguities are correctly fixed to integer values, the ambiguous carrier phase observations become equivalent to high precision pseudorange observations. The corresponding ambiguity states can be removed from the float filter. However, there are limitations in this approach: if the ambiguities are fixed to incorrect values and the filter needs to be reset, all the observation information from the previous epochs is lost since the float filter has disappeared. For implementations in this thesis, the computation of the fixed solution is based on Equations (3.18) and (3.19), which can be thought of as providing a correction to the float solution using the fixed ambiguities directly. In this way, the float filter is kept running in parallel with a fixed solution.

$$\breve{b} = \hat{b} - Q_{\hat{b}\hat{a}} Q_{\hat{a}}^{-1} (\hat{a} - \breve{a}) \tag{3.18}$$

$$Q_{\breve{b}} = Q_{\hat{b}} - Q_{\hat{b}\hat{a}} Q_{\hat{a}}^{-1} Q_{\hat{a}\hat{b}} \tag{3.19}$$

where $\hat{b}$ and $Q_{\hat{b}}$ are the float position solution vector and covariance matrix, $\breve{b}$ and $Q_{\breve{b}}$ are fixed position solution vector and covariance matrix.

As an example, Figure 3.5 shows the float and fixed solutions for a data set with 10 m baseline. It is clear that there is an increase of position accuracy after the ambiguities are correctly fixed after three data epochs.

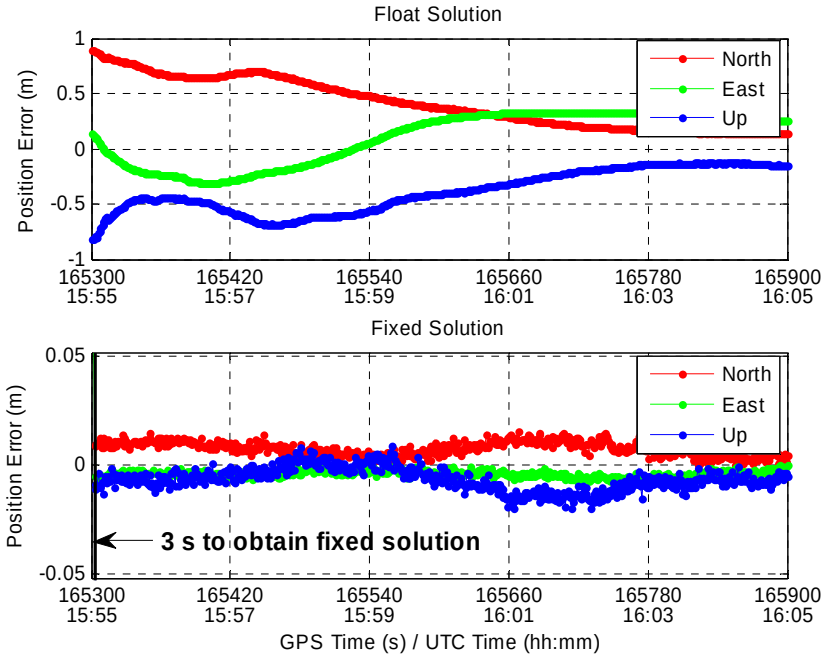

Figure 3.5: GPS L1 float and fixed solutions for a 10 m baseline

3.6 Partial Fixing

With observations on multiple frequencies available in a multiple-GNSS world, e.g., GPS and Galileo, the number of ambiguities to be fixed is increased significantly compared to current dual-frequency GPS. For example, if ten satellites are tracked on three civil frequencies for both GPS and Galileo, there will be fifty-four DD ambiguities to be fixed using three frequency observations of both systems. With so many ambiguities to be fixed, the ambiguity search space and computational load are significantly increased. In

light of this, it is possible to just fix a subset of all these ambiguities to relieve the computational burden at the expense of reducing position accuracy.

An ambiguity partial fixing method is proposed and implemented in this thesis to show the feasibility and characteristics of partial fixing. The procedure of this partial fixing strategy is described and shown as follows.

Assume $\hat{a}, \hat{z}$ are the original and transformed float ambiguity vectors, Z is the transformation matrix in the LAMBDA decorrelation, $Q_{\hat{a}}, Q_{\hat{z}}$ are the variance-covariance matrices of original and transformed float ambiguities, $Q_{\hat{b}}, Q_{\bar{b}}$ are the variance-covariance matrices of the float and fixed position solutions, and $Q_{\hat{b}\hat{a}}, Q_{\hat{b}\hat{z}}$ are the cross-covariance matrices of the original and transformed ambiguities with float position estimates.

The original ambiguity vector and its corresponding variance and covariance matrices can be expressed in terms of transformed ambiguity and their variance and covariance matrices.

$$\hat{z} = Z^T \hat{a} \Rightarrow \hat{a} = Z^{-T} \hat{z} \tag{3.20}$$

$$\begin{aligned} &Q_{\hat{z}} = Z^T Q_{\hat{a}} Z \Rightarrow Q_{\hat{a}} = Z^{-T} Q_{\hat{z}} Z^{-1} \\ &\Rightarrow Q_{\hat{a}}^{-1} = \left(Z^{-T} Q_{\hat{z}} Z^{-1} \right)^{-1} = Z Q_{\hat{z}}^{-1} Z^T \end{aligned} \tag{3.21}$$

$$Q_{\hat{b}\hat{z}} = Q_{\hat{b}\hat{a}} Z \Rightarrow Q_{\hat{b}\hat{a}} = Q_{\hat{b}\hat{z}} Z^{-1} \tag{3.22}$$

$$Q_{\hat{z}\hat{b}} = Z^T Q_{\hat{a}\hat{b}} \Rightarrow Q_{\hat{a}\hat{b}} = Z^{-T} Q_{\hat{z}\hat{b}} \tag{3.23}$$

Substituting Equations (3.20)-(3.23) to Equations (3.18) and (3.19), the fixed solutions read,

$$\begin{aligned} \breve{b} &= \hat{b} - Q_{\hat{b}\hat{a}} Q_{\hat{a}}^{-1} (\hat{a} - \breve{a}) \\ &= \hat{b} - Q_{\hat{b}\hat{z}} Z^{-1} Z Q_{\hat{z}}^{-1} Z^T (Z^{-T}\hat{z} - Z^{-T}\breve{z}) \\ &= \hat{b} - Q_{\hat{b}\hat{z}} Q_{\hat{z}}^{-1} (\hat{z} - \breve{z}) \end{aligned} \tag{3.24}$$

$$\begin{aligned} Q_{\breve{b}} &= Q_{\hat{b}} - Q_{\hat{b}\hat{a}} Q_{\hat{a}}^{-1} Q_{\hat{a}\hat{b}} \\ &= Q_{\hat{b}} - Q_{\hat{b}\hat{z}} Z^{-1} Z Q_{\hat{z}}^{-1} Z^T Z^{-T} Q_{\hat{z}\hat{b}} \\ &= Q_{\hat{b}} - Q_{\hat{b}\hat{z}} Q_{\hat{z}}^{-1} Q_{\hat{z}\hat{b}} \end{aligned} \tag{3.25}$$

The above two equations show that the fixed solutions can also be computed in terms of the transformed ambiguities instead of the original ones. In the case of partial fixing, the un-fixed subset of the ambiguities can be included in the b vector, which contains the position and other estimates. At the mean time of obtaining fixed position solutions, the float values of this remaining ambiguity set are also corrected and improved.

In the LAMBDA search process, only the transformed ambiguity vector $\hat{z}$, decorrelated matrices L, D of transformed ambiguity variance matrix $Q_{\hat{z}}$ are passed to the search function. In the case of partial fixing, it will be shown below that only the submatrices of

L, D and $\hat{z}$ that correspond to the fixed ambiguity subset are passed into the search function.

Assume $\hat{z}_1$ is the subset of ambiguities to be fixed, L_1 and D_1 are the corresponding submatrices of $\hat{z}_1$, and $Q_{\hat{z}_1}$ is submatrix of $Q_{\hat{z}}$, then

$$Q_{\hat{z}} = \begin{bmatrix} Q_{\hat{z}_2} & Q_{\hat{z}_{21}} \\ Q_{\hat{z}_{12}} & Q_{\hat{z}_1} \end{bmatrix}, L = \begin{bmatrix} L_2 & \\ L_{21} & L_1 \end{bmatrix}, D = \begin{bmatrix} D_2 & \\ & D_1 \end{bmatrix} \tag{3.26}$$

Since $Q = L^T DL$ holds true, substitute the above matrices in (3.26) to get

$$\begin{aligned} Q_{\hat{z}} &= L_{\hat{z}}^T D_{\hat{z}} L_{\hat{z}} \\ &= \begin{bmatrix} L_2 & \\ L_{21} & L_1 \end{bmatrix}^T \begin{bmatrix} D_2 & \\ & D_1 \end{bmatrix} \begin{bmatrix} L_2 & \\ L_{21} & L_1 \end{bmatrix} \\ &= \begin{bmatrix} L_2^T & L_{21}^T \\ & L_1^T \end{bmatrix}^T \begin{bmatrix} D_2 & \\ & D_1 \end{bmatrix} \begin{bmatrix} L_2 & \\ L_{21} & L_1 \end{bmatrix} \\ &= \begin{bmatrix} L_2^T D_2 & L_{21}^T D_1 \\ & L_1^T D_1 \end{bmatrix} \begin{bmatrix} L_2 & \\ L_{21} & L_1 \end{bmatrix} \\ &= \begin{bmatrix} L_2^T D_2 L_2 + L_{21}^T D_1 L_1 & L_{21}^T D_1 L_1 \\ L_1^T D_1 L_{21} & L_1^T D_1 L_1 \end{bmatrix} \\ &= \begin{bmatrix} Q_{\hat{z}_2} & Q_{\hat{z}_{21}} \\ Q_{\hat{z}_{12}} & Q_{\hat{z}_1} \end{bmatrix} \\ &\Rightarrow Q_{\hat{z}_1} = L_1^T D_1 L_1 \end{aligned} \tag{3.27}$$

The above shows that in order to fix a subset of all the ambiguities, only the subvector D_1 and submatrices $L_1, \hat{z}_1$ are needed to pass into the LAMBDA search function and the fixed solution of partial fixing can be computed according to Equations (3.24) and (3.25).

After the LAMBDA decorrelation, the ambiguity and position state vector and its corresponding variance-covariance matrix are

$$bz = \begin{bmatrix} \hat{b} \\ \hat{z}_2 \\ \hat{z}_1 \end{bmatrix} \tag{3.28}$$

$$Q_{bz} = \begin{bmatrix} Q_{\hat{b}} & Q_{\hat{b}\hat{z}_2} & Q_{\hat{b}\hat{z}_1} \\ Q_{\hat{z}_2\hat{b}} & Q_{\hat{z}_2} & Q_{\hat{z}_2\hat{z}_1} \\ Q_{\hat{z}_1\hat{b}} & Q_{\hat{z}_1\hat{z}_2} & Q_{\hat{z}_1} \end{bmatrix} \tag{3.29}$$

With the subset of ambiguities fixed, the other subset of ambiguities is corrected by the fixed ambiguities and the fixed position solution is calculated as follows.

$$\breve{B}_{|\breve{z}_1} = \hat{B} - Q_{\hat{B}\hat{z}_1} Q_{\hat{z}_1}^{-1} (\hat{z}_1 - \breve{z}_1) \tag{3.30}$$

$$Q_{\breve{B}_{|\breve{z}_1}} = Q_{\hat{B}} - Q_{\hat{B}\hat{z}_1} Q_{\hat{z}_1}^{-1} Q_{\hat{B}\hat{z}_1}^T \tag{3.31}$$

where

$$\hat{B} = \begin{bmatrix} \hat{b} \\ \hat{z}_2 \end{bmatrix}, Q_{\hat{B}} = \begin{bmatrix} Q_{\hat{b}} & Q_{\hat{b}\hat{z}_2} \\ Q_{\hat{z}_2\hat{b}} & Q_{\hat{z}_2} \end{bmatrix}, Q_{\hat{B}\hat{z}_1} = \begin{bmatrix} Q_{\hat{b}\hat{z}_1} \\ Q_{\hat{z}_1} \end{bmatrix}, \breve{B}_{|\breve{z}_1} = \begin{bmatrix} \breve{b}_{|\breve{z}_1} \\ \hat{z}_{2|\breve{z}_1} \end{bmatrix}, Q_{\breve{B}_{|\breve{z}_1}} = \begin{bmatrix} Q_{\breve{b}|\breve{z}_1} & Q_{\breve{b}\breve{z}_2|\breve{z}_1} \\ Q_{\hat{z}_2\hat{b}|\breve{z}_1} & Q_{\hat{z}_2|\breve{z}_1} \end{bmatrix}$$

The $\breve{b}_{|\breve{z}_1}$ and $\hat{z}_{2|\breve{z}_1}$ are fixed position states and corrected ambiguities based on the fixed subset of ambiguities $\breve{z}_1$, respectively.

3.7 Summary

This chapter gives an overview of each step involved in kinematic carrier phase positioning. The development of the float filter is described in detail, the methods used for multi-carrier AR are compared and the techniques for ambiguity validation and fixed solution computation are briefly explained. In Chapter 4, results of a covariance analysis based on the PCF are presented. The developed SD processor is used for simulated data processing in Chapter 5.

Chapter Four: Covariance Simulation and Analysis

A covariance analysis is conducted in this chapter to evaluate the ambiguity resolution performance using observations from different sets of GPS/Galileo frequencies over different lengths of baselines in terms of probability of correctly fixing the ambiguities. A strategy of partial fixing is evaluated to show the advantages of fixing only a subset of ambiguities when there are too many ambiguities to be fixed.

4.1 Simulation Setup

4.1.1 Methodology

The process of obtaining the integer values of ambiguities can be defined as a mapping of the real space to the integer space. Then the probability that a given integer vector $\breve{x}$ is equal to a particular integer vector z , can be assessed as (Teunissen 1998)

$$P(\breve{x} = z) = P(\hat{x} \in S_z) \int_{S_z} p_{\hat{x}}(s)ds \tag{4.1}$$

where $p_{\hat{x}}$ is the probability density function (PDF) of the float ambiguities.

However, it is difficult to quantify Equation (4.1) numerically because of the complexity of the so-called pull-in region and the computational load of the integration process (Teunissen 1998). Thus a simplification or approximation is required for computing the probability of correct fix (PCF). There have been various bounds proposed to

approximate the PCF (Verhagen 2003). A method of ambiguity bootstrapping is widely used to determining a lower bound of the PCF (Teunissen 1998, Petovello et al. 2005, O'Keefe et al. 2006) and this method is adopted in this thesis. The evaluation is based on Equations (3.16) and (3.17).

Note that in many of the references and in the remainder of this thesis, the PCF is quantified in terms of Probability of Incorrect Fix (PIF), which is equal to one minus PCF.

4.1.2 Constellation

In this study, the 30 Galileo satellites are assumed to be equally distributed in each plane. The planes are equally spaced in terms of right ascension of the ascending node and the satellites in the second and third planes are advanced by 12 and 24 degrees in argument of latitude with respect to the first plane. The ascending nodes of the three orbital planes of the simulated Galileo constellation were arbitrarily assigned right ascensions of 0, 120 and 240 degrees respectively. A real GPS constellation consisting of 30 satellites is used for the simulation. The same number of 30 satellites used for the two constellations is to make fair comparisons between GPS and Galileo (Table 4.1). The simulation was started at the second day of GPS week 1460 (January 1st, 2008) and the actual GPS almanac from that week was used. The simulated GPS and Galileo constellations are shown in Figure 4.1.

Table 4.1: GPS and Galileo constellation parameters

GNSS	GPS	Galileo
No. of Satellites	30	30
No. of Planes	6	3
Inclination Angle	55˚	56˚
Altitude (Km)	20,183	23,222

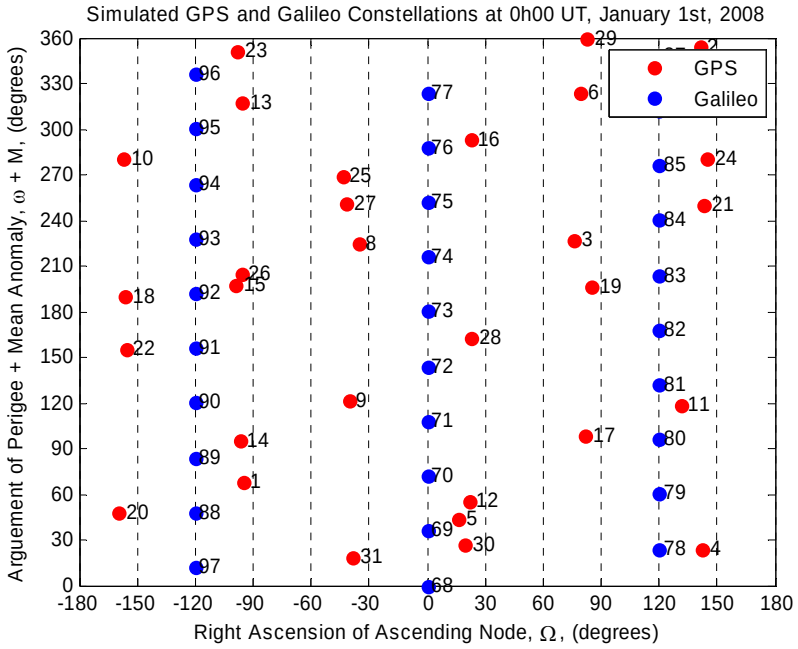

Figure 4.1: Combined GPS and Galileo constellation on January 1st, 2008 (GPS PRN: 1~30, Galileo PRN: 36~65)

4.1.3 Simulation Location and Visible Satellites

Two simulated receivers located near Calgary, Canada (51.079°N, 114.133°W) are used in the simulation. The numbers of observed GPS and Galileo satellites during the 24-hour period for the two receivers during the 24-hour period are shown in Figure 4.2.

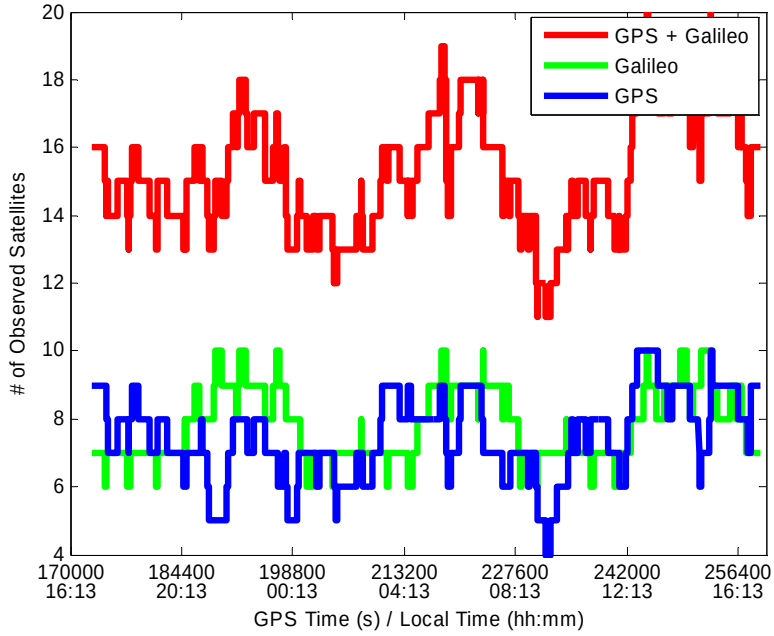

Figure 4.2: Number of observed GPS and Galileo satellites in Calgary (51.079°N, 114.133°W) with 15° cut off angle

4.1.4 Multipath and Measurement Noise

While no official documents on the range accuracy of GPS L2C, L5 and Galileo signals are publicly available, there have been studies to quantify the performance of modernized GPS signals (McDonald & Hegarty 2000) and future Galileo signals (Rodríguez et al. 2004, 2005 & 2006). Multipath and receiver noise for the pseudorange and carrier phase measurements were considered and parameterized separately in the filter. For code multipath and measurement noise, values from the above literature are adopted, and for phase multipath and measurement noise, 0.035 and 0.005 cycles of wavelength were assumed for all frequencies. Values for different frequency signals are shown Tables 4.2 and 4.3.

Table 4.2: Multipath errors (1 σ) for GPS and Galileo signals

Measurement type	GPS			Galileo		
	L1	L2	L5	E1	E5b	E5a
Code Std (cm)	60	60	40	20	40	40
Phase Std (cm)	0.70	0.85	0.89	0.70	0.87	0.89

Table 4.3: Measurement noise (1 σ) for GPS and Galileo signals

Measurement type	GPS			Galileo		
	L1	L2	L5	E1	E5b	E5a
Code Std (cm)	60	40	6.0	20	2.0	2.0
Phase Std (cm)	0.10	0.13	0.13	0.10	0.13	0.13

4.1.5 Baseline and Atmospheric Errors

Three baselines with different lengths were simulated: 4 kilometres for a short baseline, 20 kilometres for a medium baseline and 120 kilometres for a long baseline. To model the variations of the differential ionospheric and tropospheric errors, both of them were parameterized as a function of baseline length and modeled as first-order Gauss-Markov processes. A low to medium level of ionospheric activity consisting of 2.5 ppm residual L1 ionospheric error and a 4 minute correlation time was assumed for all baselines. Quiet tropospheric conditions with 0.5 ppm residual error and a 1 hour correlation time were assumed for all cases. The ionospheric and zenith tropospheric errors were not estimated

for the short baseline since both ionospheric and tropospheric effects were almost completely correlated and therefore effectively cancelled out in this case. For the medium and long baselines, the ionospheric and zenith tropospheric errors were estimated as states in the filter. The standard deviations and the time correlation parameters are listed in Table 4.4.

Table 4.4: Ionospheric and tropospheric parameters for simulations

Baseline	Ionosphere		Troposphere	
	σ [m]	τ [s]	σ [m]	τ [s]
Short (4 km)	–	–	–	–
Medium (20 km)	0.05	240	0.01	3600
Long (120)	0.30	240	0.06	3600

For each baseline, the covariances of the float solution with different subsets of GNSS signals (pseudorange and carrier phase observations) were simulated. The covariance matrices of the ambiguity states were first decorrelated using the LAMBDA algorithm and then bootstrapping was applied to compute the PCF values. In this way, the decorrelation algorithm was able to take advantage of multiple frequencies to form linear combinations most useful to successful ambiguity resolution.

4.1.6 Simulation Scenarios

Since the purpose of this research is to evaluate kinematic ambiguity resolution and positioning performance using observations on different sets of frequencies from GPS and Galileo, various scenarios of GPS/Galileo kinematic positioning are simulated herein.

For GPS, the single frequency L1 was simulated as the base scenario, both L1 & L2 and L1 & L5 were simulated to represent the cases of dual-frequency GPS, and all the three frequencies L1, L2 and L5 were used to simulate a triple-frequency GPS kinematic positioning using all GPS signals available. With respect to combined GPS/Galileo, a tightly-coupled integration approach (Julien et al. 2003) was adopted for this study and only two common frequencies between GPS and Galileo – L1 & E1 and L5 & E5a were simulated. The following six cases are evaluated in this thesis (Table 4.5).

Table 4.5: Subsets of GPS/Galileo frequencies for simulations

Case	Frequencies
①	GPS L1
②	GPS L1 & L2
③	GPS L1 & L5
④	GPS L1, L2 & L5
⑤	GPS L1 & Galileo E1
⑥	GPS L1, L5 & Galileo E1, E5a

All the simulated scenarios are listed in Table 4.6. The capital letters represent the simulation scenario for identification.

Table 4.6: Simulation scenarios for GPS, Galileo and combined GPS/Galileo

Baseline	Simulation Scenarios					
	①	②	③	④	⑤	⑥
Short (4 km)	A	B	C	D	E	F
Medium (20 km)	–	G	H	I	J	K
Long (120 km)	–	L	M	N	O	P

With GPS or Galileo operating as independent systems, it is not expected that a single frequency (GPS L1 or Galileo E1) can be used for kinematic positioning over baselines more than 10 km, so only scenario of L1 kinematic positioning over a short baseline was simulated, while scenarios of dual- or triple-frequency positioning were simulated for all baselines. As for combined GPS/Galileo positioning, with the great improvement in availability, single-frequency L1/E1 kinematic positioning was attempted for both the short and medium baselines.

4.2 Simulation Results and Analysis

This section shows the simulation results of ambiguity resolution performance for GPS/Galileo kinematic positioning over three different baselines using observations on different sets of GPS/Galileo frequencies. The results of applying a strategy to fix subsets of ambiguities are also presented to demonstrate the advantage of ambiguity partial fixing. Half-hour sessions started at the beginning of each hour were simulated for twenty-four hours. Only satellites available during the whole 30-minute session were used to avoid having to deal with the addition and removal of rising and setting satellites. The measurement sampling rate was set to 1 Hz.

4.2.1 Kinematic positioning over different baselines

Scenario A: GPS L1 kinematic positioning over the short baseline

For the 24 half-hour session simulations, there are sessions in which 5 to 10 GPS satellites were observed (4 to 9 DD observations). The results of 24 sessions for Scenario A are shown in Figure 4.3. The lines with the same colour represent different simulation sessions that have the same number of satellites observed. It is clear to see that with an increase in the number of satellites, which means enhanced satellite geometry, the GPS L1 solution takes a shorter time to get a high PCF. Instead of showing the PCF directly, the lower bound of the probability of correct fix is plotted as the upper bound of probability of incorrect fix (PIF), which is one minus PCF, for ease of interpretation. On this figure, a low value of the upper bound of the PIF is desired, and as can be seen in all scenarios, the PIF decreases as a function of time. The scale of the Y-axis is logarithmic, e.g., a PIF of 10^{-2} represents a PCF of 99%.

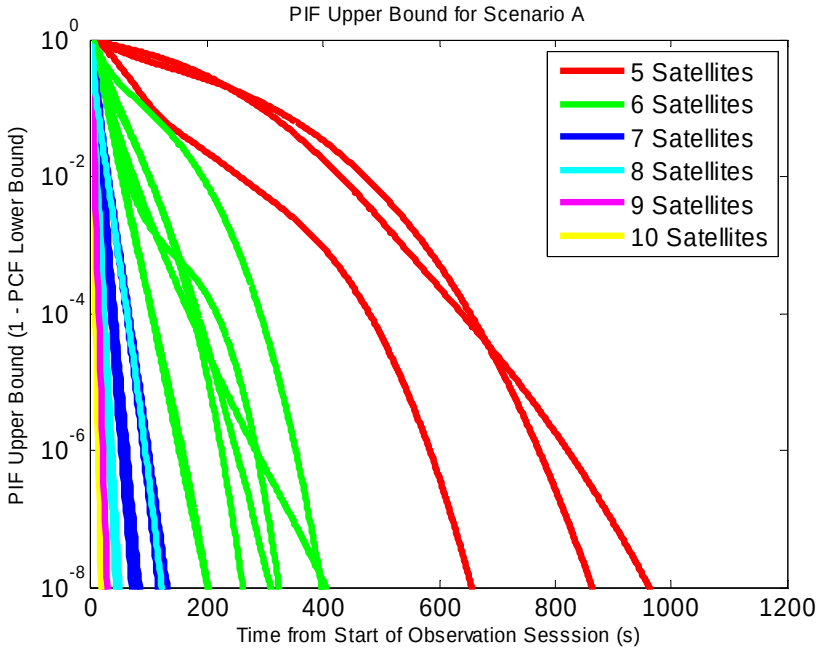

Figure 4.3: PIF upper bound for Scenario A (GPS L1) in the 24 session simulations

Scenario A, B, C, D, E, F: GPS/Galileo kinematic positioning over the short baseline

Figure 4.4 shows the results of the above six cases for the 4 km short baseline, only sessions with seven satellites observed are shown here to save space. It can be seen that all scenarios except Scenario A can achieve a very high PCF (corresponding to 10^{-8} PIF) within less than ten epochs. Scenario C, where GPS L1 and L5 observations are used, shows better performance than that of Scenario B, which uses GPS L1 and L2 observations. This phenomenon is due to the fact that better decorrelation of ambiguities can be obtained when using L1 and L5 observations than that of L1 and L2 observations since the ionospheric error estimation is more diverse for the former scenario. Scenario E, which uses observations on the GPS L1 and Galileo E1 common frequency band, shows comparable performances to those of Scenario C. This is due to the combined GPS/Galileo constellation, which significantly enhanced the geometry for ambiguity resolution, and also the differential ionospheric error is not significant over the short baseline. With using three frequencies GPS observations (Scenario D), the PIF decreases to very low levels in less than two or three epochs. This shows the advantage of adding a third frequency which can greatly benefit safety-of-life applications which generally have very high integrity requirements, e.g., 10^{-8} PIF. As shown in Scenario F, the best performance among the six scenarios is achieved when a combined GPS/Galileo dual-frequency (L1/E1 and L5/E5a) receiver is used for kinematic positioning applications.

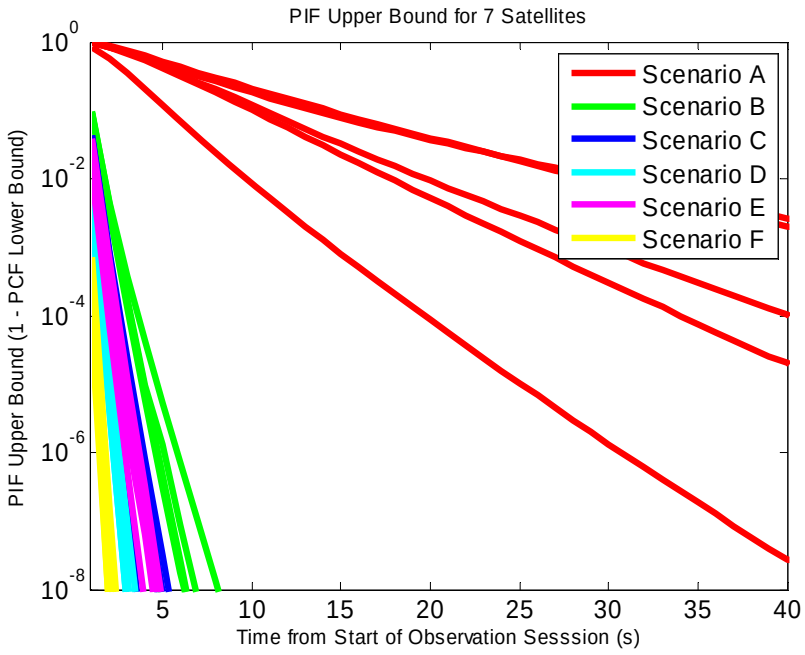

Figure 4.4: PIF upper bound for Scenario A (GPS L1), B (GPS L1 and L2), C (GPS L1 and L5), D (GPS L1, L2 and L5), E (GPS L1 and Galileo E1) and F (GPS L1, L5 and Galileo E1, E5a) over the short baseline, only sessions with seven GPS satellites observed are displayed

Scenario G, H, I, J, K: GPS/Galileo kinematic positioning over the medium baseline

The results of five simulation scenarios for the 20 km medium baseline are presented in Figure 4.5. Since the GPS L1 kinematic positioning is not expected to be applicable for baselines extending to 20 km, the single-frequency, single-system scenario is not simulated for the medium and long baselines in this study. Note that Scenario J, which simulates a combined GPS/Galileo L1/E1 single-frequency kinematic positioning, cannot achieve a PCF level feasible for ambiguity resolution, e.g. 0.99, thus even combined single frequency GPS/Galileo is not practical for medium baseline applications. While Scenario K, the combined dual-frequency GPS/Galileo still shows the best performance.

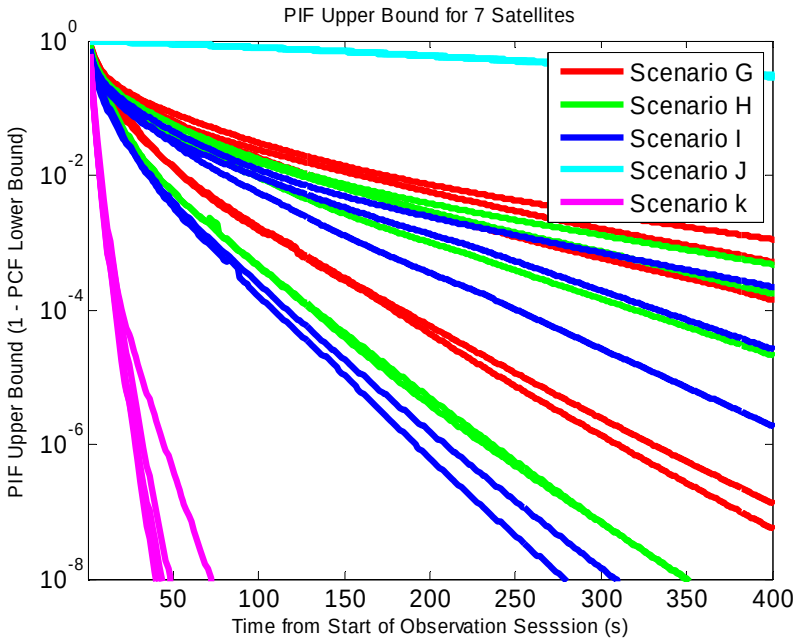

Figure 4.5: PIF upper bound for Scenario G (GPS L1 and L2), H (GPS L1 and L5), I (GPS L1, L2 and L5), J (GPS L1 and Galileo E1) and K (GPS L1, L5 and Galileo E1, E5a) over the medium baseline, only sessions with seven GPS satellites observed are displayed

Scenarios L, M, N, O, P: GPS/Galileo kinematic positioning over the long baseline

Figure 4.6 presents the results of the five simulation scenarios for the long baseline. Similar trends within different combinations of frequencies and systems can be observed as those for the medium baseline except they take longer time (or more observations) to reach the same level of PCF.

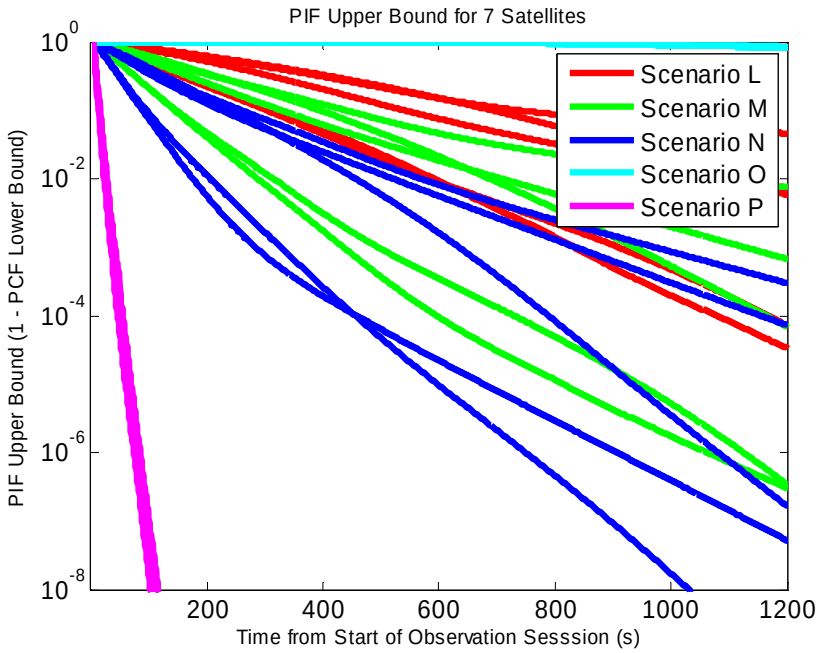

Figure 4.6: PIF upper bound for Scenario L (GPS L1 and L2), M (GPS L1 and L5), N (GPS L1, L2 and L5), O (GPS L1 and Galileo E1) and P (GPS L1, L5 and Galileo E1, E5a) over the long baseline, only sessions with seven GPS satellites observed are displayed

4.2.2 Partial Fixing

As shown in Figures 4.5 and 4.6, it takes quite a long time for a solution of all the ambiguities to achieve a high level of PCF value, especially in the case where there are many ambiguities to be fixed as those in scenarios of multi-frequencies and multi-systems, e.g., Scenarios I, K, N and P. It is possible and interesting to fix a subset of all the ambiguities to fulfill the requirements for different applications. This subsection shows the results of partial fixing ambiguities for the above scenarios. Only results of the first half-hour simulation session (where nine GPS satellites and seven Galileo satellites are observed) will be shown and the others are listed in the Appendix for completeness.

Scenario A: Partial fixing GPS L1 ambiguities over the short baseline

Figure 4.7 shows the PIF as a function of time and as a function of the number of ambiguities fixed. It can be seen that at a given time epoch, the PIF increases as more ambiguities are fixed, which is intuitive given that it is difficult to fix more ambiguities in carrier phase processing. The above phenomenon is shown through Equation (3.16): the lower bound on the PCF is a product of the probabilities associated with the conditional variance of each ambiguity. Since each probability has a value between zero and one, it is obvious that the PCF decreases as more probabilities are included in the product. It is possible to determine the position accuracy available with a certain bound of the PCF by combining the above two figures. Figure 4.8 shows the estimated position accuracy as a function of time and number of ambiguities fixed in Scenario A. It is obvious to see that the position accuracy improves with increasing time epochs and as more ambiguities are fixed. With no ambiguities fixed (float solution), the largest standard deviation of the position estimate is generated, while the best accuracy is obtained with all the ambiguities fixed. Figure 4.9 shows the obtained position accuracy with a high confidence of ambiguity fixing - the PCF is greater than 99.9999%. As can be seen from the figure, the position accuracy improves slowly with the float solution (no ambiguities fixed); while with only one ambiguity fixed, there is significant improvement in the position accuracy. Also note that it is much harder to fix the first ambiguity, and the remaining ambiguities can be fixed more quickly provided the first one is fixed.

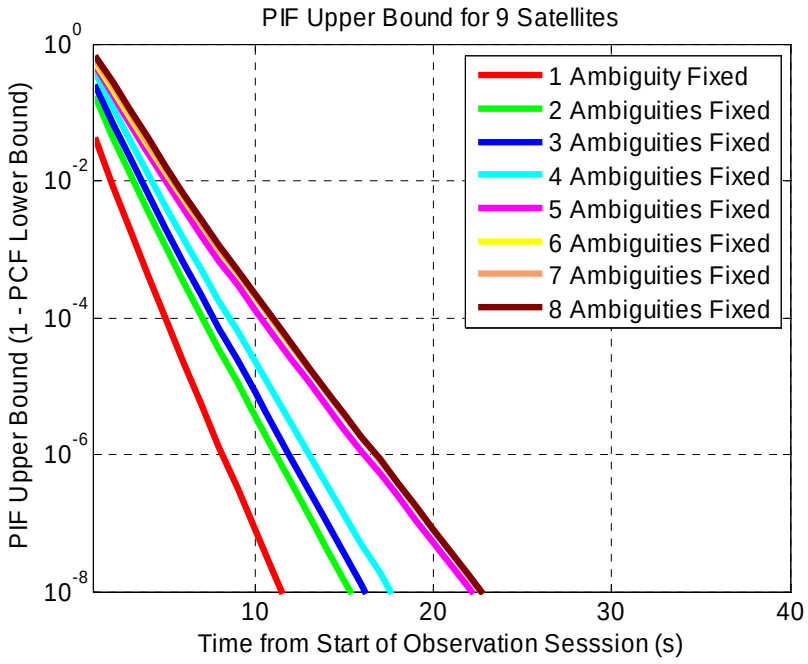

Figure 4.7: PIF as a function of time with increasing number of ambiguities fixed for Scenario A (GPS L1)

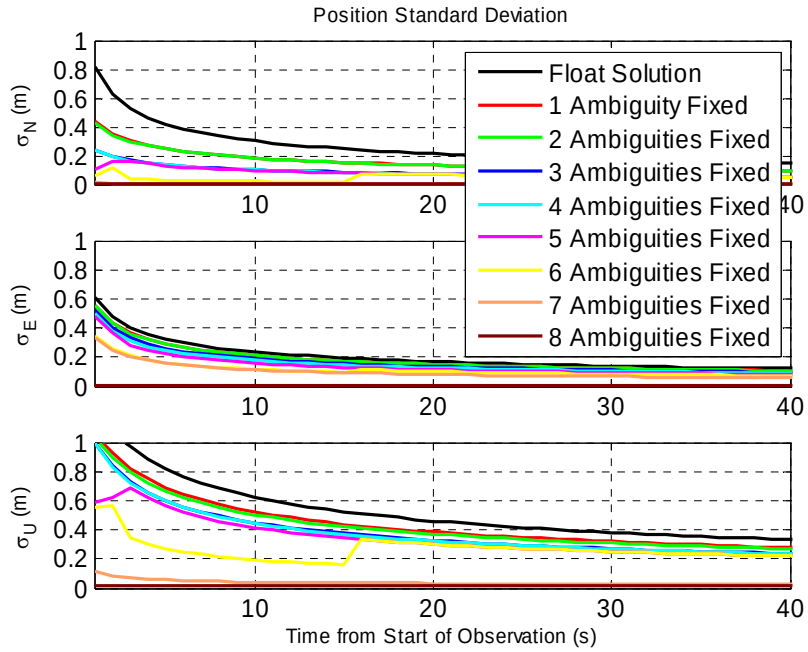

Figure 4.8: Position accuracy of float solution and fixed solution with different number of fixed ambiguities for Scenario A (GPS L1)

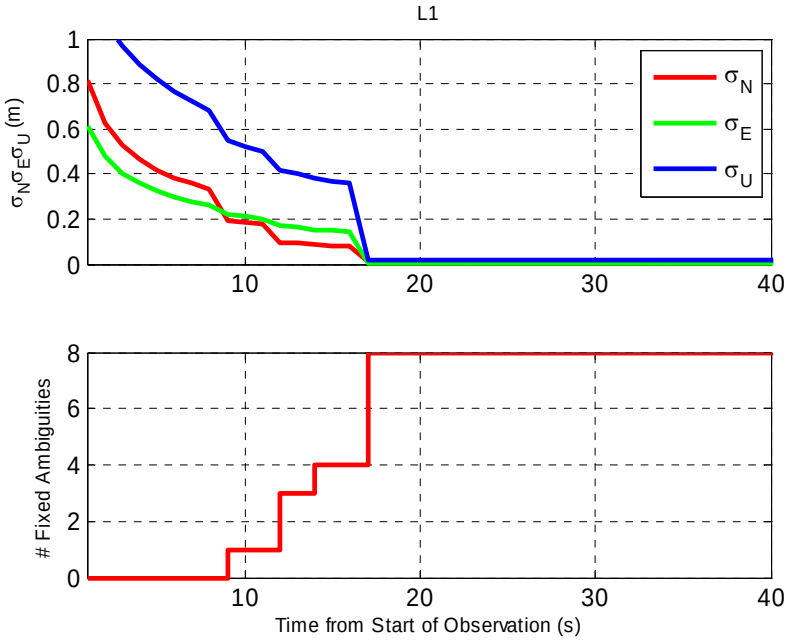

Figure 4.9: Time needed to fix different number of ambiguities at 99.9999% confidence for Scenario A (GPS L1)

Scenarios B, C, D, E, F: Partial fixing over the short baseline

Figure 4.10 shows the results of Scenario B, which uses GPS L1 and L2 observations for kinematic positioning. It is obvious that the ambiguities can be fixed faster than those in Scenario A although the number of ambiguities is increased. This is due to the higher decorrelation in the ambiguities that can be formed within LAMBDA when dual-frequency observations are used. Similar results are obtained in Scenario C (using L1 and L5 observations) and Scenario D (using L1, L2 and L5 observations) and hence are not shown. Note that in these scenarios, it is LAMBDA Z-domain ambiguities that are being fixed, not the original ambiguities. This is not a concern so long as the fixed position solution is computed using the Z-domain ambiguities. Over the short baseline without the

spatial decorrelation of ionosphere and troposphere, all the ambiguities can be fixed quite easily and the partial fixing strategy does not bring up more advantages in terms of ambiguity fixing. As shown in Figure 4.11, even though there are many ambiguities to be fixed in Scenario F (a combined dual-frequency GPS/Galileo), it takes almost the same observation time, less than two 1-second epochs, to fix either six or all thirty ambiguities. However, it still might be useful to fix only a small subset if computational load and ambiguity search space volume is an issue.

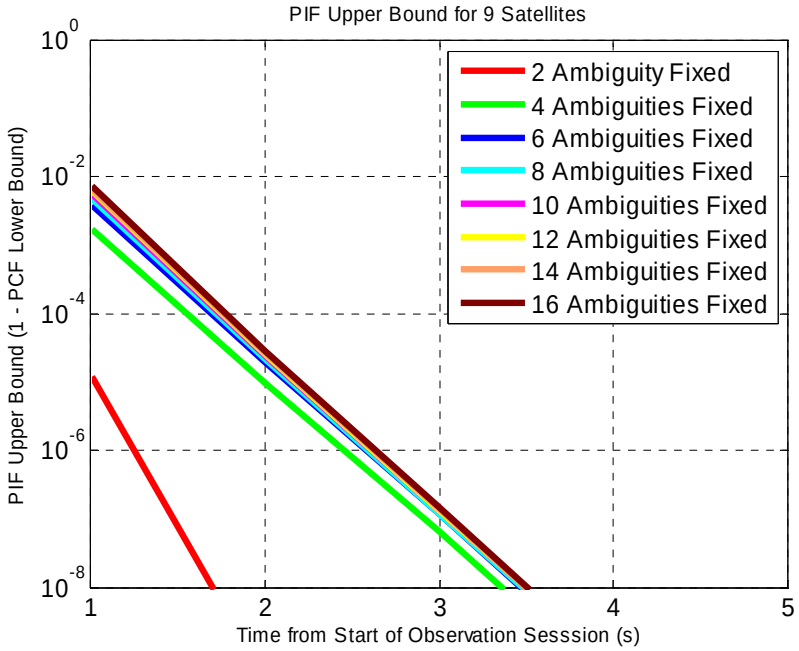

Figure 4.10: PIF as a function of time with increasing number of ambiguities fixed of Scenario B (GPS L1 and L2)

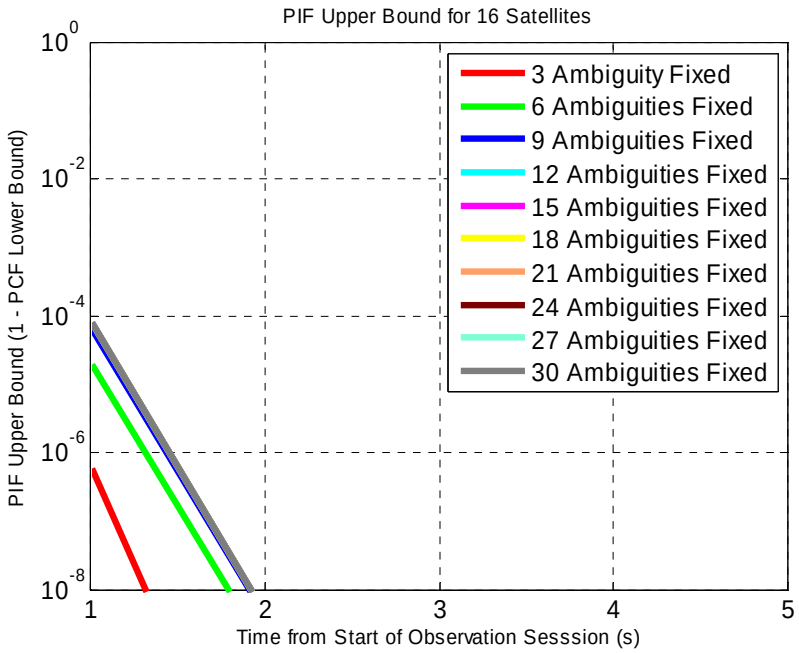

Figure 4.11: PIF as a function of time with increasing number of ambiguities fixed of Scenario F (GPS L1, L5 and Galileo E1, E5a)

Scenarios G, H, I, J, K: Partial fixing over the medium baseline

Figure 4.12 shows the results of partial fixing ambiguities for Scenario G, where GPS L1 and L2 observations are used for kinematic positioning over a 20 km baseline. As seen from the figure, the time increases as more ambiguities are needed to be fixed. After the first eight ambiguities are fixed within 80 epochs (taking 10^{-8} PIF as the threshold for fixing), it takes a much longer time to fix the remaining eight ambiguities. This clearly shows the advantage of partial fixing in the case of ionospheric and tropospheric spatial decorrelation over a medium baseline. If one wants to reduce the time to fix ambiguities and to obtain a fixed solution quickly, one can just fix the most likely to be fixed subset of ambiguities instead of fixing them all. The position accuracies are improved with more

ambiguities fixed, which is similar to the results presented in Figure 4.8 and is not shown here. The results of partial fixing for Scenario J are shown in Figure 4.13. It is found that even a single ambiguity cannot be fixed for the case of single-frequency GPS/Galileo L1/E1 since the ionospheric error cannot be properly estimated and reduced with only observations on a single frequency available even with a large, geometrically diverse, set of signals. Scenarios H, I, J and K present similar results to Scenario G and are included in the Appendix.

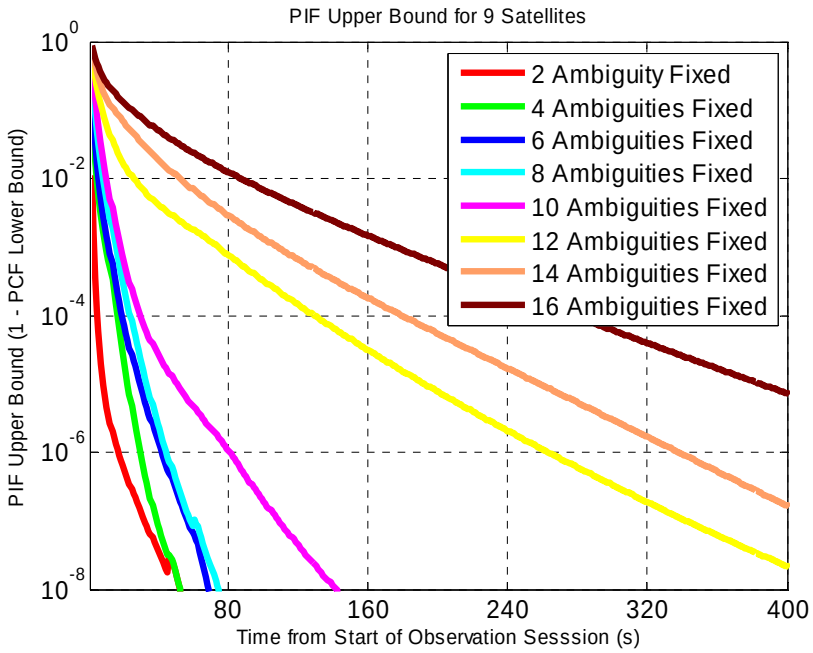

Figure 4.12: PIF as a function of time with increasing number of ambiguities fixed of Scenario G (GPS L1 and L2)

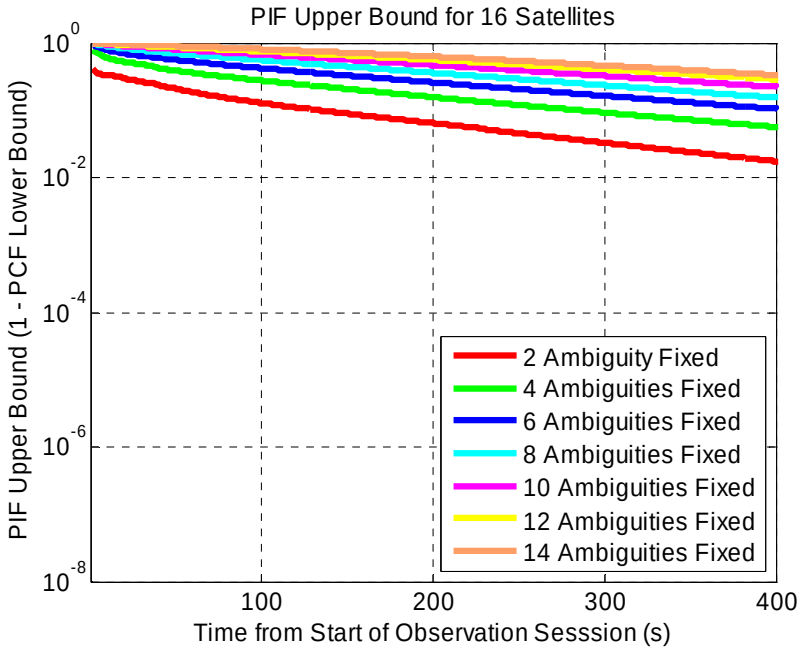

Figure 4.13: PIF as a function of time with increasing number of ambiguities fixed of Scenario J (GPS L1 and Galileo E1)

Scenarios L, M, N, O and P: Partial fixing over the long baseline

Figure 4.14 shows the results of partial fixing ambiguities for Scenario L, which gives similar results as those over the medium baseline cases except a longer time (or more observations) is needed to reach each level of PCF, and the remaining six ambiguities are still harder to fix in this case. The other scenarios, M, N, O and P present similar results since the atmospheric errors are further decorrelated over the long baseline compared to the medium one, and they are not shown here and are included in the Appendix for completeness.

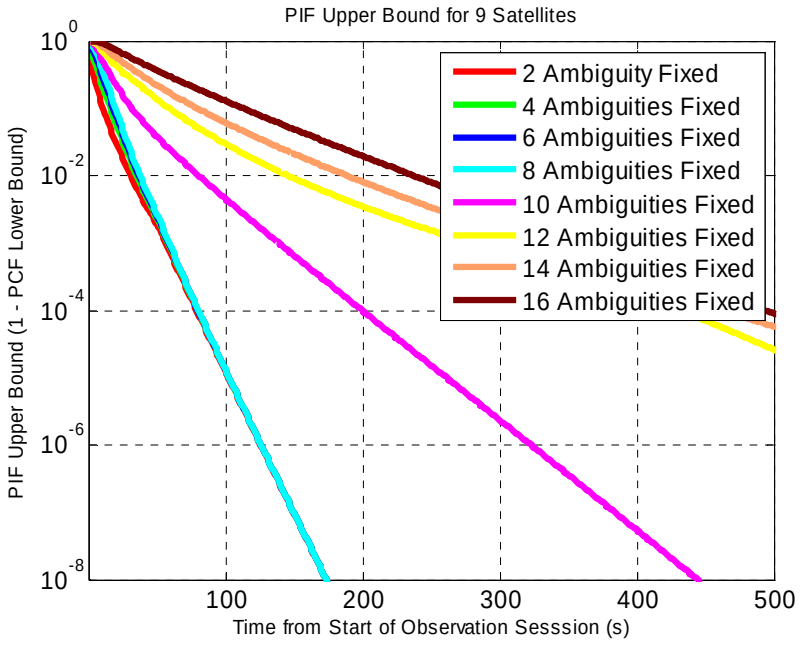

Figure 4.14: PIF as a function of time with increasing number of ambiguities fixed of Scenario L (GPS L1 and L2)

Ambiguity fixing at different confidence levels

The ambiguity fixing confidence level is varied for applications with different requirements. For example, confidence levels of 99.999999% could be required for safety-of-life applications, while only 99% or lower, is usually enough for conventional surveying and mapping applications. Figures 4.15 and 4.16 show the time needed to fix ambiguities in Scenario A at confidence levels of 99% and 99.999999%, respectively. It is clear to see that it takes less time to fix ambiguities at a lower confidence level. For example, all eight ambiguities can be fixed within 5 epochs for a 99% confidence while it takes more than 20 epochs to fix them at a 99.999999% confidence. Figures 4.17 and 4.18 show the time needed to fix ambiguity at confidence levels of 99% and 99.999999%

in Scenario N, where observations on three GPS frequencies are used for kinematic positioning over the long baseline. Figures 4.19 and 4.20 show the results of Scenario P which uses observations on two common frequencies from GPS and Galileo. The same conclusion can be drawn from Figures 4.17-20 as those of Scenario A shown in Figures 4.15 and 4.16.

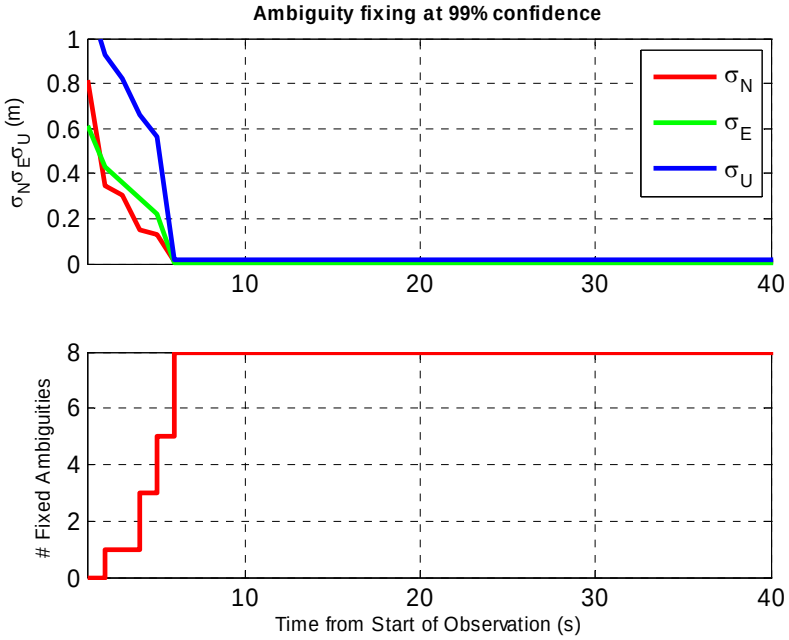

Figure 4.15: Time needed to fix different number of ambiguities at 99% confidence of Scenario A (GPS L1)

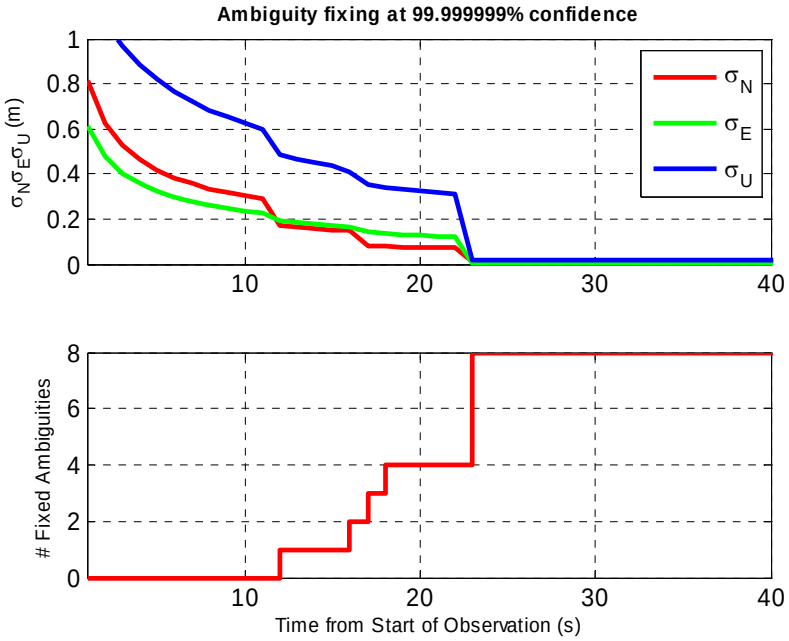

Figure 4.16: Time needed to fix different number of ambiguities at 99.999999% confidence of Scenario A (GPS L1)

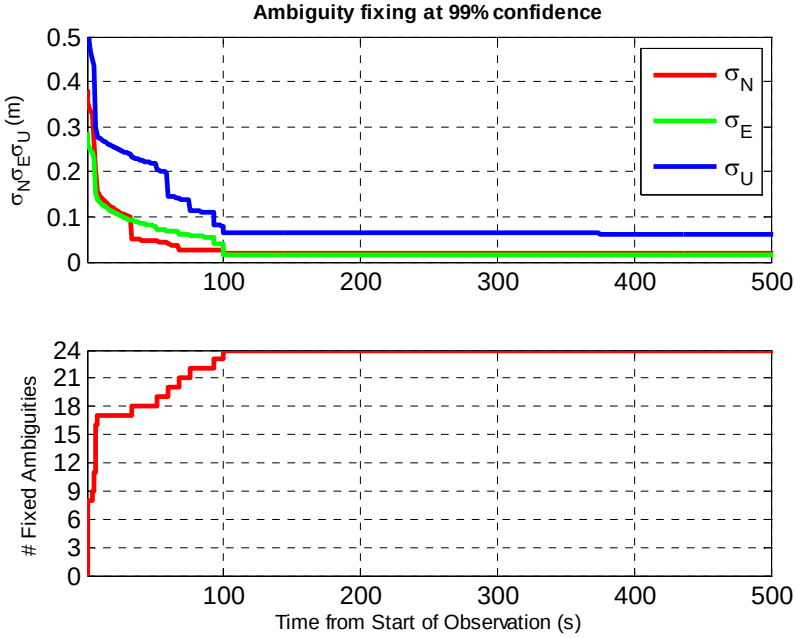

Figure 4.17: Time needed to fix different number of ambiguities at 99% confidence of Scenario N (GPS L1, L2 and L5)

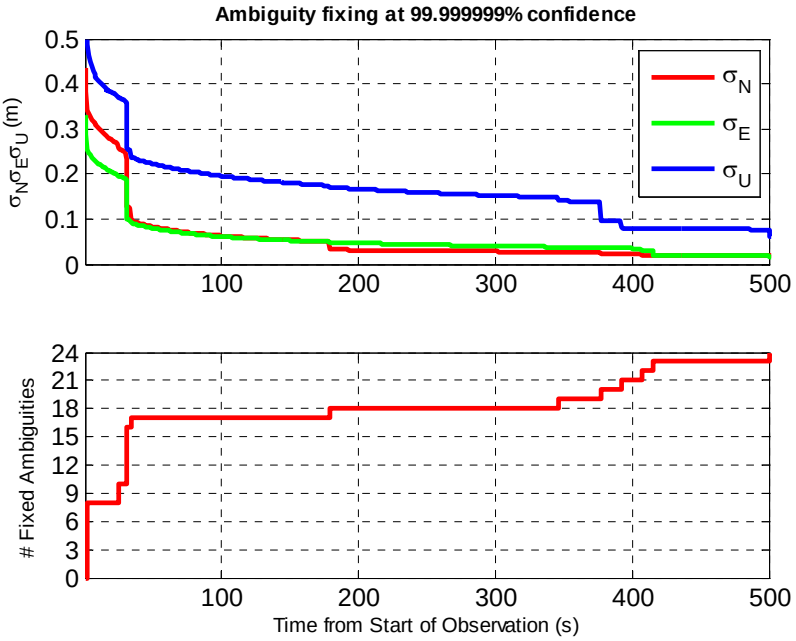

Figure 4.18: Time needed to fix different number of ambiguities at 99.999999% confidence of Scenario N (GPS L1, L2 and L5)

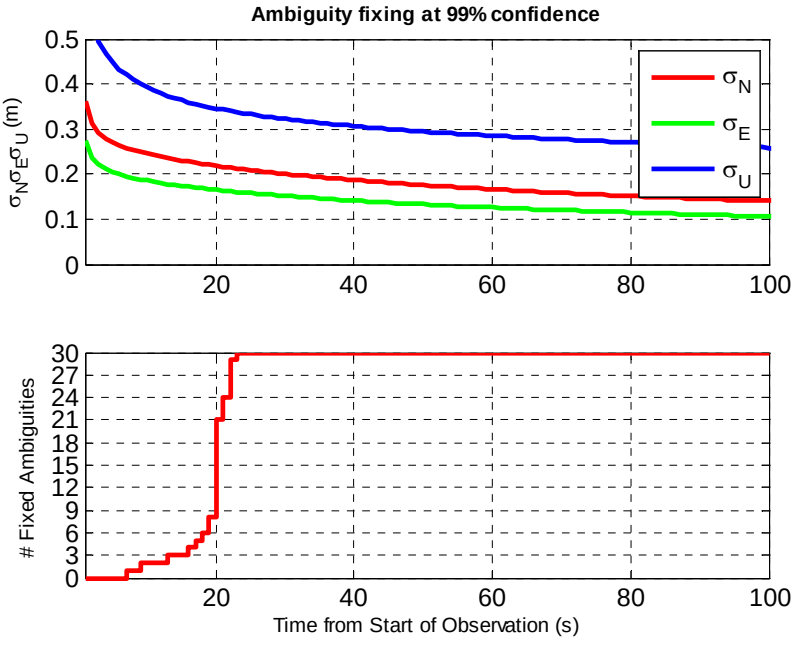

Figure 4.19: Time needed to fix different number of ambiguities at 99% confidence of Scenario P (GPS L1, L5 and Galileo E1, E5a)

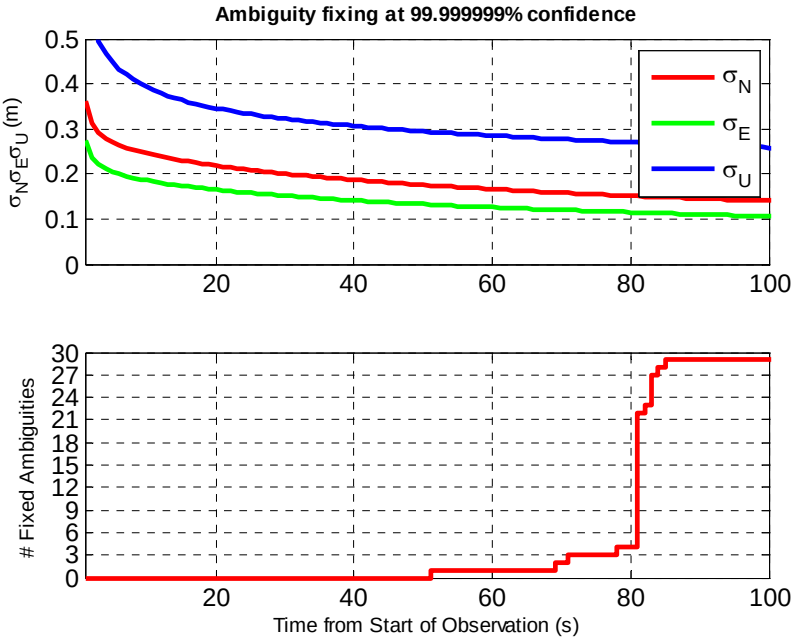

Figure 4.20: Time needed to fix different number of ambiguities at 99.999999% confidence of Scenario P (GPS L1, L5 and Galileo E1, E5a)

4.3 Summary

This chapter gives a covariance analysis of ambiguity resolution for GPS/Galileo kinematic positioning applications. It shows the constellation geometry plays an important role in carrier phase ambiguity resolution. The single-frequency combined GPS/Galileo has comparable performance with GPS L1/L2 or L1/L5 over short baselines when the spatial decorrelation of the ionospheric error is not significant. Dual-frequency combined GPS/Galileo always has the best performance for three different lengths of baselines. The strategy of partial fixing ambiguities does not show improved performance over the short baseline while significant improvements are observed over the medium and

long baselines. Simulated data from a software simulator will be processed to further investigate these results in the presence of realistic errors in Chapter 5.

Chapter Five: Testing Using Simulated Data and Results Analysis

Following the covariance analysis presented Chapter 4, a multi-frequency and multi-system carrier phase processor (capable of partial fixing) is developed and tested in this chapter. This chapter studies the AR performance of GPS/Galileo kinematic positioning using data from a software simulator. Results of using observations from different sets of GPS/Galileo frequencies will be presented in Section 5.2 and a strategy of partially fixing ambiguities is presented and analysed in Section 5.4.

5.1 Simulated Data Generation

5.1.1 GNSS Software Simulator

A multi-frequency software simulator, namely SimGNSSII™, developed and used for GPS/Galileo research by the PLAN Group of the University of Calgary, was used herein. The approach and algorithms used in the simulator were initially developed by Luo and Lachapelle (2003), Alves et al. (2003) and Julien et al. (2003). The algorithms were further enhanced and documented by Dong (2004). The simulator can generate code, phase and Doppler observations for any GPS or/and Galileo constellation that can be described using a YUMA format (Hofmann-Wellenhof et al. 2001) almanac. It operates by calculating true satellite receiver ranges and then simulating the most significant GNSS errors including orbital error, tropospheric and ionospheric delays, code and phase multipath errors and receiver noise. The levels of each error source can be adapted to

simulate many environments experienced in GNSS applications. A description of the algorithms used in the simulator can be found in Luo (2001) with applications in Alves et al. (2003) and Zhang (2005). Some important error sources that have significant effects on kinematic DGNSS positioning are described below in terms of the simulation algorithm.

5.1.2 Ionospheric Error

For ionospheric error modeling, a combined spherical harmonics (SPHA) and grid model is used. The spherical coefficients are obtained based on the Global Ionosphere Map (GIM) files from the Centre for Orbit Determination in Europe (CODE). These files are divided into four groups: January to March, April to June, July to September and October to December to form four groups of coefficients for the SPHA model. The spherical harmonic expansion defines a global grid of vertical total electron content (VTEC) values with the assumption of a single ionosphere layer around the Earth. To get the TEC values above the area of interest, the pierce point of the observation from each satellite is calculated first, and then the surrounding four grid values are interpolated to the pierce point. Since the GIM model only represents the global trend of ionospheric variation, a local area ionospheric variation is also added using a second set of spherical harmonic expansion coefficients to increase the spatial resolution of the ionospheric error. The temporal resolution of the ionosphere is realized by updating the magnitudes of the expansion coefficients in a time-variant way using a first-order Gauss-Markov model. The generated vertical ionospheric error was multiplied by an elevation mapping function

to get the slant ionospheric delay for each user station (Luo 2001). The level of ionospheric error can be varied through a parameter in the simulation option file. Figure 5.1 shows a sample time series of DD ionospheric errors simulating a high level of ionospheric activity. It can be seen from the figure that the GPS L1 phase DD ionospheric error varies with the local time, the RMS of the errors is about 7 ppm, i.e., 7 mm over a 1-km baseline though its maximum can reach 28 ppm.

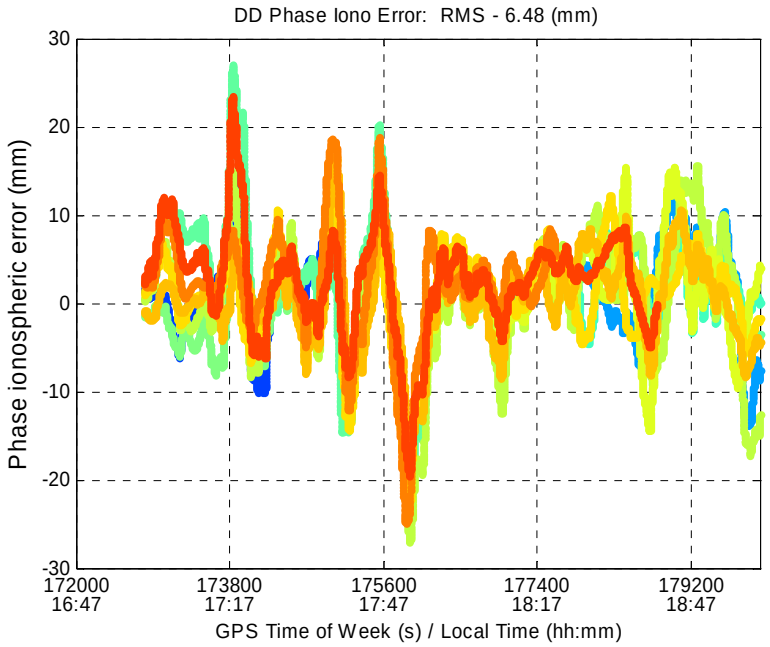

Figure 5.1: GPS L1 phase DD ionospheric errors over a 1 km baseline for all visible satellites during 2 hours

5.1.3 Multipath

Multipath is also one of the dominant error sources in DGNSS applications. It is caused by the mixture of direct and indirect signals from various reflectors around the receiver

antenna. The magnitude of multipath is dependent on the properties of the reflector, the distance between the reflector and the antenna, the gain pattern of the antenna, and the characteristics of the tracking loops used in the receiver. To simplify the simulation, only one reflected signal from the ground is assumed in modeling multipath in this case (Luo 2001). The magnitudes of code and phase multipath are simulated according to Table 4.2. Figure 5.2 shows the L1 phase multipath errors for four satellites observed at one station. It can be seen that the phase multipath errors for different satellites present the same trends: the errors are time-correlated and the magnitude of the error varies between ±6 mm, which is equivalent to 0.03 cycles of wavelength on the L1 frequency as set in the data generation.

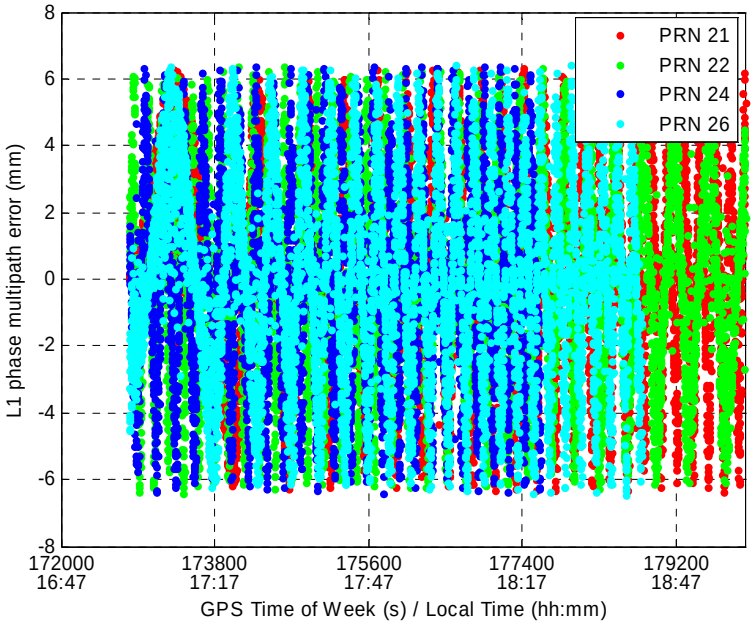

Figure 5.2: Single phase multipath of PRN 21, 22, 24 and 26 during 2 hours

5.1.4 Receiver Noise

Receiver noise is simulated as white noise. The magnitude of the receiver noise on different GPS/Galileo frequencies is simulated according to Table 4.3. A sample plot of the phase receiver noise of the GPS L1 observations is shown in Figure 5.3. It can be seen that the receiver noise of the L1 phase observations ranges between ±2 mm with an RMS of 0.6 mm.

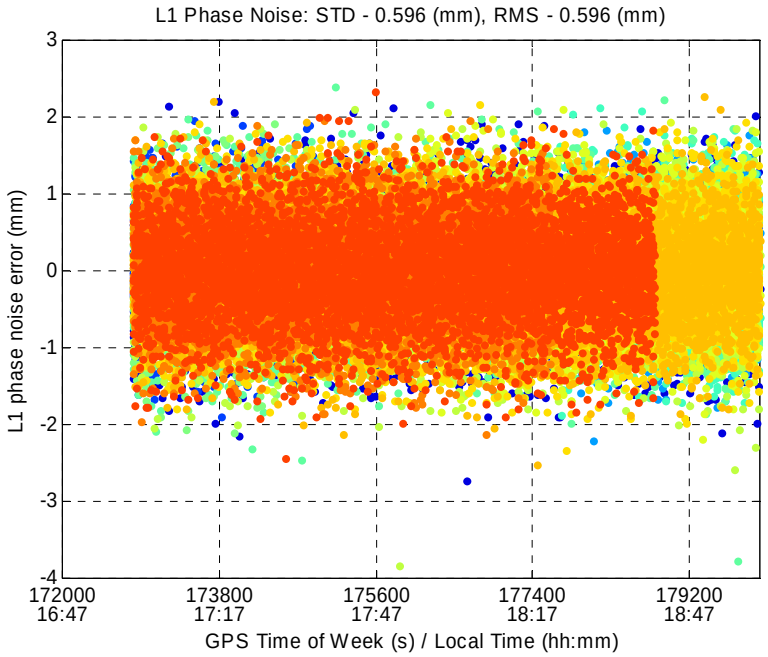

Figure 5.3: Phase receiver noise of GPS L1 observations during 2 hours

Based on the descriptions in Section 2.3, the orbital and tropospheric errors do not have significant effects on kinematic positioning over baselines less than 10 km with maximum values of 0.8 mm and 2 mm respectively under normal conditions (Cosentino et al. 2005).

5.2 Simulation Description and Processing Strategy

5.2.1 Simulation Description

One of the objectives of this thesis is to evaluate the AR performance of kinematic positioning using observations on different subsets of GPS/Galileo frequencies, the same six cases as those in Chapter 4 (see Table 4.5) are investigated herein. In contrast to the medium and long baselines simulated in Chapter 4, three different short baselines - 1 km, 5 km and 10 km are investigated in this chapter using software simulated data. This is to restrict the investigation to the region of normal RTK operations on baselines of less than 10 km.

Since this research is only focused on short baselines (no greater than 10 km), the orbital and tropospheric errors are not significant on kinematic positioning (based on the conclusions given in Section 2.3) in these cases and they are ignored in the data generation. To account for the effect of the ionospheric error, two conditions are simulated: a benign condition without ionospheric error and a severe condition with L1 DD ionospheric RMS errors of 7 ppm though their maximum value can reach nearly 30 ppm (shown in Figure 5.1). Since ionospheric error is the only distance dependent error in these cases, the scenarios without ionospheric error over the 5 and 10 km baselines are identical to that over a 1 km baseline (Scenario A) and have been removed. In all, four scenarios are simulated as listed in Table 5.1.

Table 5.1: Simulation Scenarios

Baseline (km)	DD Ionosheric Error RMS (ppm)	
	0	7
1	A	B
5	-	C
10	-	D

5.2.2 Processing Strategy: Full Ambiguity Resolution

The simulated data was processed using the SD processor described in Chapter 3. The North, East and Up position components and the between-receiver differenced clock offset are estimated as states with a random walk dynamics model in a Kalman filter to simulate a slowly walking user. Since the rover station was assumed to be in slowly moving kinematic mode, the spectral density of the position states was set to 0.05 m/s. For the clock state, a very large value of 10,000 m/s was set in order for the clock estimate to essentially be free from epoch to epoch. This condition is necessary to maintain the equivalence of the single- and double-differencing estimation models. As mentioned in Chapter 4, the so-called tight-coupling approach is used for Cases ⑤ and ⑥ where observations on common GPS and Galileo frequencies are available. The float solutions were first obtained and then passed to LAMBDA for fixing. The interest in this study is the ambiguity convergence period to get fixed solutions, and that is the reason for

resetting the filter. The results of partial fixing of the float ambiguities are presented in Section 5.4.

In order to answer the question of which sets of GNSS observations should be used in future GPS/Galileo kinematic positioning, statistics are obtained and compared for the above scenarios. This was done by dividing the 24-hour data sets into 10-minute samples and processing them with the phase processing strategy described above. The time to first fix (time required to fix and validate the full set of ambiguities) was then recorded for each simulation run, in addition to whether the correct ambiguity set had been obtained or not. The statistics were obtained by processing all the 144 simulation runs.

5.3 Result and Analysis

5.3.1 Simulation results of different cases for Scenario B

A subset of simulation results is presented in this section. Results for different cases (using observations on different frequencies) in Scenario B (a 1 km baseline with high ionospheric error) are presented and compared. The statistics from the simulation results of 24-hour data set for all the six cases are then presented and discussed in terms of several figures of merit.

Case ①: GPS L1 Observations (base case)

As an example, Figure 5.4 shows the GPS L1 DD float ambiguity values for all the observed satellites. It can be seen that the 8 DD float ambiguities converge to their corresponding integer values (all zeros in this case) in the float filter. In this 10 minute simulation, PRN 21 is the base satellite.

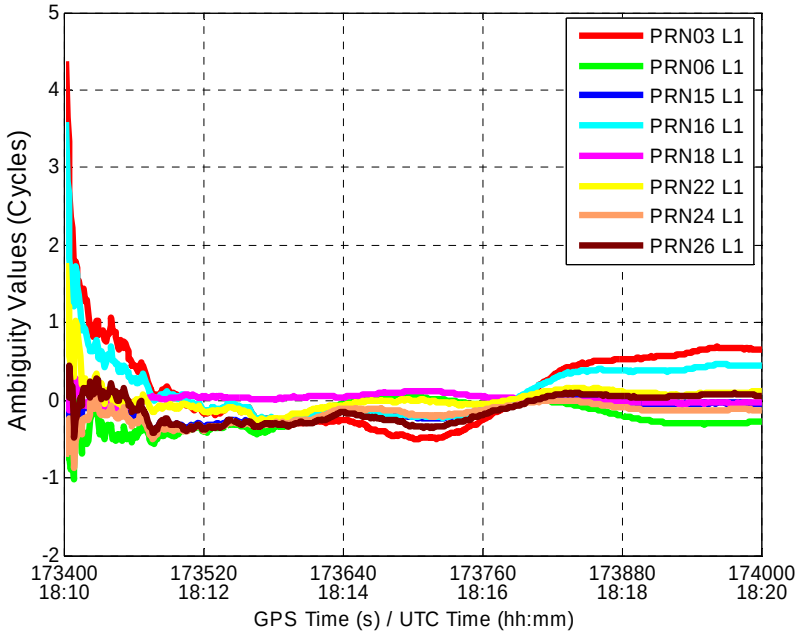

Figure 5.4: Float DD ambiguities of all the GPS L1 observations over a 1 km baseline with high ionospheric error

Figure 5.5 shows the values of the ratio test and the PCF obtained in ambiguity validation. In this study, the thresholds for ratio testing and PCF are set to 2 and 0.9, respectively. The ratio threshold is derived from experience and the PCF threshold is not as stringent as that used in the covariance simulations shown in Chapter 4, and it is to simulate GNSS applications in land surveying such as conventional RTK. After passing

the ratio and PCF thresholds, the ambiguities are deemed as fixed and the fixed position solution is computed according to Equations (3.18) and (3.19).

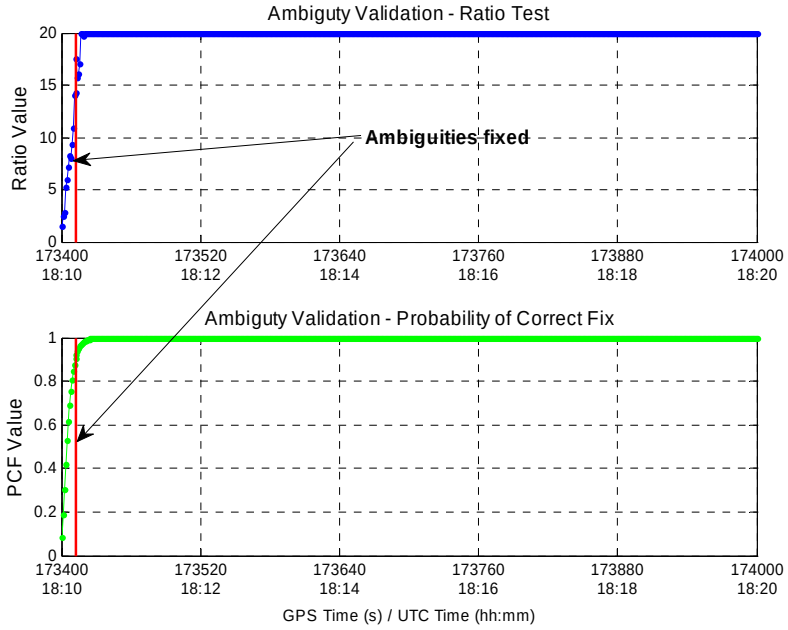

Figure 5.5: Ratio test value and probability of correct fix ambiguities using GPS L1 observations over a 1 km baseline with high ionospheric error

Figure 5.6 shows the GPS L1 DD fixed ambiguities. It is found all the ambiguities are correctly fixed to zeros, which are the integer ambiguities set in the data generation. Note that only the results for the first two minutes are shown and the float values are displayed before the fixed values are obtained.

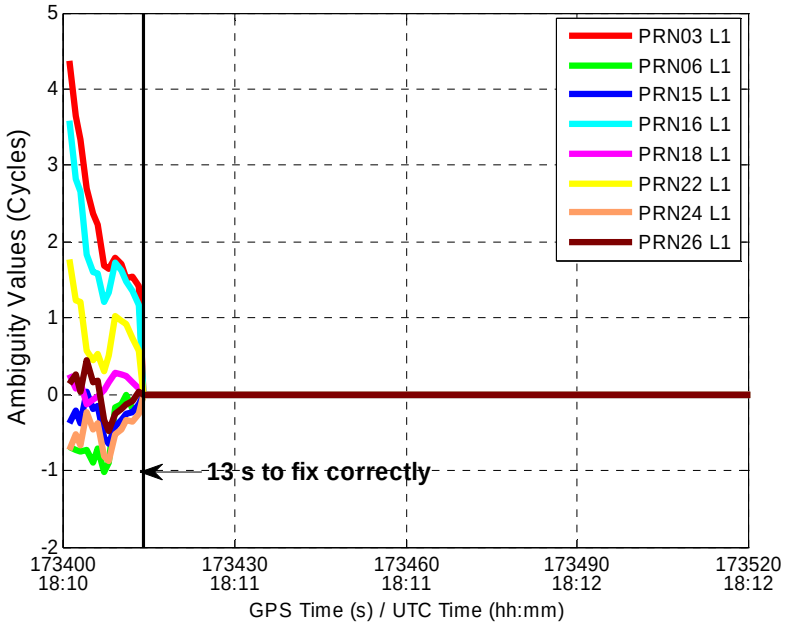

Figure 5.6: Fixed DD ambiguities of all the GPS L1 observations over a 1 km baseline with high ionospheric error

Figures 5.7 and 5.8 show the position errors in Case ①. The North, East and Up position error components from the SD float solution are shown in Figure 5.7, while Figure 5.8 shows the position error of the fixed solution. Note that it takes 13 seconds to correctly fix and validate all GPS L1 ambiguities and the float solution is shown before obtaining the fixed solution. When the ambiguities are correctly fixed, millimetre level position accuracies are obtained. Figures 5.9 and 5.10 show the position errors and standard deviation ($\pm 3\sigma$) together, it can be seen that the position errors are completely bounded by the standard deviation.

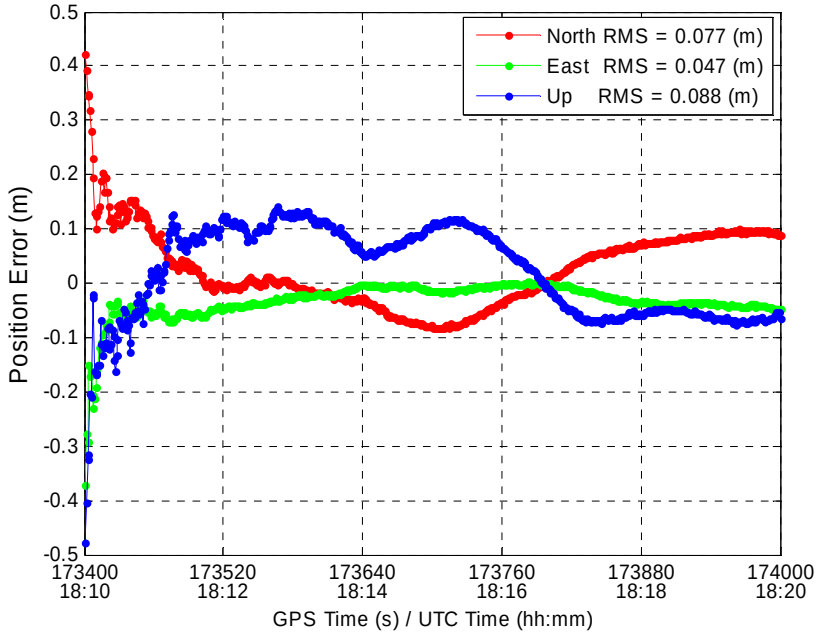

Figure 5.7: Position errors of the float solution using GPS L1 observations over a 1 km baseline with high ionospheric error

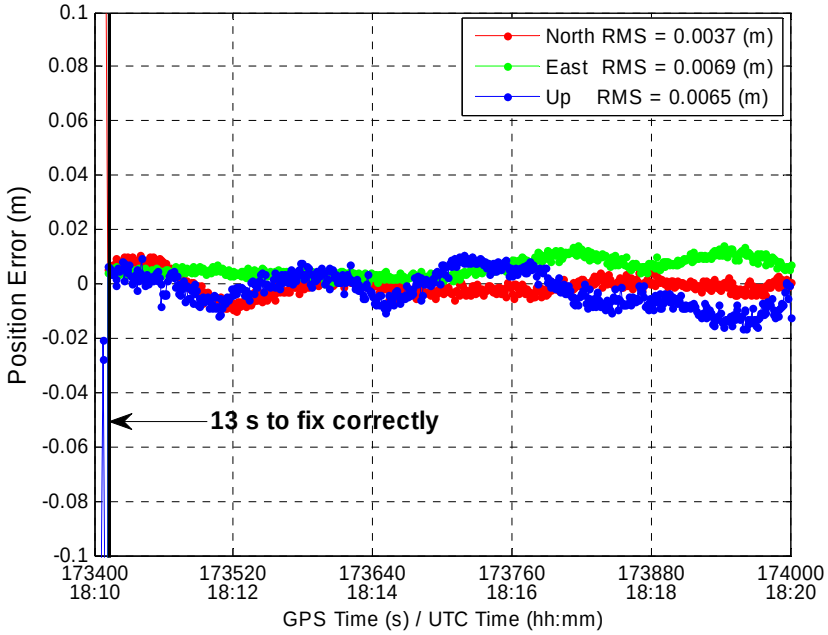

Figure 5.8: Position errors of the fixed solution using GPS L1 observations over a 1 km baseline with high ionospheric error

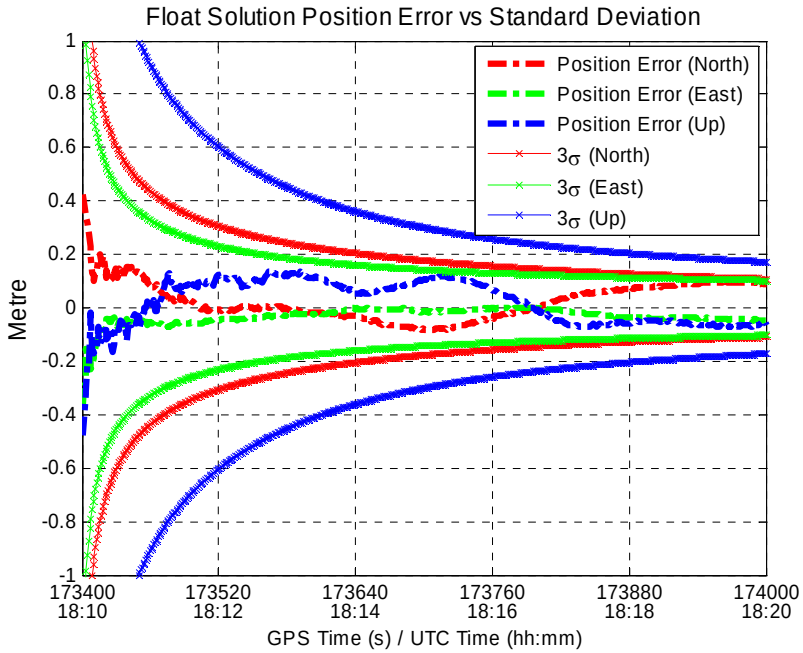

Figure 5.9: Position errors versus estimated standard deviation for the float solution using GPS L1 observations over a 1 km baseline with high ionospheric error

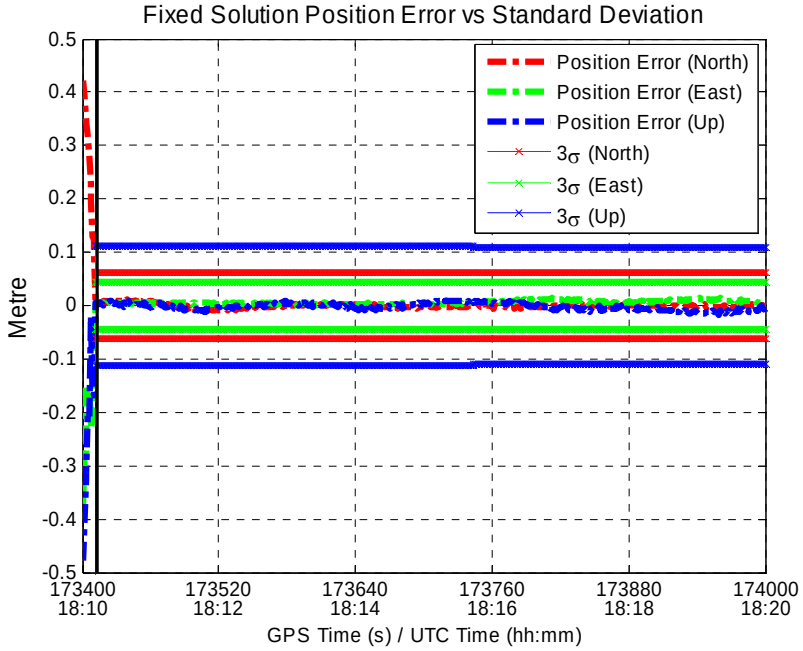

Figure 5.10: Position errors versus estimated standard deviation for the fixed solution using GPS L1 observations over a 1 km baseline with high ionospheric error

Cases ② and ③: Dual-frequency GPS Observations

Figures 5.11-15 show results for Cases ② and ③, where GPS L2 or L5 observations are added to the filter compared to Case ①. With the additional observations on another frequency from the same GNSS (GPS in these cases), it is found that similar float position estimates are obtained. However, it takes much less time, only 3 seconds in both cases, to fix ambiguities (shown in Figure 5.12). This is due to the fact the LAMBDA algorithm, when operating on multiple frequency float ambiguities, is able to form linear combinations of ambiguities with longer wavelengths (for example the first step in dual frequency LAMBDA forms a wide-lane implicitly before search for an even better linear combination (Teunissen 1998)). The LAMBDA Z-domain ambiguities are then much easier to fix compared to the GPS L1 ambiguities in Case ①. Using L1 and L2 observations should lead to better AR performance due to the longer wide-lane wavelength compared to that of L1 and L5, however, this benefit is not significantly observed in this simulation run since these are over short baseline cases where the ionospheric errors are small.

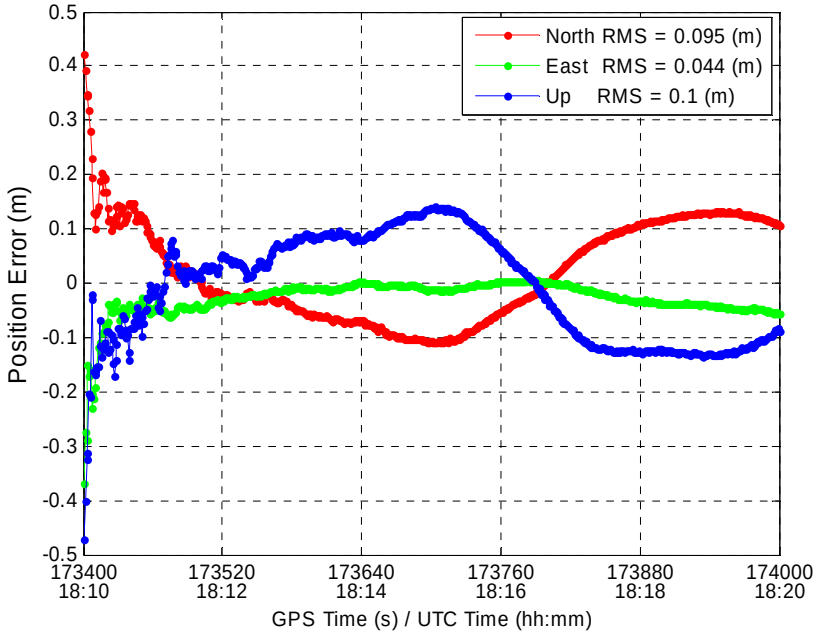

Figure 5.11: Position errors of the float solution using GPS L1 and L2 observations over a 1 km baseline with high ionospheric error

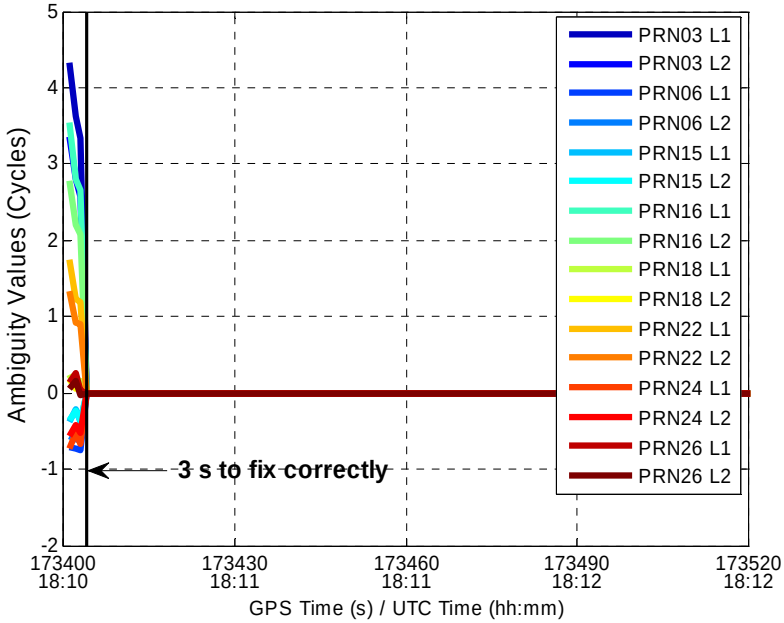

Figure 5.12: Fixed ambiguities of all the GPS L1 and L2 observations over a 1 km baseline with high ionospheric error

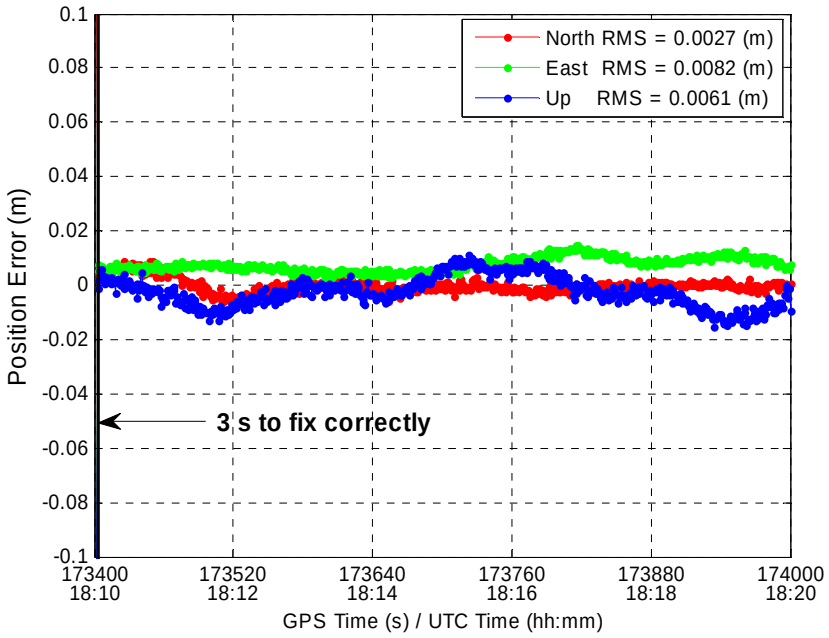

Figure 5.13: Position errors of the fixed solution using GPS L1 and L2 observations over a 1 km baseline with high ionospheric error

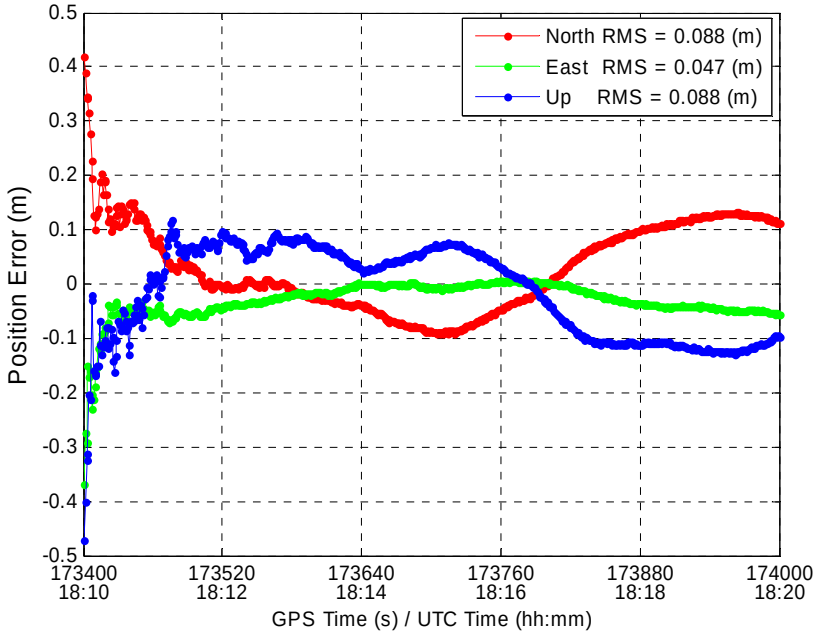

Figure 5.14: Position errors of the float solution using GPS L1 and L5 observations over a 1 km baseline with high ionospheric error

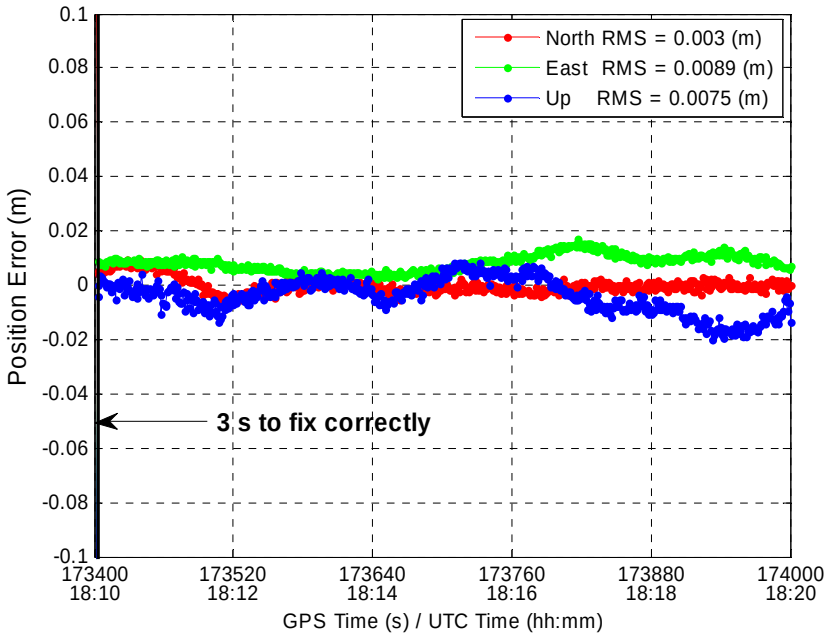

Figure 5.15: Position errors of the float solution using GPS L1 and L5 observations over a 1 km baseline with high ionospheric error

Case ④: Triple-frequency GPS Observations

Figures 5.16 and 5.17 show position errors of the float and fixed solutions using observations on all three GPS frequencies (L1, L2 and L5). The float solution presents similarities to those in Cases ①, ② and ③, while it only takes 2 seconds to fix all the ambiguities in this case since three frequencies are now available to LAMBDA, implicitly giving it the benefits of three carrier ambiguity resolution when the algorithm searches for an optimal set of linear combinations of ambiguities on three frequencies.

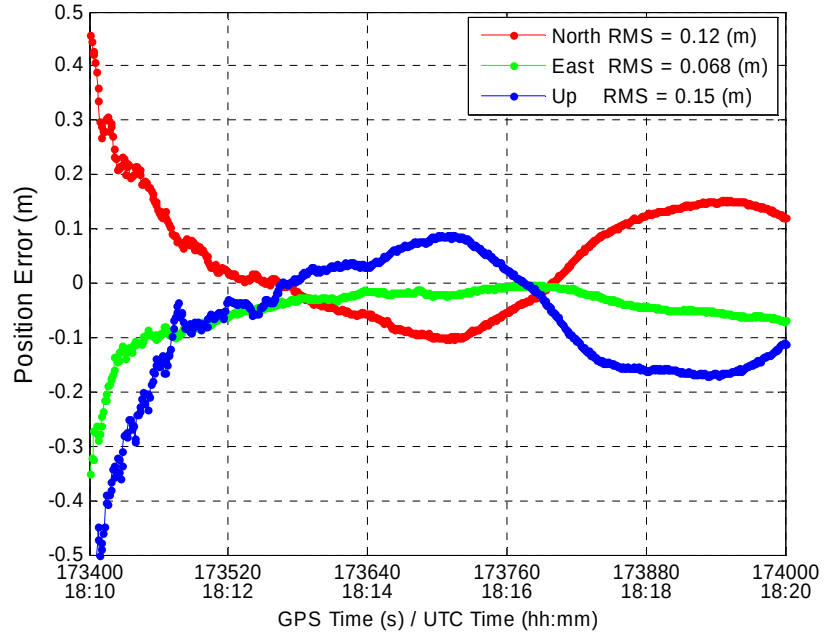

Figure 5.16: Position errors of the float solutions using GPS L1, L2 and L5 observations over a 1 km baseline with high ionospheric error

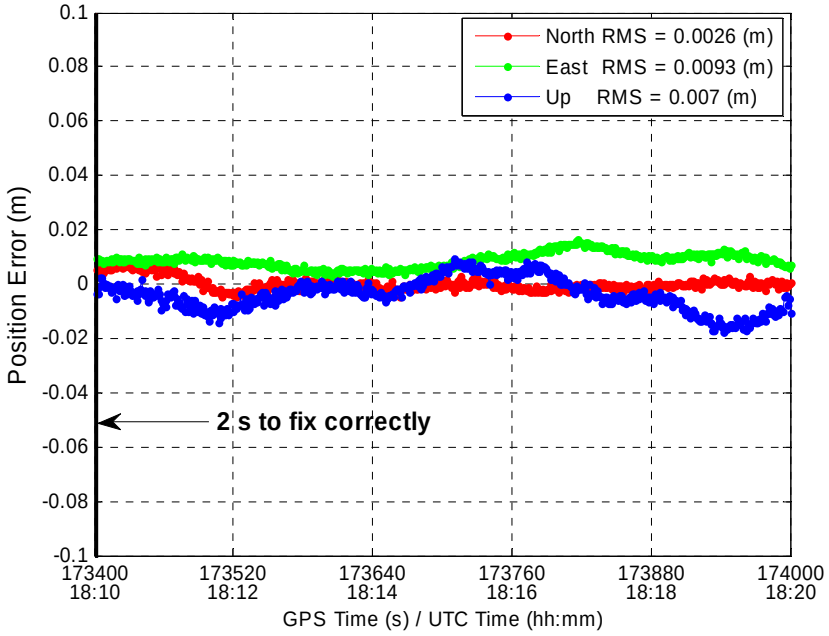

Figure 5.17: Position errors of the fixed solutions using GPS L1, L2 and L5 observations over a 1 km baseline with high ionospheric error

Case ⑤: Single-frequency GPS and Galileo Observations

Figures 5.18 and 5.19 present the results when GPS L1 and Galileo E1 observations are used for kinematic positioning. As shown in Figure 5.18, better float position estimates are obtained compared to that of GPS L1. This is due to the enhanced satellite geometry when the two systems are used together. The improved geometry also leads to faster ambiguity fixing (3 epochs) compared to cases ①-④, where only GPS observations are used for kinematic positioning.

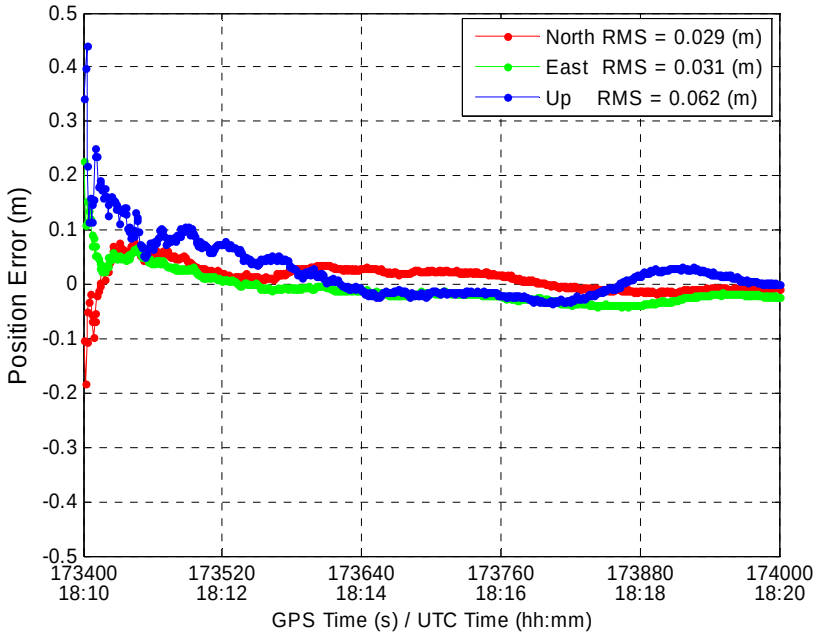

Figure 5.18: Position errors of the float solution using GPS L1 and Galileo E1 observations over a 1 km baseline with high ionospheric error

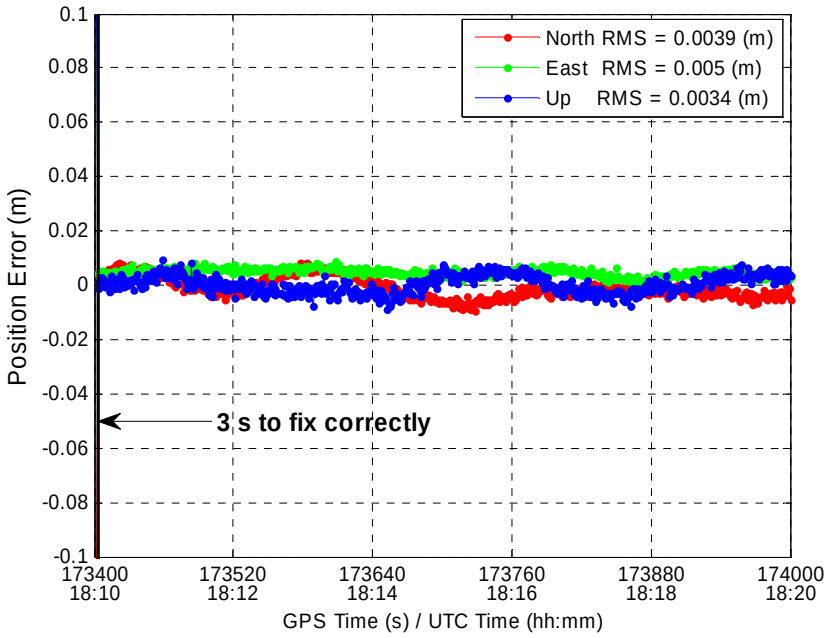

Figure 5.19: Position errors of the fixed solution using GPS L1 and Galileo E1 observations over a 1 km baseline with high ionospheric error

Case ⑥: Dual-frequency GPS and Galileo Observations

Figures 5.20 and 5.21 show the results for Case ⑥, where observations on two common frequencies, L1 and E1 or L5 and E5a, from GPS and Galileo are used. It is obvious that the positioning accuracy of the float solution is improved significantly due to the enhanced geometry of combined GPS/Galileo, and the ambiguities can also be quickly fixed in 2 seconds with the availability of observations on two common frequencies. It shows the dual-frequency combined GPS/Galileo has the best AR performance in all six cases and conforms to the results in Chapter 4 based on the covariance simulations.

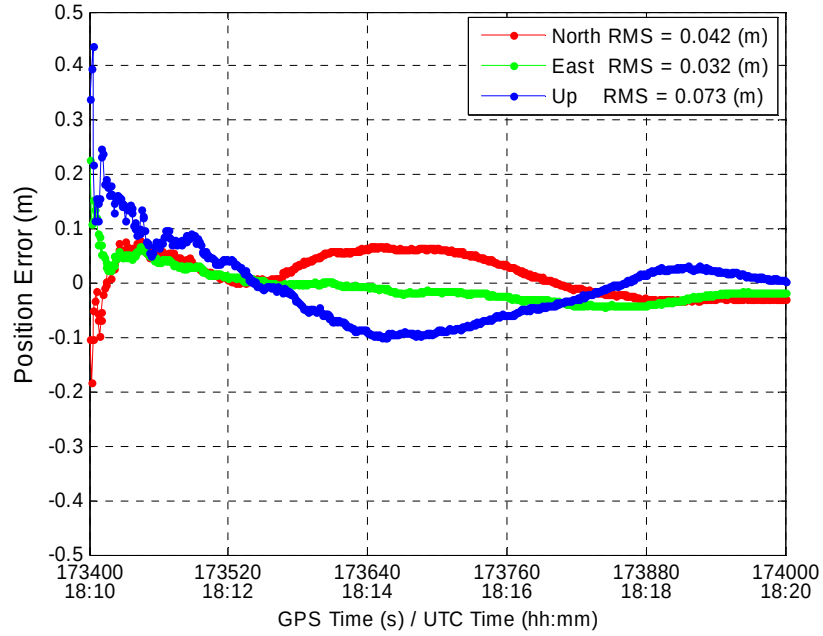

Figure 5.20: Position errors of the float solution using GPS L1, L5 and Galileo E1, E5a observations over a 1 km baseline with high ionospheric error

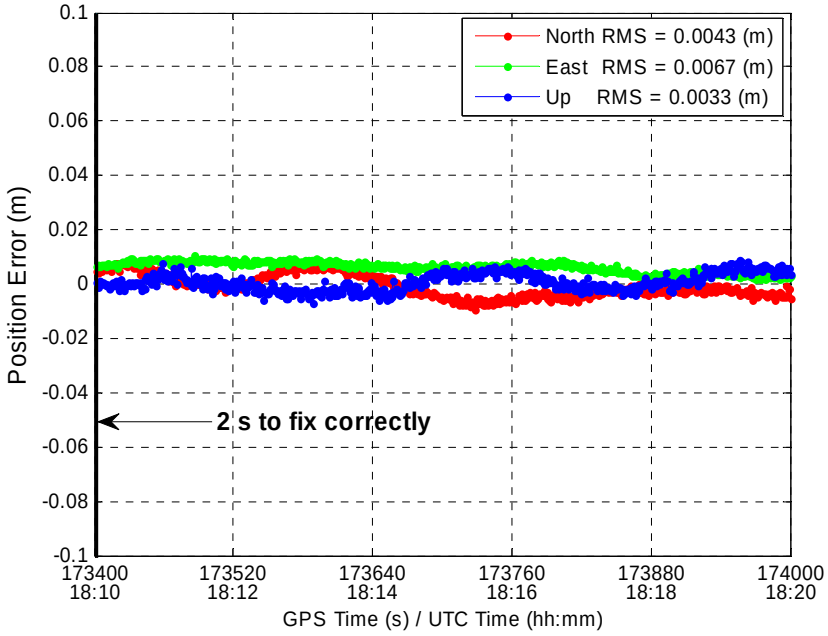

Figure 5.21: Position errors of the fixed solution using GPS L1, L5 and Galileo E1, E5a observations over a 1 km baseline with high ionospheric error

5.3.2 Statistics of Simulation Results

To get a better understanding of the kinematic positioning performance using observations on different subsets of GPS/Galileo frequencies, the 24-hour simulated data set was divided into 10-minute samples (Subsection 5.2.2). Statistics on these multiple samples are obtained and compared in terms of the following figures of merit.

1) Mean Time To First Fix Ambiguities (MTTFFA): the time to first fix and successful validation of each 10-minute sample is calculated. The total time is summed over all samples and the average time is calculated as the MTTFFA.
2) Percent of Correct Fix Ambiguities (PCFA): the number of 10-minute samples which have ambiguities correctly fixed over the 144 samples in the 24-hour simulated data set.
3) Percent of Incorrect Fix Ambiguities (PIFA): the number of 10-minute samples which have ambiguities incorrectly fixed over the 144 samples in the 24-hour simulated data set.
4) Percent of No Fix Ambiguities (PNFA): the number of samples that the ambiguities cannot be fixed in the whole 10-minute duration over the 144 samples in the 24-hour simulated data set.

Note that the above figures of merit are calculated over 10-minute samples and the sum of three percentages is 100%.

Table 5.2 shows the statistics of the simulation results for various cases in Scenario A - the 1 km baseline without ionospheric error. It can be seen that the MTTFFA is 57 seconds when using GPS L1 observations. There are some samples whose ambiguities cannot be fixed or are fixed to incorrect values in the 10-minute duration. With the addition of observations on other frequencies, the MTTFFA decreases and ambiguities over all samples can be fixed and no incorrect fixing occurs. These results are as expected. What is most interesting however, is that the inclusion of additional observations on the same frequency (Case ⑤) results in a greater improvement than adding signals on multiple frequencies (Cases ② and ③). This shows that when spatially correlated errors are small, there is more benefit from additional geometry than there is from additional frequency diversity.

Table 5.2: Mean time to first fix ambiguities, percentage of correct fix, percentage of incorrect fix and percentage of no fix for GPS/Galileo kinematic positioning over a 1 km baseline without ionospheric error

Case	Observations	MTTFFA	PCFA (%)	PIFA (%)	PNFA (%)
①	L1	56.6	93.75	5	1.25
②	L1, L2	8.2	100	0	0
③	L1, L5	8.6	100	0	0
④	L1, L2, L5	3.1	100	0	0
⑤	L1, E1	6.8	100	0	0
⑥	L1, E1, L5, E5a	2.0	100	0	0

The statistics of the simulation results for a 1 km baseline with high ionospheric error (Scenario B) is shown in Table 5.3. The same conclusion can be made as in the case of no ionospheric error. There are some samples with incorrect-fixes and no-fixes due to the ionospheric effect. It is observed that the MTTFFA when using GPS L1 and L5 observations is higher than that of using L1 and L2. This is likely due to the fact that L1-L5 results in a shorter wavelength wide-lane ambiguity which can be formed implicitly in the LAMBDA decorrelation. Comparing Case ② (using GPS L1 and L2) to Case ⑤ (using GPS L1 and Galileo E1), it is found that it takes much less time to gain the MTTFFA for the latter though incorrect-fixes occur in some samples. This shows again

the benefit of the enhanced geometry of the GPS/Galileo combination in the case that the differential ionospheric error is relatively low. In this case, adding observations on the same frequency from another GNSS (namely Galileo) has superior performance than adding observations on another frequency from the existing GNSS (namely GPS). Comparing the results of using observations on all GPS frequencies – L1, L2 and L5 (Case ④) to that of using observations on two common frequencies of GPS and Galileo (Case ⑥), also shows the benefit of enhanced geometry on the ambiguity resolution in terms of decreased MTTFFA.

Table 5.3: Mean time to first fix ambiguities, percentage of correct fix, percentage of incorrect fix and percentage of no fix for GPS/Galileo kinematic positioning over a 1 km baseline with high ionospheric error

Case	Observations	MTTFFA	PCFA (%)	PIFA (%)	PNFA (%)
①	L1	63.8	90.00	8.75	1.25
②	L1, L2	8.1	100.00	0	0
③	L1, L5	13.1	98.75	1.25	0
④	L1, L2, L5	3.4	100.00	0	0
⑤	L1, E1	3.3	98.75	1.25	0
⑥	L1, E1, L5, E5a	2.0	100.00	0	0

Table 5.4 shows the statistics for a 5 km baseline with high ionospheric error present (Scenario C). The same trend can be observed in this scenario. Besides the decrease of MTTFFA in Cases ⑤ and ⑥ where GPS and Galileo are combined, it is also found that there are fewer incorrect-fixes, which means the enhanced geometry also improves the reliability of carrier phase ambiguity resolution.

Table 5.4: Mean time to first fix ambiguities, percentage of correct fix, percentage of incorrect fix and percentage of no fix for GPS/Galileo kinematic positioning over a 5 km baseline with high ionospheric error

Case	Observations	MTTFFA	PCFA (%)	PIFA (%)	PNFA (%)
①	L1	204.7	47.50	32.50	20.00
②	L1, L2	122.5	80.00	13.75	6.25
③	L1, L5	154.0	78.75	10.00	11.25
④	L1, L2, L5	148.3	77.50	13.75	8.75
⑤	L1, E1	98.7	85.00	3.75	11.25
⑥	L1, E1, L5, E5a	118.8	88.75	1.25	10.00

Simulation results for the 10 km baseline (Scenario D) are shown in Table 5.5. In this case, ambiguities in most of the samples cannot be fixed due to the significant effect of high ionospheric errors. However, the ability to identify the wrong ambiguity sets is still observed in Cases ⑤ and ⑥, where the geometry is augmented due to the combination of

the two systems. For example, the PIFA is 7.50% and 2.50% for Cases ⑤ and ⑥, where GPS and Galileo are combined on single and dual frequencies, while the figure of merit is 21.25% and 15.00% for Cases ② and ④.

Table 5.5: Mean time to first fix ambiguities, percentage of correct fix, percentage of incorrect fix and percentage of no fix for GPS/Galileo kinematic positioning over a 10 km baseline with high ionospheric error

Case	Observations	MTTFFA	PCFA (%)	PIFA (%)	PNFA (%)
①	L1	222.0	17.50	47.50	35.00
②	L1, L2	148.2	37.50	21.25	41.25
③	L1, L5	165.5	46.25	11.25	42.50
④	L1, L2, L5	153.3	41.25	15.00	43.75
⑤	L1, E1	244.0	37.50	7.50	55.00
⑥	L1, E1, L5, E5a	250.0	37.50	2.50	60.00

5.4 Partial Fixing

While the previous section dealt with selecting subsets of the available GPS/Galileo observations, using these to estimate a float position solution and the corresponding ambiguities, and then fixing all of the ambiguities, this section shows the results obtained

by estimated these ambiguities but not necessarily fixing all of them. Partial fixing of ambiguities is demonstrated for three different cases in Scenarios B, C and D. The case of using GPS L1 observations (Case ①) for kinematic positioning is presented as the base case, while Cases ④ and ⑥ are presented as scenarios where the number of ambiguities is increased to a significant level when using a triple-frequency GPS and dual-frequency GPS/Galileo, respectively. Results from the first 10-minute period of simulated data are shown in this section. In the ambiguity validation stage, the thresholds for the ratio testing and the PCF are set to 2 and 99.99%, respectively. A high PCF threshold is selected to simulate kinematic positioning with high integrity requirements. This is done to show the benefit of partial fixing, since the PCF decreases as more ambiguities are fixed. By setting it high, the goal is to show that high PCF can be maintained by fixing only a small number of ambiguities. The corresponding position accuracies are then shown to demonstrate the positioning accuracy associated with fixing various numbers of ambiguities compared to the float (none fixed) and fixed (all fixed) results presented in Section 5.3 above.

5.4.1 Results Over 1 Km Short Baseline

Case ①: GPS L1 Observations (base case)

Ambiguity partial fixing with 4, 6 and 8 fixed ambiguities in the GPS L1 case are shown first, where there are 8 ambiguities in total in this case. By passing them to LAMBDA, the original ambiguities are decorrelated via the transformation matrix Z^T as shown in Equation (3.20). For example, the Z^T matrix at the first epoch is

$$Z^T = \begin{bmatrix} 0 & 0 & 0 & 1 & 3 & -2 & 1 & 0 \\ -1 & -1 & 1 & 1 & 1 & 0 & -1 & 1 \\ 1 & 0 & 2 & -1 & 0 & 0 & 1 & -3 \\ 0 & -2 & 0 & -2 & 0 & 3 & 0 & 1 \\ 2 & 2 & 0 & -2 & 1 & -1 & -2 & 0 \\ 0 & 0 & 2 & 0 & 0 & 0 & -1 & -1 \\ 0 & 1 & -1 & 0 & -2 & 0 & 0 & 0 \\ 0 & 0 & 1 & 0 & 0 & 0 & -1 & 0 \end{bmatrix} \tag{5.1}$$

From Equation (5.1), it is found that the decorrelated ambiguities are a mixture or combination of the original ones. For example, the first decorrelated ambiguity is a linear combination of the 4th, 5th, 6th and 7th original ambiguities as in

$$\hat{N}_1 = a_4 + 3a_5 - 2a_6 + a_7 \tag{5.2}$$

With partial fixing, the partial subset of fixed ambiguities starts from the last ambiguity in the Z-domain ambiguity vector, since the decorrelated (Z-domain) ambiguities are mostly placed in an order of decreasing conditional variance as a by-product of the LAMBDA decorrelation algorithm (de Jonge & Tiberius 1996). It was shown in Chapter 4 that the smaller the conditional variance, the higher the PCF, which means a higher probability to fix the ambiguity and as a result it makes sense to first fix the ambiguity with the smallest (unconditional) variance and then fix the ambiguity with the smallest conditional variance (conditioned on the first ambiguity being fixed correctly) and so on.

For example, the decorrelated ambiguities are divided into two groups in case ①: a subset which is to be fixed and another one which is unfixed. Following Equation (3.28), the ambiguities can be written with the position states together as,

$$bz^T = \begin{bmatrix} \hat{b} & \hat{N}_1 & \cdots & \hat{N}_4 & \hat{N}_5 & \cdots & \hat{N}_8 \end{bmatrix}^T \tag{5.3}$$

With partially fixing a subset of ambiguities, e.g., $\breve{N}_5, \breve{N}_6, \breve{N}_7, \breve{N}_8$, the remaining ambiguities and position estimates become

$$\breve{B}^T = \begin{bmatrix} \breve{b}_{|\breve{N}_5 \cdots \breve{N}_8} & \breve{N}_{1_{|\breve{N}_5 \cdots \breve{N}_8}} & \cdots & \breve{N}_{4_{|\breve{N}_5 \cdots \breve{N}_8}} \end{bmatrix}^T \tag{5.4}$$

where $_{|\breve{N}_5 \cdots \breve{N}_8}$ indicates the fixed position states and remaining ambiguities are conditioned on the fixed ambiguities $\breve{N}_5, \breve{N}_6, \breve{N}_7, \breve{N}_8$.

Figure 5.22 shows the position errors of the float solution using the GPS L1 observations. The position errors of the North and East components are in the sub-decimetre levels while the Up component can reach 19 cm. Figure 5.23 shows the position errors and standard deviation together, it is found that the position errors are bounded by the $\pm 3\sigma$ standard deviation.

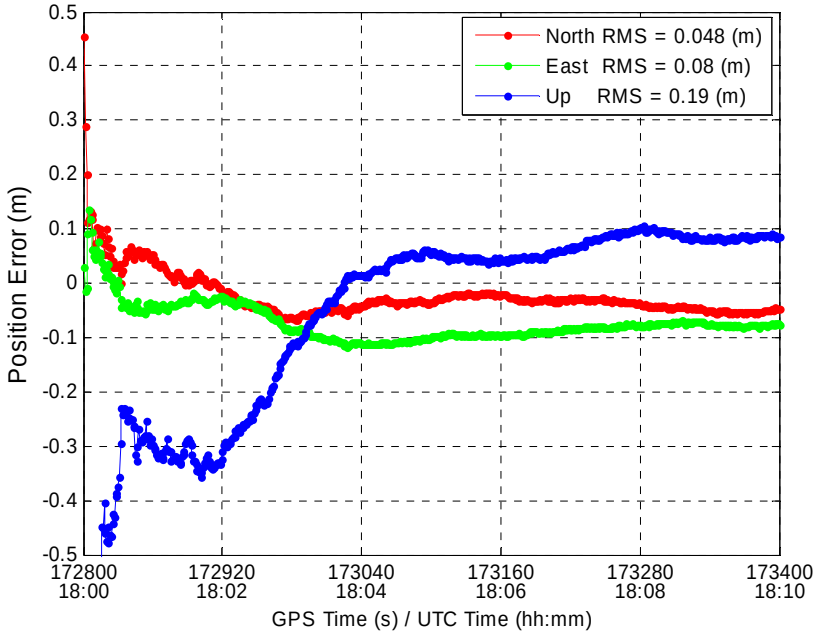

Figure 5.22: Position error for the float solution using all GPS L1 observations over a 1 km baseline with high ionospheric error

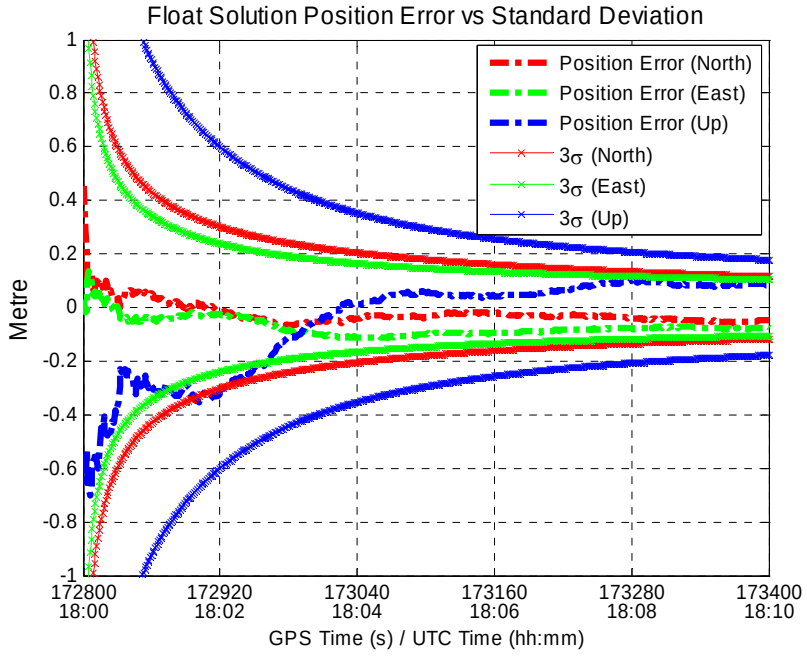

Figure 5.23: Position error versus estimated standard deviation for the float solution using all GPS L1 observations over a 1 km baseline with high ionospheric error

Figure 5.24 shows the float and fixed values of the fixed partial subset of 4 ambiguities, which are the last four ambiguities in the ambiguity vector. It is seen that there are abrupt changes of the float ambiguities, which is due to the changes of Z-transformation matrices as shown in Figure 5.28. In this case, the 4 float ambiguities are fixed and validated in 37 epochs.

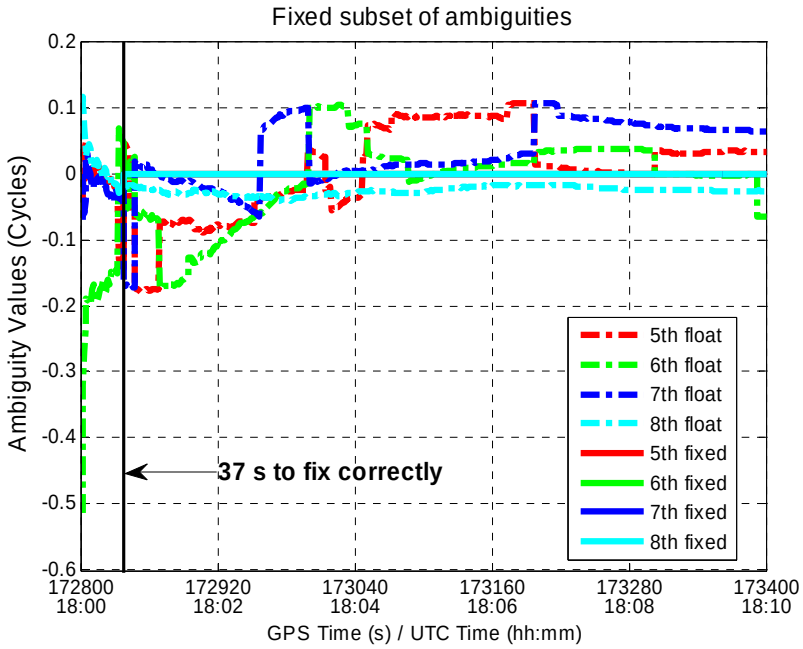

Figure 5.24: Float and fixed values of the fixed partial subset (4 ambiguities) in the GPS L1 case over a 1 km baseline with high ionospheric error. After 37 seconds, all of the Z-domain ambiguities are fixed to zero. The corresponding float ambiguities are discontinuous because the transformation from the original to decorrelated ambiguities changes during the 10 minute interval, meaning that a different Z-domain float ambiguity set is sent for partial fixing after each change in Z matrices.

Figure 5.25 shows the ambiguity values of the remaining unfixed subset (the first four ambiguities in the ambiguity vector) before (in dashed lines, first four ambiguities in Equation (5.3)) and after (in solid lines, ambiguities in Equation (5.4)) the subset

ambiguities being fixed. It is found that these ambiguities are corrected after correctly fixing the subset of other ambiguities.

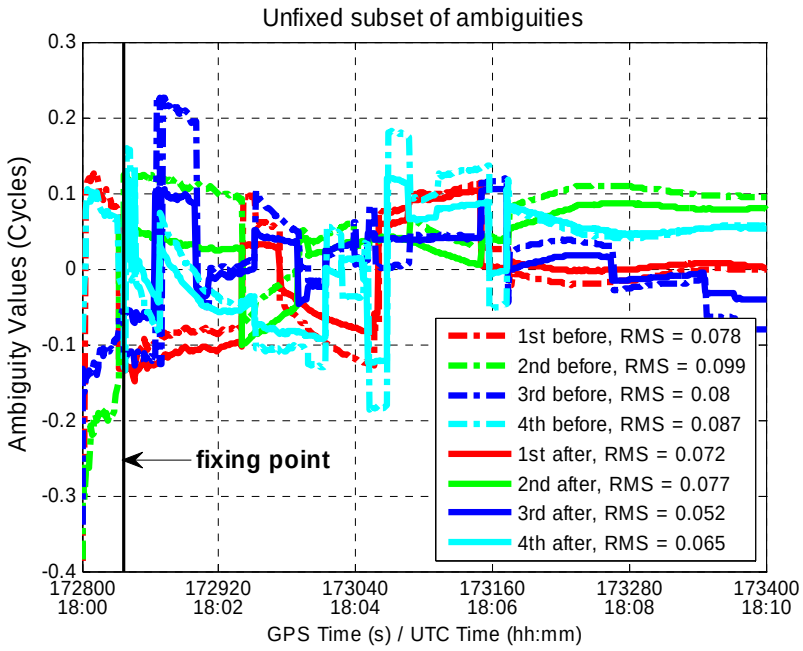

Figure 5.25: The values of the unfixed partial subset (4 ambiguities) before and after the partial ambiguity fixing in the GPS L1 case over a 1 km baseline with high ionospheric error. Note that for each ambiguity the solid (float subject to the other ambiguities being fixed) is closer to zero than the float value. As shown in Figure 5.28, the plots are discontinuous due to changes in the LAMBDA decorrelation.

Figure 5.26 shows the position errors with partially fixing the four ambiguities. Comparing with the position errors of the float solution (shown in Figure 5.22), the position accuracies are improved and they are still at the centimetre level. Figure 5.27 shows the position errors are bounded by the $\pm 3\sigma$ standard deviation. The discontinuities of the position errors are due to changes in the Z-transformation matrix as will be discussed later.

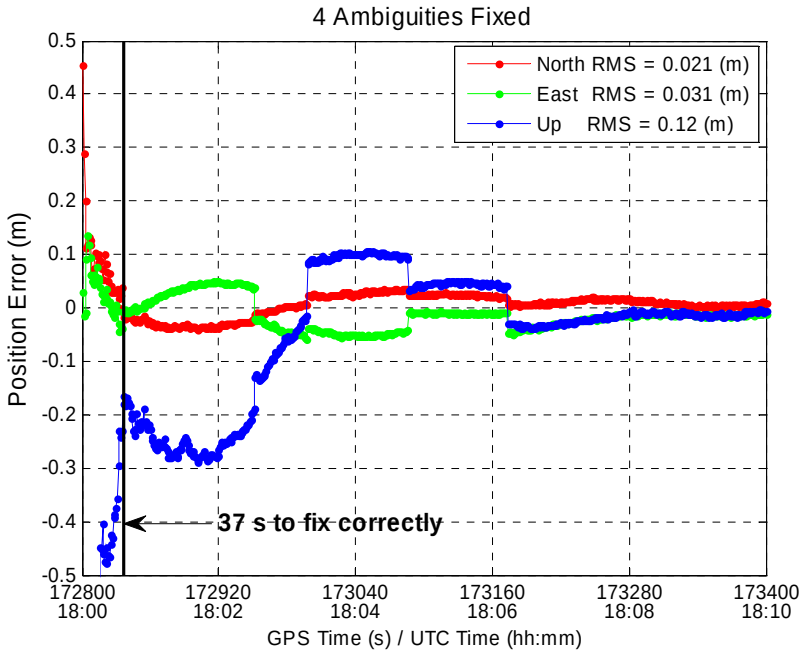

Figure 5.26: Position errors with 4 ambiguities correctly fixed in the Case ① (GPS L1) over a 1 km baseline with high ionospheric error

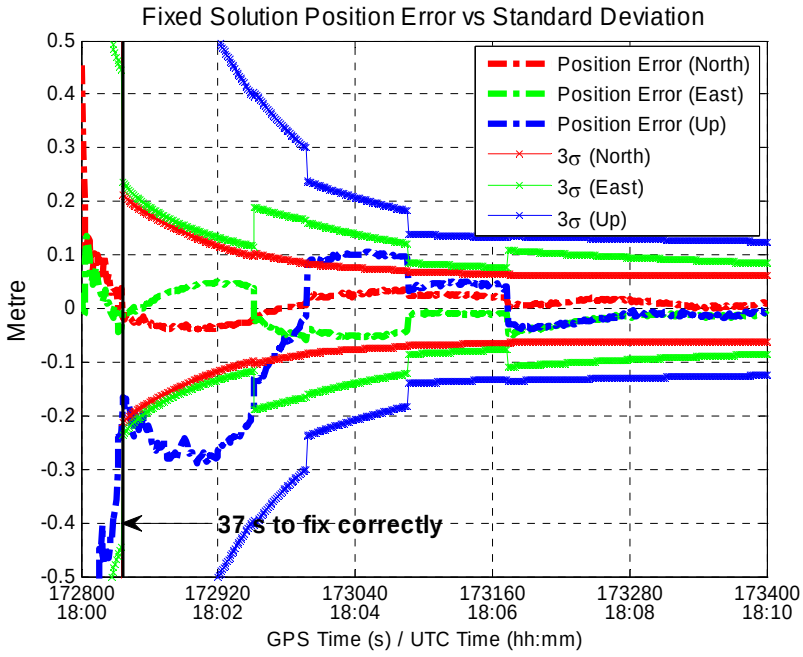

Figure 5.27: Position errors versus estimated standard deviation with 4 ambiguities correctly fixed in the Case ① (GPS L1) over a 1 km baseline with high ionospheric error

Figure 5.28 shows the changes of the decorrelation matrix, Z^T in LAMBDA for different epochs. Variations in the LAMBDA decorrelation at different epochs were observed and proved by Teunissen (1998). The changes of decorrelation matrices lead to discontinuities of the Z-domain ambiguities and position estimates.

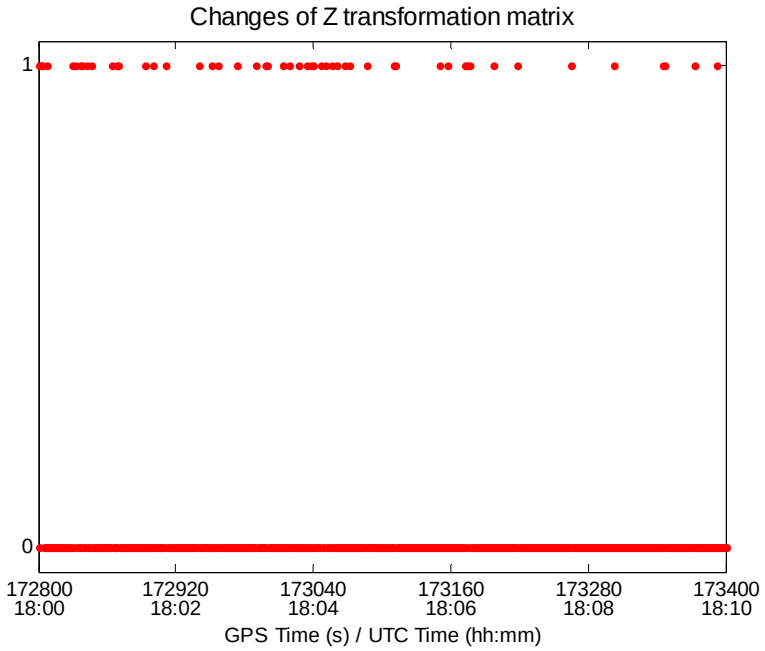

Figure 5.28: Changes in the decorrelation transformation matrix for the Case ① (GPS L1) over a 1 km baseline with high ionospheric error: 0 - the Z matrix is not changed compared to the previous epoch, 1 - the Z matrix is changed compared to the previous epoch

Figures 5.29 to 5.31 show the results for partially fixing 6 ambiguities. Similar trends in the ambiguity values of the fixed and unfixed subsets are shown compared to those obtained by fixing 4 ambiguities, and the position accuracies are further improved and they are still at centimetre levels. With fixing six instead of four ambiguities, the time to first fix increases from 37 to 44 seconds.

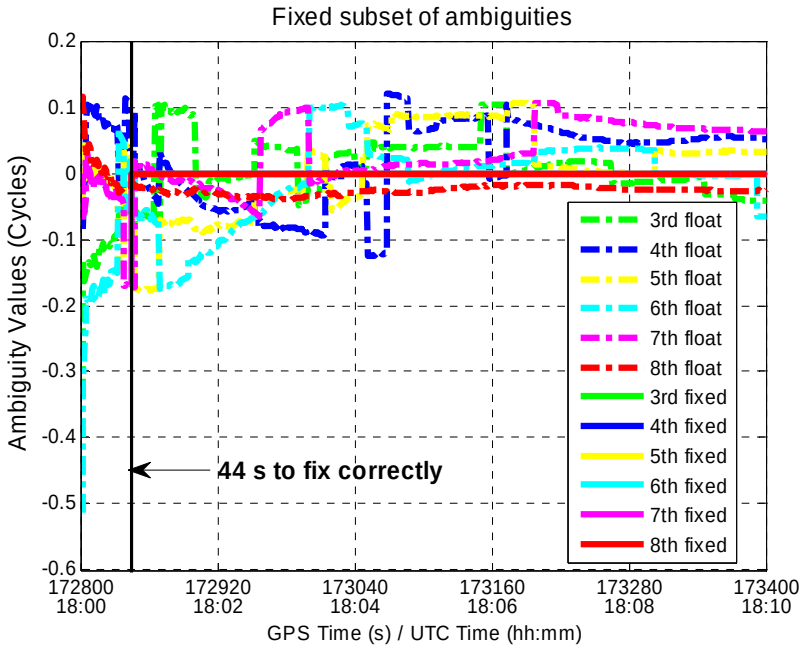

Figure 5.29: Float and fixed values of the fixed partial subset (6 ambiguities) in the Case ① (GPS L1) over a 1 km baseline with high ionospheric error

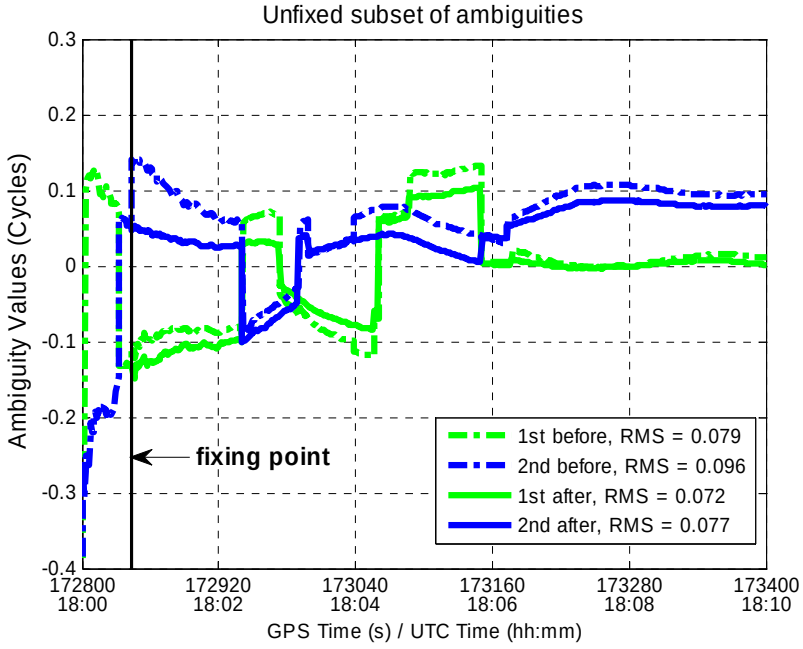

Figure 5.30: The values of the unfixed partial subset (2 ambiguities) before and after the partial ambiguity fixing in the Case ① (GPS L1) over a 1 km baseline with high ionospheric error

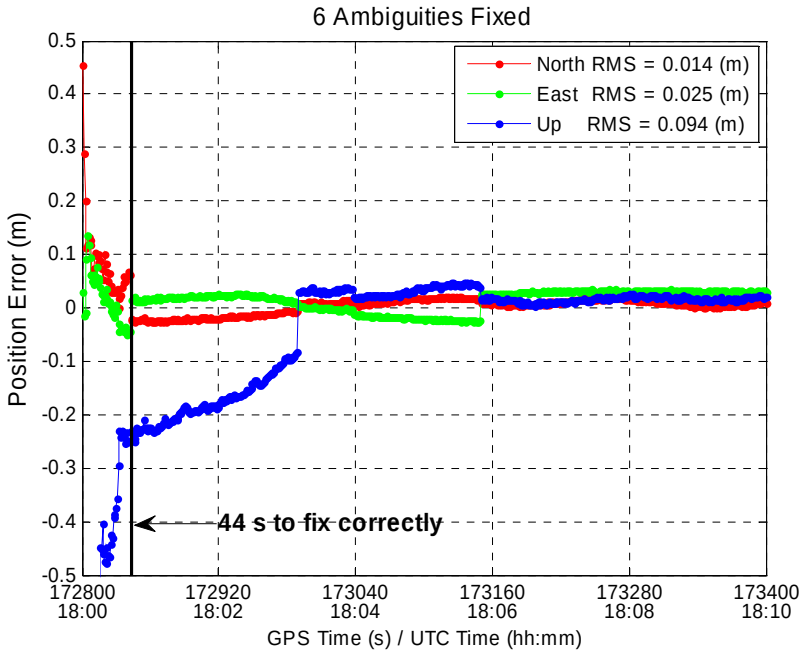

Figure 5.31: Position error with 6 ambiguities correctly fixed in the Case ① (GPS L1) over a 1 km baseline with high ionospheric error

Figures 5.32 and 5.33 show the results for fixing all 8 ambiguities in the GPS L1 case. Though it takes longer time to fix them all (51 s) comparing to fixing four (37 s) or six (44s) of them, the position accuracies are significantly improved to millimetre levels. This shows that ambiguity partial fixing can reduce the time to first fix while at the sacrifice of decreasing position accuracies.

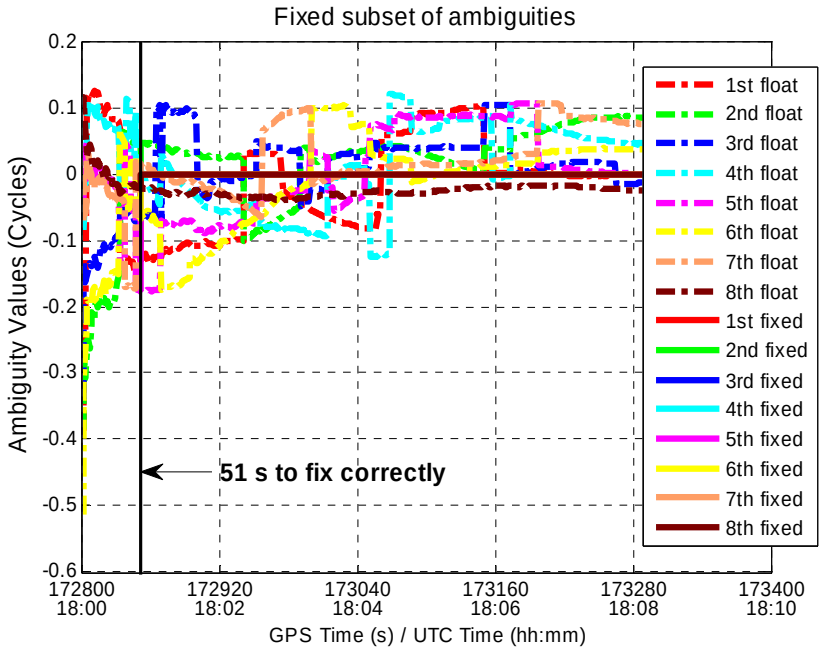

Figure 5.32: Float and fixed values of the fixed partial subset (8 ambiguities) in the Case ① (GPS L1) over a 1 km baseline with high ionospheric error

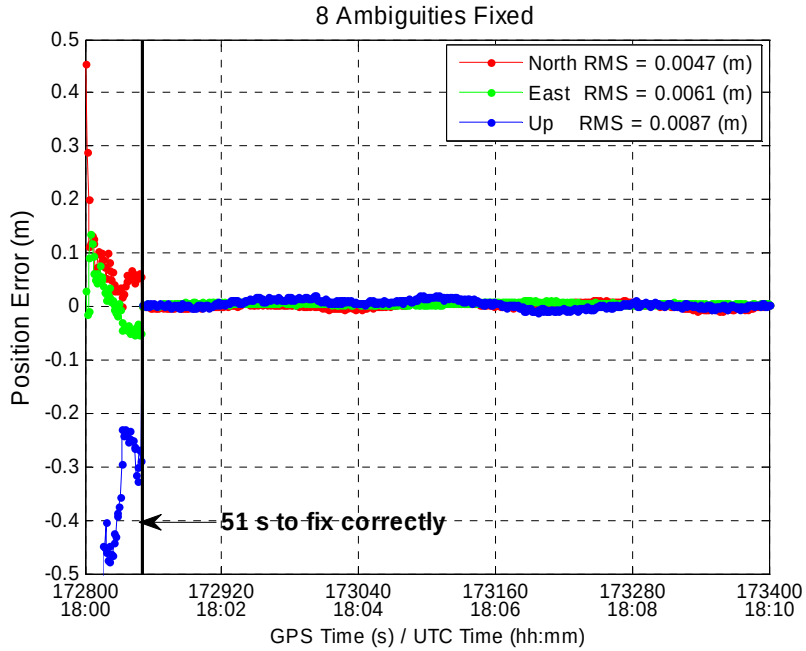

Figure 5.33: Position errors with all 8 ambiguities correctly fixed in the Case ① (GPS L1) over a 1 km baseline with high ionospheric error

The above results for partial fixing are interesting since trade-offs can be made on the time to fix ambiguities and position accuracies. If a fixed position solution needed to be obtained quickly and the requirements for position accuracies are not very high, e.g., millimetre level, a fixed solution with only fixing a subset of all float ambiguities could be a good option for this kind of application. Furthermore, fixing a subset quickly does not preclude the user from continuing to fix more ambiguities as a function of time. As such this method could be used to provide a temporary improvement in positioning accuracy while the full ambiguity set is still being validated. The advantages of partial fixing will be further demonstrated for the multi-frequency multi-GNSS cases below.

Case ④: Triple-frequency GPS Observations

Figures 5.34-37 show the results of partially fixing different numbers of ambiguities when multiple frequency GPS observations are used (24 ambiguities in total). The selection of partial ambiguity sets also starts from the last one in the ambiguity vector, which is a mixture of ambiguities on all three frequencies after the LAMBDA decorrelation. The same trends as the case of using GPS L1 observations can be observed and it takes a shorter time to get fixed solutions since greater ambiguity decorrelation is achieved with three-frequency GPS observations. Changes in the decorrelation matrices and the values of ambiguities are not shown due to the similarities with Case ①.

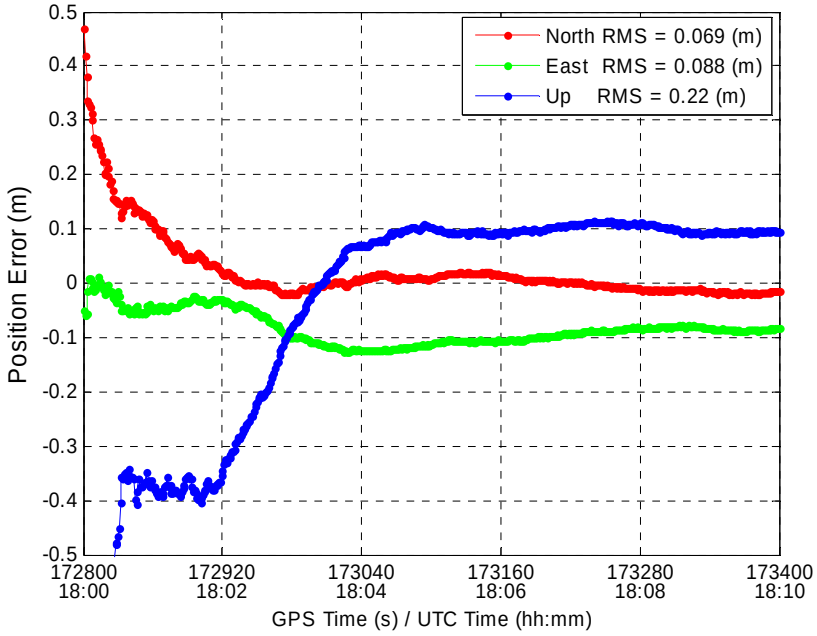

Figure 5.34: Position errors of the float solution using GPS L1, L2 and L5 observations over a 1 km baseline with ionospheric error

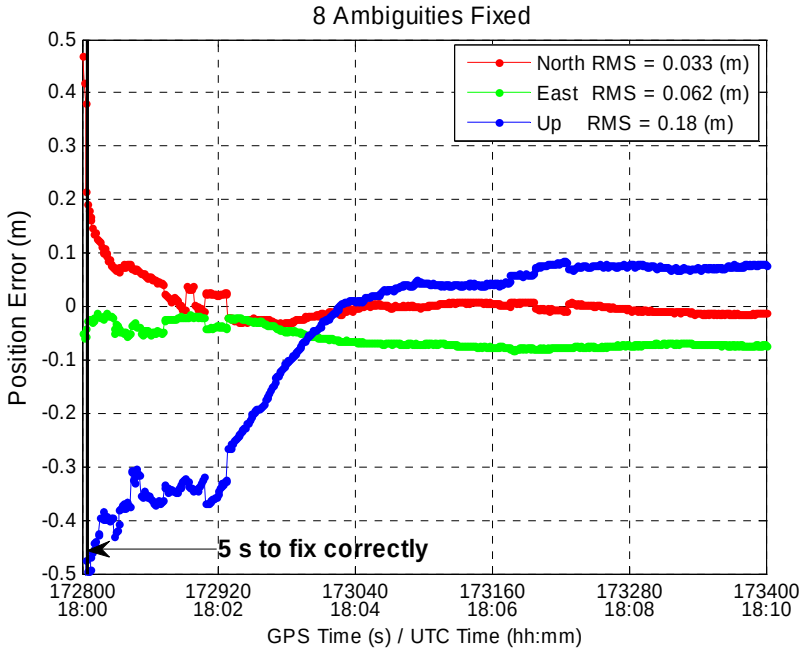

Figure 5.35: Position errors with 8 ambiguities correctly fixed in the GPS L1, L2 and L5 case over a 1 km baseline with high ionospheric error

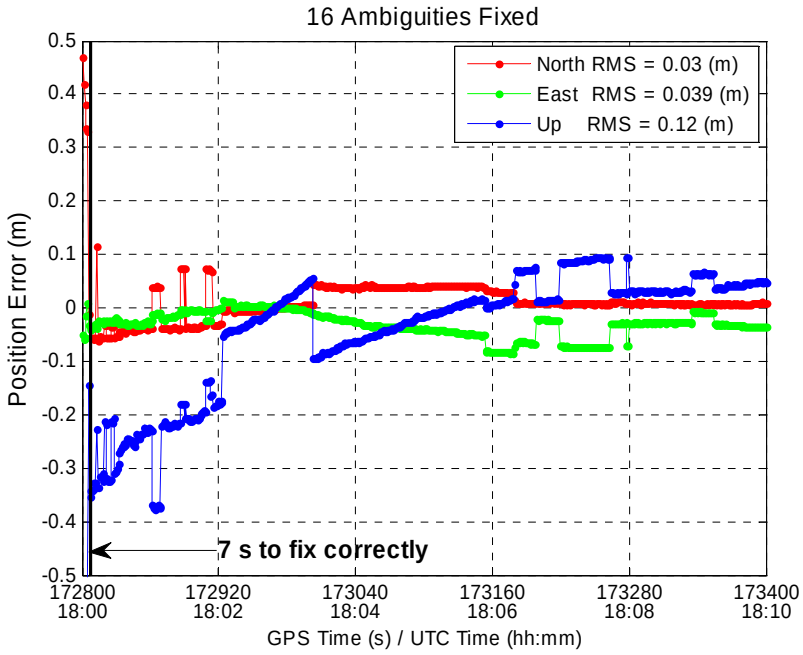

Figure 5.36: Position errors with 16 ambiguities correctly fixed in the GPS L1, L2 and L5 case over a 1 km baseline with high ionospheric error

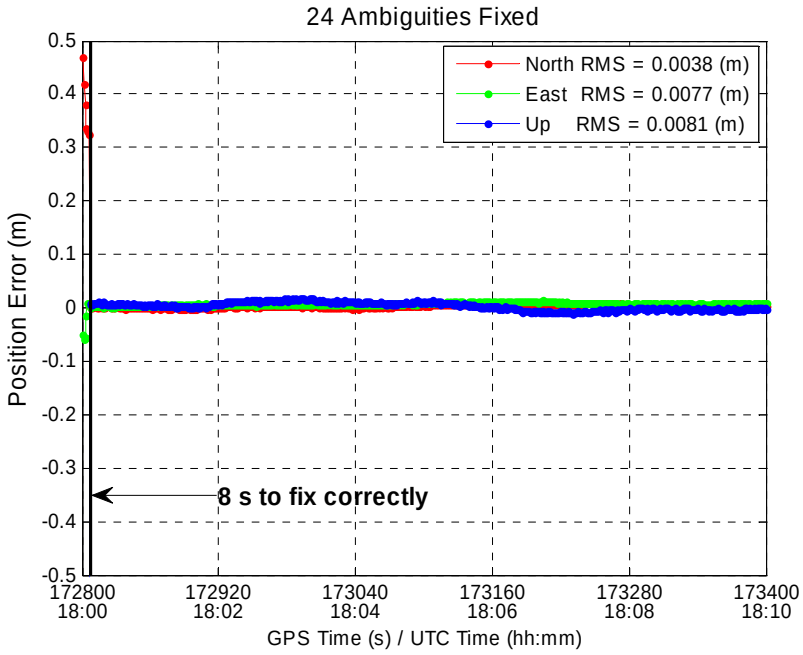

Figure 5.37: Position errors with 24 ambiguities correctly fixed in the GPS L1, L2 and L5 case over a 1 km baseline with high ionospheric error

Case ⑥: Dual-frequency GPS and Galileo Observations

Figures 5.38-41 show the results of partial fixing ambiguities on two common frequencies of GPS/Galileo (30 ambiguities in total). The position accuracies improve as more ambiguities are fixed while it takes more or less the same amount of time to fix different numbers of ambiguities. This is due to the fact that the enhanced satellite geometry improves the float ambiguity estimates and the conditional variances for different ambiguities are small and thus the PCF value for each ambiguity is very close to one, making fixing additional ambiguities relatively easy.

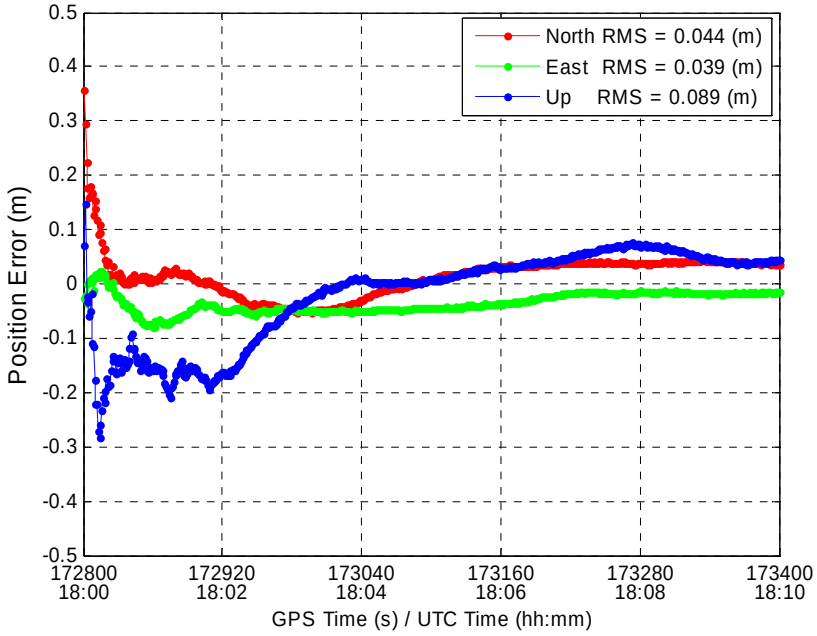

Figure 5.38: Position errors of float solutions in the GPS L1, L5 and Galileo E1, E5a case over a 1 km baseline with high ionospheric error

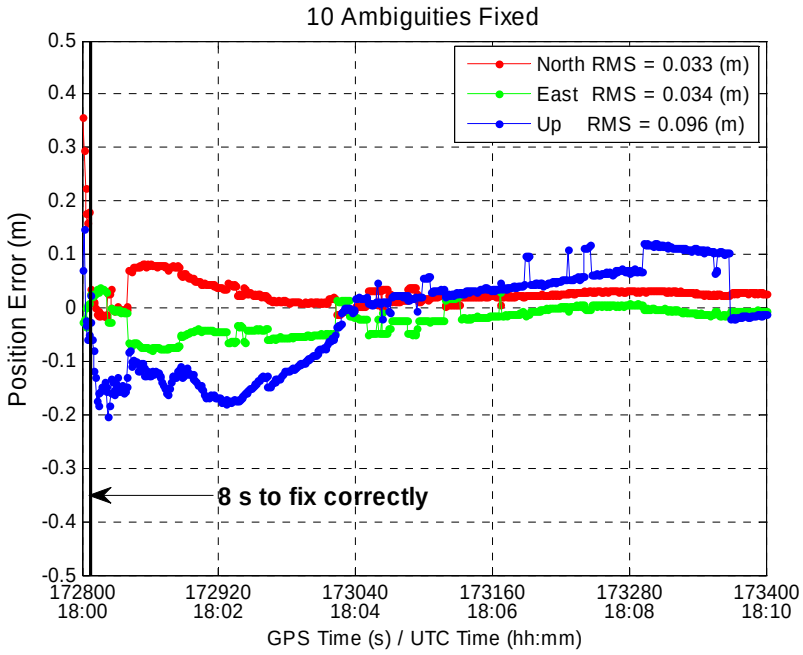

Figure 5.39: Position errors with 10 ambiguities correctly fixed in the GPS L1, L5 and Galileo E1, E5a case over a 1 km baseline with high ionospheric error

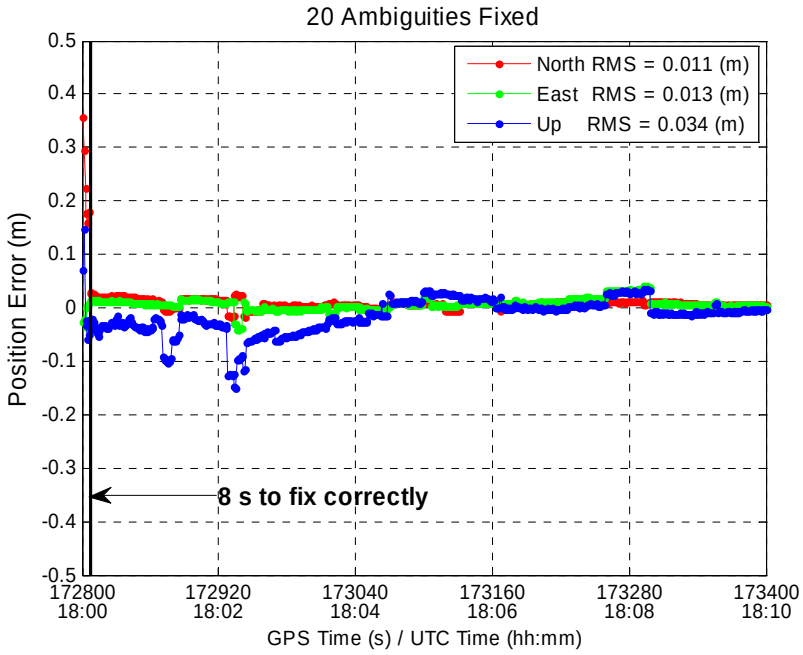

Figure 5.40: Position errors with 20 ambiguities correctly fixed in the GPS L1, L5 and Galileo E1, E5a case over a 1 km baseline with high ionospheric error

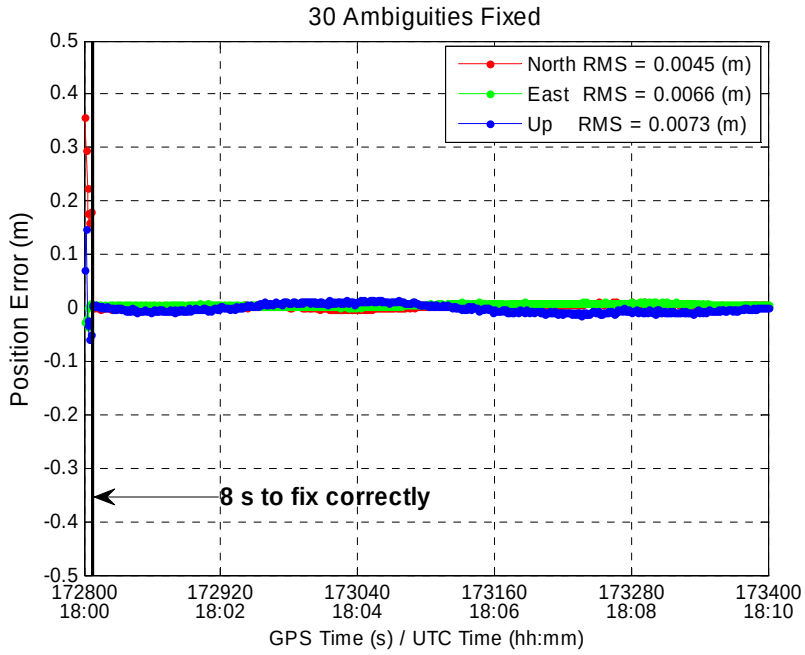

Figure 5.41: Position errors with 30 ambiguities correctly fixed in the GPS L1, L5 and Galileo E1, E5a case over a 1 km baseline with high ionospheric error

5.4.2 Summary of Results with Partial Fixing Over Different Baselines

The results of partial fixing ambiguities using observations on different subsets of GPS/Galileo frequencies over three different baselines are summarized in Tables 5.6-8. For the three simulated cases in this single simulation run, the position errors decrease with an increase in the number of fixed ambiguities. When single- or triple-frequency GPS observations are used, the time to correctly fix ambiguities (TTCFA) increases with more and more ambiguities fixed. However, there is no significant difference for TTCFA when GPS and Galileo observations are used together. This is due to the fact that the enhanced geometry of GPS/Galileo improves the accuracies of float ambiguities, thus the differences of the PCF values with fixing different numbers of ambiguities are not

significant. Over the 10 km baseline, the float ambiguities are significantly biased by spatially decorrelated ionosphere, which leads to the failure of fixing all ambiguities, while it is still possible to fix a partial set of them and the partial fixed position solutions are generally better than the float ones as shown in Table 5.8.

Table 5.6: Position errors, TTCFA with fixing different numbers of ambiguities using subsets of GPS/Galileo observations over a 1 km baseline with high ionospheric error

Observations	No. Fixed	Position Error (cm)			TTCFA (s)
		North	East	Up	
GPS L1 (①)	Float	4.8	8.0	19.0	-
	4	2.1	3.1	12.0	37
	6	1.4	2.5	9.4	44
	8	0.5	0.6	0.9	51
GPS L1, L2, L5 (④)	Float	6.9	8.8	22.0	-
	8	3.3	6.2	18.0	5
	16	3.0	3.9	12.0	7
	24	0.4	0.8	0.8	8
GPS L1, L5 and Galileo E1, E5a (⑥)	Float	4.4	3.9	8.9	-
	10	3.3	3.4	9.6	8
	20	1.1	1.3	3.4	8
	30	0.5	0.7	0.7	8

Table 5.7: Position errors, TTCFA with fixing different number of ambiguities using subsets of GPS/Galileo observations over a 5 km baseline with high ionospheric error

Observations	No. Fixed	Position Error (cm)			TTCFA (s)
		North	East	Up	
GPS L1 (①)	Float	3.9	9.6	26.0	-
	4	6.4	8.5	16.0	95
	6	3.9	6.7	12.0	107
	8	1.4	3.1	2.8	117
GPS L1, L2, L5 (④)	Float	10.0	12.0	35.0	-
	8	8.9	11.0	29.0	17
	16	4.8	5.0	19.0	25
	24	1.8	3.8	3.4	26
GPS L1, L5 and Galileo E1, E5a (⑥)	Float	9.7	3.6	16.0	-
	10	6.6	3.9	22.0	25
	20	2.6	2.6	5.7	25
	30	1.9	3.2	3.2	25

Table 5.8: Position errors, TTCFA with fixing different number of ambiguities using subsets of GPS/Galileo observations over a 10 km baseline with high ionospheric error

Observations	No. Fixed	Position Error (cm)			TTCFA (s)
		North	East	Up	
GPS L1 (①)	Float	5.9	11.0	32.0	-
	4	12.0	13.0	25.0	114
	6	14.0	22.0	29.0	146
	8	-	-	-	No fix
GPS L1, L2, L5 (④)	Float	16.0	15.0	51.0	-
	8	14.0	15.0	45.0	26
	16	8.6	7.9	28.0	36
	24	-	-	-	No Fix
GPS L1, L5 and Galileo E1, E5a (⑥)	Float	9.9	3.4	16.0	-
	10	5.0	7.9	23.0	33
	20	-	-	-	No fix
	30	-	-	-	No fix

5.5 Summary

This chapter presents the results of AR performance evaluation using observations on different subsets of GPS/Galileo frequencies and the partial fixing ambiguity in three selected GPS/Galileo cases. The results show that better AR performance can be obtained

when using multiple-frequency GPS observations and a combined dual-frequency GPS/Galileo is better than a three-frequency GPS in terms of position accuracies and time to fix ambiguities. With partially fixing a subset of all ambiguities, the position accuracies improves as more ambiguities are fixed while it generally takes a longer time to fix more and more ambiguities. The partial fixing is effective when it is hard to fix all ambiguities to get the best position solutions and it shows better positioning accuracies than the float solutions. However, in most cases studied, full fixing could be obtained several seconds after partial fixing, suggesting that the best potential applications for partial fixing are those that require improved position solutions in very short periods of time, before full fixing of all available ambiguities is possible.

Chapter Six: Conclusions and Recommendations for Future Work

The overall goal of this research was to investigate ambiguity resolution (AR) performance of GPS/Galileo kinematic positioning using observations from different subsets of frequencies. To meet this goal a single difference carrier phase GNSS processor was developed and a novel strategy for partial fixing ambiguities was implemented. Covariance simulations of ambiguity resolution performance based on the geometry of observed satellites were carried out under various scenarios using observations on different subsets of GPS or/and Galileo frequencies. An evaluation of AR performance was also performed using a phase processor with software simulated GPS/Galileo observations. The phase processor was used both on different subsets of GPS and Galileo frequencies and to test the strategy of partial fixing ambiguities in the LAMBDA decorrelated Z-ambiguity domain. The findings in each chapter and recommendations for future work are summarized as follows.

6.1 Key Findings

1) It was found that single-differencing was superior to double-differencing in carrier phase GNSS positioning applications in terms of ease of implementation. Hence the single-differencing scheme was used in a carrier phase processor development.

2) It was shown that the LAMBDA method is better than the various cascading AR approaches in terms of the flexibility of carrier phase processing with multi-carrier GNSS observations.

3) With an increase in the number of observed satellites, which means enhanced satellite geometry, it took a shorter time to get a specific level of PCF for all scenarios of the covariance simulations performed.

4) Through covariance analysis, it was found that single-frequency combined GPS/Galileo had comparable performance with GPS L1/L2 or L1/L5 over the short baseline (it took around 5 seconds to reach 10^{-8} PIF for three cases) when the spatial decorrelation of the ionospheric error was not significant. The triple-frequency GPS L1/L2/L5 only showed slightly improved performance to GPS L1/L2 or L1/L5 - the former only took 2 seconds less than the later to reach 10^{-8} PIF over the short baseline.

5) Dual-frequency combined GPS/Galileo had the best performance among all six cases of frequency combinations over three different baselines - 4 km, 20 km and 120 km using covariance simulation, which took about 2, 50 and 100 seconds to reach 10^{-8} PIF, respectively.

6) Using covariance analysis, the strategy of partial fixing ambiguities did not show improved performance over the short baseline while significant improvements

were observed over the medium and long baselines where the tropospheric and ionospheric errors were significantly decorrelated. The time to fix different number of ambiguities (took 10^{-8} PIF as a threshold) over short baseline was less than 10 seconds, while it was more than 1000 seconds for medium and long baselines.

7) The different applications require fixing ambiguities with different PCF thresholds. It took 15 seconds less to fix ambiguities at 99% PCF level for surveying applications than fixing them at 99.999999% PCF level for safety-of-life applications using GPS L1 observations. The difference was more significant (reached to a hundred of seconds) when other sets of observations were used.

8) For results of the software simulator generated data, the MTTFFA (Mean Time To First Fix Ambiguities) decreased from more than 60 epochs using GPS L1 observations to less than 10 seconds when using two or three frequency GPS/Galileo observations over the 1 km and 5 km baselines. Multi-carrier observations provided better ability to identify the wrong ambiguity sets over the 10 km baseline where the ionospheric error was prominent. The combined dual-frequency GPS/Galileo showed better performance than a three-frequency GPS - 2 versus 3 seconds to fix ambiguities over the 1 km baseline and 88.75% versus 77.50% of PCFA (percent of correct fix ambiguities) over the 5 km baseline and 2.50% versus 15.00% of PIFA (percent of incorrect fix ambiguities) over the 10 km baseline, which confirmed conclusions 4) and 5).

9) With partial ambiguity fixing, the position accuracies improved from decimetre levels (float solution with no ambiguity fixed) to less than a decimetre with subsets of ambiguities fixed and to 0.5~3 centimetres when all ambiguities were fixed. It generally took longer time (1 to 20 seconds) to fix more ambiguities. The partial fixing was effective when it was hard to fix all ambiguities to get the best fixed position solutions and it showed higher positioning accuracies than the float solutions.

6.2 Recommendations for Future Work

Though efforts have been made to study the AR performance of GPS/Galileo kinematic positioning using observations on different subsets of frequencies, there are still many unanswered questions related to this topic. The following are some recommendations for future work.

1) The work in this thesis was based on the Kalman filter covariance analysis and processing of software simulated data. One important assumption was made regarding the time reference frame of GPS and Galileo: their time reference systems were accurately synchronized with each other thus the approach of tightly-coupling GPS/Galileo is adopted. However, the assumption may not hold true in the case when real data is used. The synchronization accuracy of 5 ns (equivalent to 1.5 m) is not accurate enough to make double-differencing between

GPS and Galileo, thus each system has to use its own base satellite. Though the coordinate reference frames of both systems are realizations of ITRF, the discrepancy between WGS84 (for GPS) and GTRF (for Galileo) has to be carefully considered and dealt with through conversion parameters between two systems for very high precision applications such as geodynamics etc.

2) In Chapter 5, the AR performance evaluations were performed over short baselines that are not greater than 10 km. It was shown that even combined GPS/Galileo cannot fix ambiguities quickly in the case of a large ionospheric bias present in the observations. It has been expected that long baseline kinematic positioning can be achieved with the combination of GPS and Galileo. The ionospheric bias is prominent over long baselines. An effective method to eliminate or reduce the ionospheric error is through an approach of stochastic ionospheric modeling as shown in Liu (2003) and Zhang (2005). Implementation of this method in the processor will be of great importance for future work.

3) As found by Teunissen & Verhagen (2008), the foundation of ratio test used in ambiguity validation was not correct, a validation criteria based on fixed failure rate was proposed and showed better performance (Verhagen 2007). Ambiguity validation in carrier phase GNSS positioning is still an open problem and needs further investigation.

4) Observations were generated using a software simulator in Chapter 5. Given that

GPS L5 and Galileo will not be fully operational for quite some time (10 years away in the current schedule), the next step in the investigation would be to use simulated data that has been generated in a hardware simulator and actually received by a functioning GPS/Galileo receiver.

5) In the ambiguity partial fixing strategy implemented in this thesis, the selection of a subset of ambiguities was done in an arbitrary way: a certain number of ambiguities were extracted from the ambiguity vector starting from the last entry in the vector. However, this subset of ambiguities might not necessarily have the smallest PCF among all possible subsets with the same number of ambiguities. This was due to the fact that the conditional variances in LAMBDA decorrelation were not completely sorted in a decreasing order. Further decorrelation can be pursued to make the conditional variances sorted in a more decreasing order as those shown in Chang et al. (2005). Practical application of the partial ambiguity fixing to RTK surveying should be further investigated. For example, criteria to choose the number of fixed ambiguities based on a trade-off between probability of correct fix and position solution accuracy should be carefully considered.

References

Allain, D.J. and C.N. Mitchell (2008) "Ionospheric Delay Corrections for Single-frequency GPS Receivers over Europe using Tomographic Mapping", *GPS Solutions*, doi: 10.1007/s10291-008-0107-y

Alves, P. (2001) "The Effect of Galileo on Carrier Phase Ambiguity Resolution", In *Proceedings of 14th International Technical Meeting of the Satellite Division (ION GPS-01)*, 11-14 September, Salt Lake City, UT, pp. 2086-2095

Alves, P., Y.W. Ahn and G. Lachapelle (2003) "The Effects of Network Geometry on Network RTK Using Simulated GPS Data", In *Proceedings of 16th International Technical Meeting of the Satellite Division (ION GPS/GNSS 2003)*, 9-12 September, Portland, OR, pp. 1417-1427

Aragón Ángel, M.A. and F. Amarillo Fernández (2006) "Advanced Ionospheric Modelling for GNSS Single Frequency Users", In *Proceedings of 2006 IEEE/ION Position, Location And Navigation Symposium (PLANS 2006)*, 25-27 April, 2006, San Diego, CA, pp. 110-120

ARINC, Inc. (2004) *NAVSTAR GPS Space Segment / Navigation User Interfaces, ICD-GPS-200D*, El Segundo, CA, GPS NAVSTAR JPO SNC/CZ, Published on 7 December, 2004

Avila-Rodriguez, J.-A., G.W. Hein, S. Wallner, J.-L. Issler, L. Ries, L. Lestarquit, A. de Latour, J. Godet, F. Bastide, T. Pratt and J. Owen (2007) "The MBOC Modulation: The Final Touch to the Galileo Frequency and Signal Design", In *Proceedings of 20th International Technical Meeting of the Satellite Division (ION GNSS 2007)*, 25-28 September, 2007, Fort Worth, TX, pp. 1515-1529

Avila-Rodriguez, J.-A., G.W. Hein, S. Wallner, J.-L. Issler, L. Ries, L. Lestarquit, A. de Latour, J. Godet, F. Bastide, T. Pratt and J. Owen (2008) "The MBOC Modulation: The Final Touch to the Galileo Frequency and Signal Design", *NAVIGATION: Journal of the Institute of Navigation*: Vol. 55, No. 1, pp. 15-28

Avila-Rodriguez, J.-A., M. Irsigler, G.W. Hein and T. Pany (2005) "Performance of a Galileo PRS/GPS M-Code Combined Service", In *Proceedings of Institute of Navigation National Technical Meeting (ION NTM-2005)*, 21-24 January 2005, San Diego, CA, pp. 754-768

Belabbas, B., S. Schlueter and M.Z. Sadeque (2005) "Impact of NeQuick Correction Model to Positioning and Timing Accuracy using the Instantaneous Pseudo Range Error of Single Frequency Absolute Positioning Receivers", In *Proceedings of 18th International Technical Meeting of the Satellite Division (ION GNSS 2005)*, 13-16 September, 2005, Long Beach, CA, pp. 711-722

Bilich, A., K.M. Larson and P. Axelrad (2008) "Modeling GPS Phase Multipath with SNR: Case Study from the Salar de Uyuni, Boliva", *Journal of Geophysical Research*: Vol. 113, No. B04401, doi: 10.1029/2007JB005194

Black, H.D., and A. Eisner (1984) "Correcting Satellite Doppler Data for Tropospheric Effects", *Journal of Geophysical Research*: Vol. 89, No. D2, pp. 2616-2626

Bonhoure, B., I. Vanschoenbeek, M. Boschetti and J. Legenne (2008) "GPS - Galileo Urban Interoperability Performance with the GPS - Galileo Time Offset", In *Proceedings of 21st International Technical Meeting of the Satellite Division (ION GNSS-2008)*, 16-19 September, 2008, Savannah, GA, pp. 971-981

Bonillo-Martínez, C., M. Toledo-López and M. Romay-Merino (1999) "The Benefits of the GPS Three Frequencies on the Ambiguity Resolution Techniques", In *Proceedings of 12th International Technical Meeting of the Satellite Division (ION GPS-99)*, 14-17 September, Nashville, TN, pp. 1737-1746

Brown, R.G. and P.Y.C. Hwang (1997) *Introduction to Random Signals and Applied Kalman Filtering*, Third Edition, John Wiley & Sons, Inc., New York

Cao, W., K. O'Keefe and M.E. Cannon (2007) "Partial Ambiguity Fixing within Multiple Frequencies and Systems", In *Proceedings of 20th International Technical Meeting of the Satellite Division (ION GNSS 2007)*, 25-28 September, 2007, Fort Worth, TX, pp. 1515-1529

Chang, X.-W., X. Yang and T. Zhou (2005) "MLAMBDA: A modified LAMBDA Method for Integer Least-squares Estimation", *Journal of Geodesy*: Vol. 79, No. 9, pp. 552-565

Cocard, M., S. Bourgon, O. Kamali and P. Collins (2008) "A Systematic Investigation of Optimal Carrier-phase Combinations for Modernized Triple-frequency GPS", *Journal of Geodesy*: Vol. 82, No. 9, pp. 555-564

Conley, R., R. Cosentino, C. J. Hegarty, E.D. Kaplan, J.L. Leva, M. Uijt de Haag and K. V. Dyke (2005) "Performance of Stand-Alone GPS", In *Understanding GPS: Principles and Applications*, Eds. Kaplan, D. K. and C. J. Hegarty, Artech House, Inc., pp. 301-378

Cosentino, R.J., D.W. Diggle, M. Uijt de Haag, C.J. Hegarty, D. Milbert and J. Nagle (2005) "Differential GPS", In *Understanding GPS: Principles and Applications*, Eds. Kaplan, D. K. and C. J. Hegarty, Artech House, Inc., pp. 379-458

China Satellite Navigation Project Center (CSNPC) (2008) "Overview of Compass/ Beidou Navigation Satellite System", Available at http://www.unoosa.org/pdf/icg/2008/expert/2-1a.pdf, last accessed on 9 January, 2009

Dai, L., D. Eslinger and T. Sharpe (2007) "Innovative Algorithms to Improve Long Range RTK Reliability and Availability", In *Proceedings of Institute of Navigation National Technical Meeting (ION NTM-2006)*, San Diego, CA., 22-24 January, 2007, pp. 860-872

Dai, L., D. Eslinger, T. Sharpe and R. Hatch (2008) "Partial Search Carrier-Phase Integer Ambiguity Resolution", U.S. Patent Application No. 20080297408, Filed on 12 May, 2008

Department of Defence (2008) *Global Positioning System Standard Positioning Service (GPS SPS) Performance Standard*, 4th Edition, September 2008

Dellago, R., E. Detoma and F. Luongo (2003) "Galileo-GPS Interoperability And Compatibility: A Synergetic Viewpoint", In *Proceedings of 16th International Technical Meeting of the Satellite Division (ION GPS/GNSS 2003)*, 9-12 September, Portland, OR, pp. 542-548

de Jonge, P.J., and C.C.J.M., Tiberius (1996) *The LAMBDA Method for Integer Ambiguity Estimation: Implementation Aspects*, LGR Series, No. 12, Delft Geodetic Computing Centre, Delft University of Technology, 1996

Dong, L. (2004) *SimGNSSII™ Algorithm Design Document*, Internal Report, PLAN Group, Department of Geomatics Engineering University of Calgary, 31 March, 2004, Calgary, Canada

Ericson, S. (1999) "A Study of Linear Phase Combinations in Considering Future Civil GPS Frequencies", In *Proceedings of Institute of Navigation National Technical Meeting (ION NTM-99)*, San Diego, CA, 25-27 January, 1999, pp. 677-686

Essifeller, B., C. Tiberius, P. Thomas, B. Robert, T. Schueler and G. Heinrichs (2001) "Real-Time Kinematic in the Light of GPS Modernization and Galileo", In *Proceedings of 14th International Technical Meeting of the Satellite Division (ION GPS-01)*, 11-14 September, Salt Lake City, UT, pp. 650-662

ESA Galileo Project Office (2008) *GIOVE-A+B (#102) Navigation Signal-In-Space Interface Control Document*, Published on 8 August, 2008, Noordwijk, The Netherlands

ESA / European GSA (2008) *Galileo Open Service Signal In Space Interface Control Document (OS SIS ICD)*, Draft 1, Published on 14 February, 2008, Brussels, Belgium

Falcone, M. (2008) "Galileo Programme Status", In *Proceedings of 21st International Technical Meeting of the Satellite Division (ION GNSS-2008)*, 16-19 September, 2008, Savannah, GA, pp. 453-492

Falcone, M., P. Erhard and G.W. Hein (2005) "Galileo", In *Understanding GPS: Principles and Applications*, Eds. Kaplan, D. K. and C. J. Hegarty, Artech House, Inc., pp. 559-594

Feairheller, S. and R. Clark (2005) "Other Satellite Navigation Systems", In *Understanding GPS: Principles and Applications*, Eds. Kaplan, D. K. and C. J. Hegarty, Artech House, Inc., pp. 595-634

Feess, W.A., and S.G. Stephens (1987) "Evaluation of GPS Ionospheric Time-Delay Model", *IEEE Transaction on Aerospace and Electronic Systems*: Vol. 23, No. 3, pp. 332-338

Feng, Y. (2004) "A Complete Geometry-Free Approach to Three Carrier Ambiguity Resolutions", In *Proceedings of International Symposium on GPS/GNSS*, 6-8 December, Sydney, Australia

Feng, Y. (2005) "Long-Range Kinematic Positioning Using Three Frequency GNSS Signals", In *Proceedings of Institute of Navigation National Technical Meeting (ION NTM-2005)*, 24-26 January, San Diego, CA, pp. 694-702

Feng, Y. and C. Rizos (2008) "Network-based Geometry-free Three Carrier Ambiguity Resolution and Phase Bias Calibration", *GPS Solutions*: Vol. 13, No. 1, pp. 43-56

Forssell, B., M. Martin-Neira and R.A. Harris (1997) "Carrier Phase Ambiguity Resolution in GNSS-2", In *Proceedings of 10th International Technical Meeting of the Satellite Division (ION GPS-97)*, 16-19 September, Kansas City, MI, pp. 1727-1736

Fyfe, P., K. Davis, I. Jeng, C. Kelley and C. Mosley (2002) "GPS and Galileo - Interoperability for Civil Aviation Applications", In *Proceedings of 15th International Technical Meeting of the Satellite Division (ION GPS-02)*, 24-27 September, Portland, OR, pp. 289-302

Gower, A. (2008) "The System: The Promise of OCX", *GPS World*, September, 2008, Available at http://sidt.gpsworld.com/gpssidt/article/articleDetail.jsp?id=545023, last accessed on 23 December, 2008

Grewal, M.S. and A.P. Andrews (2001) *Kalman Filtering: Theory and Practice Using MATLAB*, Second Edition, John Wiley & Sons, Inc., New York

Guo, J. and R.B. Langley (2003) "A New Tropospheric Propagation Delay Mapping Function for Elevation Angles Down to 2°", In *Proceedings of 16th International Technical Meeting of the Satellite Division (ION GPS/GNSS 2003)*, 9-12 September, Portland, OR, pp. 368-376

Hahn J. and E. Powers (2004) "GPS and Galileo Timing Interoperability", In *Proceedings of European Navigation Conference (ENC-GNSS 2004)*, 16-19 May, Rotterdam, Netherlands

Hatch, R. (1996) "The Promise of a Third Frequency", *GPS World*: Vol. 7, No. 5, pp. 55-58

Han S., and C. Rizos (1999) "The Impact of Two Additional Civilian GPS Frequencies on Ambiguity Resolutions Strategies", In *Proceedings of the Institute of Navigation 55th Annual Technical Meeting (ION AM-99)*, 28-30 June, Cambridge, MA, pp. 315-321

Hein, G.W., J. Godet, J.L. Issler, J.C. Martin, P. Erhard, R. Lucas-Rodriguez and T. Pratt (2002) "Status of Galileo Frequency and Signal Design", In *Proceedings of 15th International Technical Meeting of the Satellite Division (ION GPS-02)*, 24-27 September, Portland, OR, pp. 266-277

Hein, G.W. (2007) "Towards a GNSS System of Systems", In *Proceedings of 20th International Technical Meeting of the Satellite Division (ION GNSS 2007)*, 25-28 September, 2007, Fort Worth, TX, pp. 22-30

Hein, G.W., J. Rodriguez, S. Wallner, B. Eissfeller , T. Pany and A. Hartl. (2007) "Envisioning A Future GNSS Systems of Systems: Part 1", *Inside GNSS*: Vol. 2, No. 1, pp. 58-67

Hofmann-Wellenhoff, B., H. Lichtenegger, and J. Collins (2001) *Global Positioning System: Theory and Practice*, 5th Edition, Springer-Verlag, Berlin

Hopfield, H.S. (1970) *Tropospheric Effect on Electromagnetically Measured Range: Prediction from Surface Weather Data*, Applied Physics Laboratory, Johns Hopkins University, Baltimore, MD

Hoque, M.M., and N. Jakowski (2008) "Estimate of Higher Order Ionospheric Errors in GNSS Positioning", *Radio Science*: Vol. 43, RS5008, doi: 10.1029/2007RS003817

Huang, J. and F. van Graas (2006) "Comparison of Tropospheric Decorrelation Errors in the Presence of Severe Weather Conditions in Different Areas and Over Different Baseline Lengths", In *Proceedings of 19th International Technical Meeting of the Satellite Division (ION GNSS 2006)*, 26-29 September, 2006, Fort Worth, TX, pp. 2769-2787

IGS (2008) *IGS Product Table*, International GNSS Service, Available at http://igscb.jpl.nasa.gov/components/prods.html, last accessed on 23 December, 2008

Information Analytical Centre (2008) *GLONASS Constellation Status*, available at http://www.glonass-ianc.rsa.ru/, last accessed on 13 February, 2009

Inside GNSS (2007a) *EU Finance Ministers Approve Galileo Funds*, Available at http://www.insidegnss.com/node/403, last accessed on 23 December, 2008

Inside GNSS (2007b) *Transport Ministers Put Galileo Back on Track*, Available at http://www.insidegnss.com/node/419, last accessed on 23 December, 2008

Ji, S. (2007) *Assessing the New GNSS System Performance*, PhD Thesis, Department of Land Surveying and Geo-Informatics, The Hong Kong Polytechnic University, Hong Kong

Ji, S., W. Chen, C. Zhao, X. Ding and Y. Chen (2007) "Single epoch ambiguity resolution for Galileo with the CAR and LAMBDA methods", *GPS Solutions*: Vol. 11, No. 4, pp. 259-268

Julien, O., P. Alves, M.E. Cannon and W. Zhang (2003) "A Tightly Coupled GPS/Galileo Combination for Improved Ambiguity Resolution", In *Proceedings of European Navigation Conference (ENC-GNSS 2003)*, 22-25 April, Graz, Austria, 14 pp

Jung, J. (1999) "High Integrity Carrier Phase Navigation for Future LAAS Using Multiple Civilian GPS Signals", In *Proceedings of 12th International Technical Meeting of the Satellite Division (ION GPS-99)*, 14-17 September, Nashville, TN, pp. 727-736

Jung, J., P. Enge and B. Pervan (2000) "Optimization of Cascade Integer Resolution with Three Civil GPS Frequencies", In *Proceedings of 13th International Technical Meeting of the Satellite Division (ION GPS-00)*, 19-22 September, 2000, Salt Lake City, UT, pp. 2191-2201

Kaplan, D.K. (2005) "Introduction", In *Understanding GPS: Principles and Applications*, Eds. Kaplan, D. K. and C. J. Hegarty, Artech House, Inc., pp. 1-20

Kintner, P.M., B.M. Ledvina and E.R. de Paula (2006) "GPS and Ionospheric Scintillations", *Space Weather*: Vol. 5, S09003, doi: 10.1029/2006SW000260.

Klobuchar, J.A. (1996) "Ionospheric Effects on GPS", In *Global Positioning System, Theory and Application*, Vol. 1, Eds, Parkinson, B. and Spilker, J., American Institute of Aeronautics and Astronautics, Inc., pp. 485-514

Klobuchar J. A. (1987) "Ionospheric Time-delay Algorithm for Single Frequency Users", *IEEE Transaction on Aerospace and Electronic Systems*: Vol. 23, No. 3, pp. 325-331

Klobuchar J. A. (2001) "Eye on the Ionosphere: Correction Methods for GPS Ionospheric Range Delays", *GPS Solutions*: Vol. 5, No. 2, pp. 91-92

Lau, L. and P.A. Cross (2007) "Development and Testing of a New Ray-tracing Approach to GNSS Carrier-phase Multipath Modeling", *Journal of Geodesy*: Vol. 81, No. 11, pp. 713-732

Lawrence, D. (2009) "A New Method for Partial Ambiguity Resolution", In *Proceedings of Institute of Navigation International Technical Meeting (ION ITM-2009)*, 26-28 January, Anaheim, CA, pp. 652-663

Lawrence, D., R.B. Langley, D. Kim, F.C. Chan and B. Pervan (2006) "Decorrelation of Troposphere across Short Baselines", In *Proceedings of 2006 IEEE/ION Position, Location And Navigation Symposium (PLANS 2006)*, 25-27 April, 2006, San Diego, CA, pp. 94-102

Leandro, R., M. Santos and R.B. Langley (2006) "UNB Neutral Atmosphere Models: Development and Performance", In *Proceedings of Institute of Navigation National Technical Meeting (ION NTM-2006)*, Monterey, CA, 18-20 January, 2006, pp. 564-573

Luo, N., and G. Lachapelle (2003) "Relative Positioning of Multiple Moving Platforms using GPS", *IEEE Transactions on Aerospace and Electronic Systems*: Vol. 39, No. 3, pp. 936-948

Madden, D. (2008) "GPS Program Update", In *Proceedings of 21st International Technical Meeting of the Satellite Division (ION GNSS-2008)*, 16-19 September, 2008, Savannah, GA, pp. 412-430

McDonald, K.D. (2005) "GPS Modernization: Global Positioning System Planned Improvements", In *Proceedings of the Institute of Navigation 61st Annual Technical Meeting (ION AM-2005)*, 27-29 June, Cambridge, MA, pp. 36-53

Merrigan, M.J., E.R. Swift, R.F. Wong and J.T. Saffel (2002) "A Refinement to the World Geodetic System 1984 Referece Frame", In *Proceedings of 15th International Technical Meeting of the Satellite Division (ION GPS-02)*, 24-27 September, Portland, OR, pp. 289-302

Michael, T. and C. Hegarty (2003) "Performance Evaluations of the New GPS L5 and L2 Civil (L2C) Signals", In *Proceedings of Institute of Navigation National Technical Meeting (ION NTM-2003)*, 22-24 January, Anaheim, CA, pp. 521-535

Mowlam, A. (2004) "Baseline Precision Results Using Triple Frequency Partial Ambiguity Sets", In *Proceedings of 17th International Technical Meeting of the Satellite Division (ION GNSS-2004)*, 21-24 September, Long Beach, CA, pp. 2509-2518

Mowlam, A. and P.A. Collier (2004) "Fast Ambiguity Resolution Performance using Partially-Fixed Multi-GNSS Phase Observations", In *Proceedings of International Symposium on GPS/GNSS*, 6-8 December, Sydney, Australia

Neil, A.E. (1996) "Global Mapping Functions for the Atmosphere Delay at Radio Wavelengths", *Journal of Geophysical Research*: Vol. 101, No. B2, pp. 3227-3246

Ochieng, W.Y., K. Sauer, P.A. Cross, K.F. Sheridan, J. Iliffe, S. Lannelongue, N. Ammour and K. Petit (2001) "Potential Performance Levels of a Combined Galileo/GPS Navigation System", *Journal of Navigation*: Vol. 54, No. 2, pp. 185-197

Ochieng, W.Y., K.F. Sheridan, K. Sauer, X. Han, P.A. Cross, S. Lannelongue, N. Ammour and K. Petit (2002) "An Assessment of the RAIM Performance of a Combined Galileo/GPS Navigation System Using the Marginally Detectable Errors (MDE) Algorithm", *GPS Solutions*: Vol. 5, No. 3, pp. 42-51

O'Donnell, M., T. Watson, J. Fisher, S. Simpson, G. Brodin, E. Bryant and D. Walsh (2002) "A Study of Galileo Performance - GPS Interoperability and Discriminators for Urban and Indoor Environments", In *Proceedings of 15th International Technical Meeting of the Satellite Division (ION GPS-02)*, 24-27 September, Portland, OR, pp. 2160-2172

O'Keefe, K. (2001) "Availability and Reliability Advantages of GPS/Galileo Integration", In *Proceedings of 14th International Technical Meeting of the Satellite Division (ION GPS-01)*, 11-14 September, Salt Lake City, UT, pp. 2096-2104

O'Keefe, K., M.G. Petovello, G. Lachapelle and M.E. Cannon (2006) "Assessing Probability of Correct Ambiguity Resolution in the Presence of Time-correlated Errors", *NAVIGATION: Journal of the Institute of Navigation*: Vol. 53, No. 4, pp. 269-282

O'Keefe, K., M. Petovello, W. Cao, G. Lachapelle and E. Guyade (2008) "Comparing of Multi-carrier Ambiguity Resolution methods for Geometry-Based GPS and Galileo Low Earth Orbiting Satellite Attitude Determination", *International Journal of Navigation and Observation*, Available at http://www.hindawi.com/journals/ijno/aip.592073.html, last accessed on 7 May, 2009

Polischuk, G. M., V.I. Kozlov, V.V. Ilitchov, A.G. Kozlov, V.A. Bartenev, V.E. Kossenko, N.A. Anphimov, S.G. Revnivykh, S.B. Pisarev, A.E. Tyulyakov, B.V. Shebshaevitch, A.B. Basevitch and Y.L. Vorokhovsky (2002) "The Global Navigation Satellite System GLONASS: Development and Usage in the 21st Century", In *Proceedings of 34th Annual Precise Time and Time Interval Meeting (PTTI-2002)*, 3-5 December, 2002, Reston, VA, pp. 151-160

Ray, J.K. (2006) "What Receiver Technologies Exist for Mitigating GNSS Pseudorange and Carrier Phase Multipath?", *Inside GNSS*: Vol. 1, No. 6, pp. 25-27

Revnivykh, S. (2007) *GLONASS Status and Progress*, Presentation on 47th CGSIC meeting, Fort Worth, Texas, USA, 24-25 September, 2007

Revnivykh (2008) "GLONASS Status and Progress", In *Proceedings of 21st International Technical Meeting of the Satellite Division (ION GNSS-2008)*, 16-19 September, 2008, Savannah, GA, pp. 431-452

Saastamoinen, J. (1972) "Contributions to the Theory of Atmospheric Refraction", *Bulletin Geodesique*: Vol. 105, No. 1, pp. 279-298

Saastamoinen, J. (1973) "Contributions to the Theory of Atmospheric Refraction, part II: Refraction Corrections in Satellite Geodesy", *Bulletin Geodesique*: Vol. 107, No. 1, pp. 13-34

Sauer, K., U. Vollath and F. Amarillo (2004) "Three and Four Carriers for Reliable Ambiguity Resolution", In *Proceedings of European Navigation Conference (ENC-GNSS 2004)*, 16-19 May, Rotterdam, Netherlands

Schlötzer, S. and S. Martin (2005) "Performance Study of Multi Carrier Ambiguity Resolution Techniques for Galileo and Modernized GPS", In *Proceedings of 18th International Technical Meeting of the Satellite Division (ION GNSS 2005)*, 13-16 September, 2005, Long Beach, CA, pp. 142-151

Schüler, E., and T. Schüler (2007) "Active GNSS Network and the Benefits of Combined GPS+Galileo Positioning", *Inside GNSS*: Vol. 2, No. 8, pp. 46-55

Schüler, E., T. Schüler, and B. Eissfeller (2007) "Joint GPS/Galileo Precise Positioning Performance Using Active Reference Networks", In *Proceedings of 20th International Technical Meeting of the Satellite Division (ION GNSS 2007)*, 25-28 September, 2007, Fort Worth, TX, pp. 661-667

Schaffrin, B. and E. Grafarend (1986) "Generating Classes of Equivalent Linear Models by Nuisance Parameter Elimination, Applications to GPS Observations", *Manuscripta Geodaetica*: Vol. 11, pp. 262-271

Shen, Y. and G. Xu (2008) "Simplified Equivalent Representation of GPS Observation Equations", *GPS Solutions*: Vol. 12, No.2, pp. 99-108

Sheridan, K., W.Y. Ochieng, K. Sauer, P.A. Cross, K.F. Sheridan, J. Iliffe, S. Lannelongue, N. Ammour and K. Petit (2001) "Performance Potential of a Combined Galileo/GPS Navigation System", In *Proceedings of European Navigation Conference (ENC-GNSS 2001)*, 8-11 May, Sevilla, Spain

Suman, G., A. Jovancevic and J. Noronha (2004) "Interoperability between GPS and Galileo", In *Proceedings of 17th International Technical Meeting of the Satellite Division (ION GNSS-2004)*, 21-24 September, Long Beach, CA, pp. 670-680

Teunissen, P.J.G. (1993) *Least-squares Estimation of the Integer GPS Ambiguities*, Invited lecture, Section IV Theory and Methodology, IAG General Meeting, Beijing, China, August, also in Delft Geodetic Computing Centre LGR series, No. 6, 16 pp

Teunissen, P.J.G. (1994) "A New Method for Fast Carrier Phase Ambiguity Estimation", In *Proceedings of IEEE Position, Location and Navigation Symposium (PLANS'94)*, 11-15 April, 1994, Las Vegas, NV, pp. 562-573

Teunissen, P. J. G. and A. Kleusberg (1998) "GPS Observation Equations and Positioning Concepts", In *GPS for Geodesy*, Eds. Kleusberg, A. and P. J. G. Teunissen, Springer-Verlag, pp. 175-217

Teunissen, P.J.G., P. Joosten and C.C.J.M., Tiberius (1999) "Geometry-free Ambiguity Success Rates in Case of Partial Fixing", In *Proceedings of Institute of Navigation National Technical Meeting (ION NTM-99)*, San Diego, CA, 25-27 January, 1999, pp. 201-207

Teunissen, P. J. G., P. Joosten and C.C.J.M., Tiberius (2002) "A Comparison of TCAR, CIR and LAMBDA GNSS Ambiguity Resolution", In *Proceedings of 15th International Technical Meeting of the Satellite Division (ION GPS-02)*, 24-27 September, Portland, OR, pp. 2799-2808

Teunissen, P. J. G. and S. Verhagen (2007a) "GNSS Carrier Phase Ambiguity Resolution: Challenges and Open Problems", In *Proceedings of the Scientific Meetings of the IAG General Assembly 2007*, 2-13 July 2007, Perugia, Italy

Teunissen, P. J. G. and S. Verhagen (2007b) "On GNSS Ambiguity Acceptance Tests", *International Global Navigation Satellite Systems Society IGNSS Symposium 2007*, 4-6 December, 2007, Sydney, Australia, 13 pp

Teunissen, P.J.G. and S. Verhagen (2008) "GNSS Ambiguity Resolution: When and How to Fix or not to Fix?", In *International Association of Geodesy Symposia Vol 132: VI Hotine-Marussi Symposium on Theoretical and Computational Geodesy* (Xu, P., J. Liu and A. Dermanis Eds), pp. 143-148, doi: 10.1007/978-3-540-74584-6_22

Tiberius, C.C.J.M., T. Pany, B. Eissfeller, K. de Jong, P. Joosten and S. Verhagen (2002a) "Integral GPS-Galileo Ambiguity Resolution", In *Proceedings of European Navigation Conference (ENC-GNSS 2002)*, 28-30 May, Kopenhagen, Denmark

Tiberius, C.C.J.M., T. Pany, B. Eissfeller, P. Joosten and S. Verhagen (2002b) "0.99999999 Confidence Ambiguity Resolution with GPS and Galileo", *GPS Solutions*: Vol. 6, No. 2, pp. 96-99

Taylor, J., J.J. Pace Jr., P.J. Mendicki and A.J. Dorsey (2008) "GPS Control Segment Upgrade Goes Operational - Enhanced Phased Operations Transition Details", In *Proceedings of Institute of Navigation National Technical Meeting (ION NTM-2008)*, 28-30 January, San Diego, CA, pp. 992-1006

U.S. PNT National Executive Committee (2007) *Selective Availability*, Available at http://pnt.gov/public/sa/, last accessed on 23 December, 2008

U.S. PNT National Executive Committee (2008) *Joint Statement on GPS and Galileo Cooperation*, Available at http://pnt.gov/public/docs/2008-10-EC-statement.shtml, last accessed on 23 December, 2008

Verhagen, S. (2002) "Performance Analysis of GPS, Galileo and Integrated GPS-Galileo", In *Proceedings of 15th International Technical Meeting of the Satellite Division (ION GPS-02)*, 24-27 September, Portland, OR, pp. 2208-2215

Verhagen, S. (2004) "Integer Ambiguity Validation: An Open Problem?", *GPS Solutions*: Vol. 8, No. 1, pp. 36-43

Verhagen, S. (2005) "On the Reliability of Integer Ambiguity Resolution", *NAVIGATION: Journal of the Institute of Navigation*: Vol. 52, No. 2, pp. 99-110

Verhagen, S. (2006) "Improved Performance of Multi-Carrier Ambiguity Resolution Based on the LAMBDA Method", In *Proceedings of 3th ESA Workshop on Satellite Navigation User Equipment Technologies (NAVITEC'2006)*, 11-13 December, Noordwijk, The Netherlands

Verhagen, S. (2007) "Reliable Positioning with the Next Generation Global Navigation Satellite Systems", In *Proceedings of 3rd International Conference on Recent Advances in Space Technologies (RAST '07)*, 14-16 June, Istanbul, Turkey, pp. 618-623

Vollath, U. and K.D. Doucet (2007) *Multiple-GNSS and FDMA High Precision Carrier-Phase Based Positioning*, US Patent No. 7312747, Issued on 25 December, 2007

Vollath, U. and K.D. Doucet (2008) *GNSS Signal Processing with Partial Fixing of Algorithms*, U.S. Patent Application No. 20080165054, Filed on 12 November, 2007

Vollath, U., S. Birnbach and H. Landau (1998) "Analysis of Three-Carrier Ambiguity Resolution (TCAR) Technique for Precise Relative Positioning in GNSS-2", In *Proceedings of 11th International Technical Meeting of the Satellite Division (ION GPS-99)*, 15-18 September, Nashville, TN, pp. 417-426

Ward, P.W., J.W. Betz and C.J. Hegarty (2005) "Satellite Signal Acquisition, Tracking, and Data Demodulation", In *Understanding GPS: Principles and Applications*, Eds. Kaplan, D. K. and C. J. Hegarty, Artech House, Inc., pp. 153-241

Wallner, S., J.-A. Avila-Rodriguez, J.-H. Won, G.W. Hein and J.-L Issler (2008) "Revised PRN Code Structures for Galileo E1 OS", In *Proceedings of 21st International Technical Meeting of the Satellite Division (ION GNSS 2008)*, 16-19 September, 2008, Savannah, GA, pp. 887-899

Wübbena, G. and S. Willgalis (2001) "State Space Approach for Precise Real Time Positioning in GPS Reference Networks", In *Proceedings of the International*

Symposium on Kinematic Systems in Geodesy, Geomatics and Navigation 2001 (KIS 01), 5-8 June, 2001, Banff, Canada, pp. 72-79

Zhang, W., M.E. Cannon, O. Julien and P. Alves (2003) "Investigation of Combined GPS/Galileo Cascading Ambiguity Resolution Schemes", In *Proceedings of 16th International Technical Meeting of the Satellite Division (ION GPS/GNSS 2003)*, 9-12 September, Portland, OR, pp. 2599-2610

Zhang, W. (2005) *Triple Frequency Cascading Ambiguity Resolution for Modernized GPS and Galileo*, UCGE Report Number 20228, Department of Geomatics Engineering, the University of Calgary, Calgary, Canada, July 2006

APPENDIX A: PARTIAL FIXING OVER DIFFERENT BASELINES

Scenarios C, D, E: Partial fixing over the short baseline

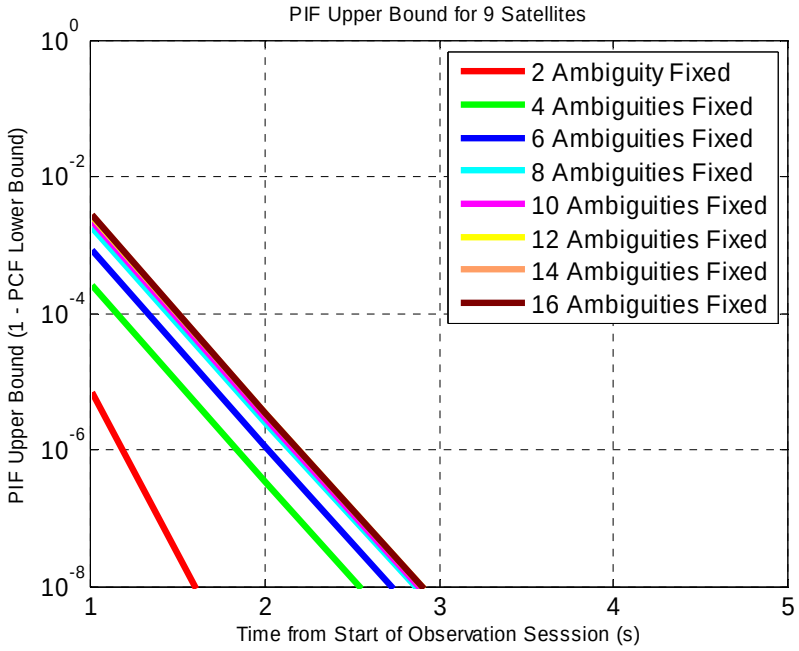

Figure A.1: PIF as a function of time with increasing number of ambiguities fixed of Scenario C (GPS L1 and L5)

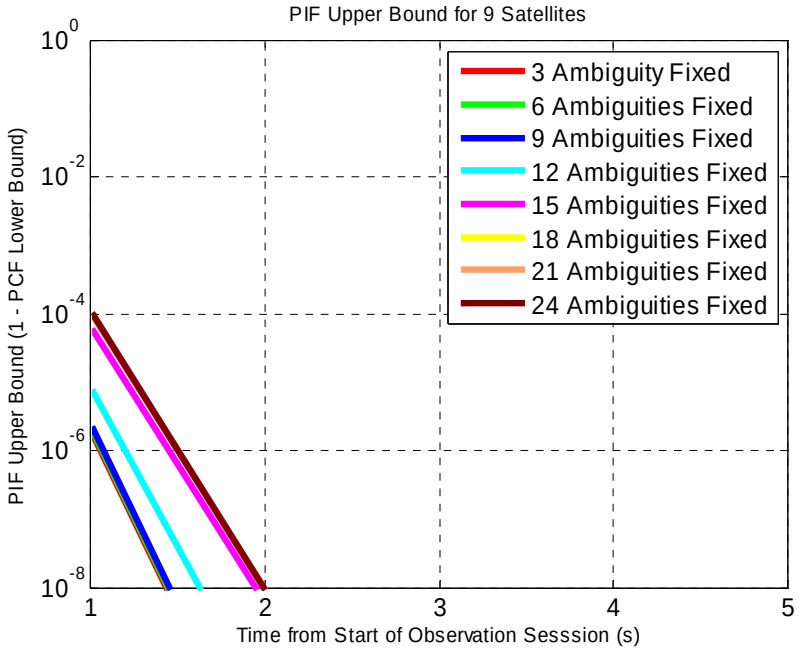

Figure A.2: PIF as a function of time with increasing number of ambiguities fixed of Scenario D (GPS L1, L2 and L5)

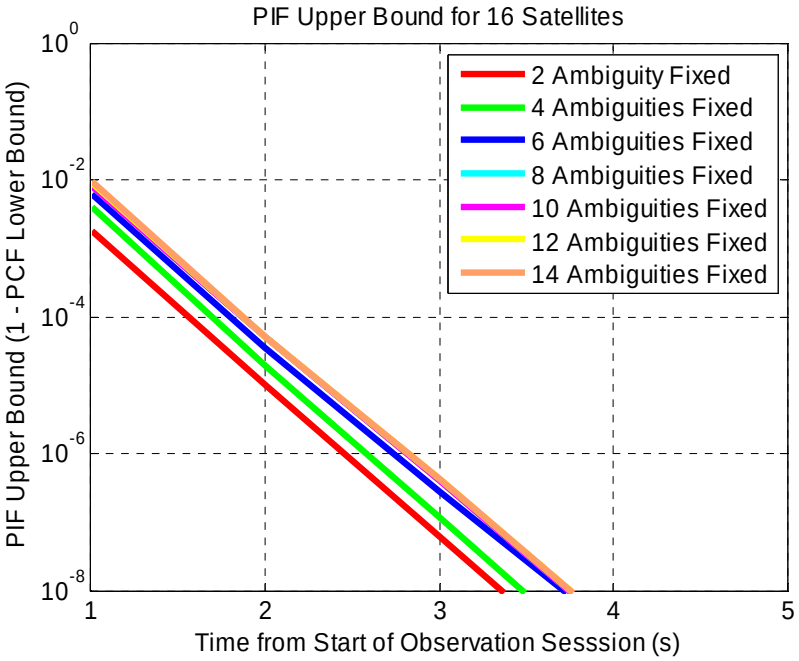

Figure A.3: PIF as a function of time with increasing number of ambiguities fixed of Scenario E (GPS L1 and Galileo E1)

Scenarios H, I, K: Partial fixing over the medium baseline

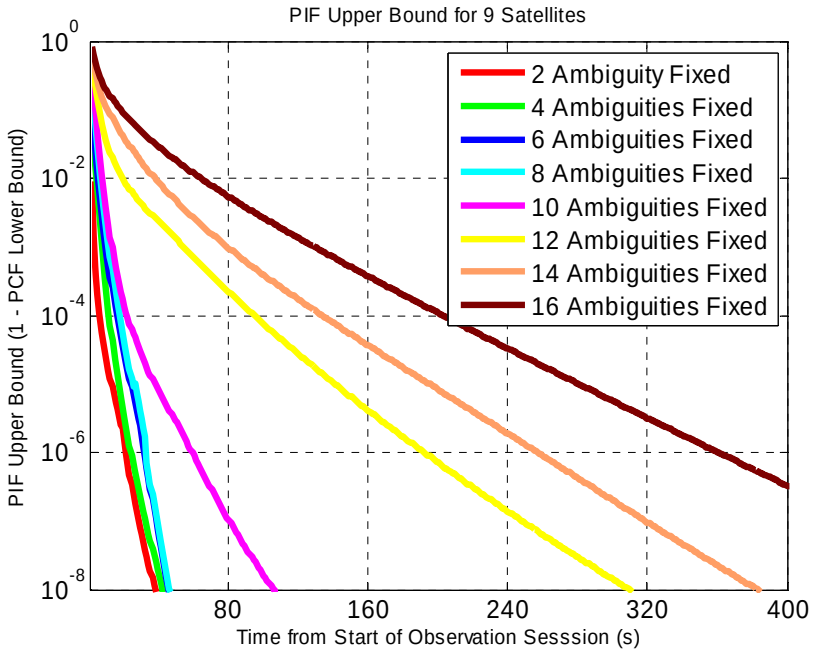

Figure A.4: PIF as a function of time with increasing number of ambiguities fixed of Scenario H (GPS L1 and L5)

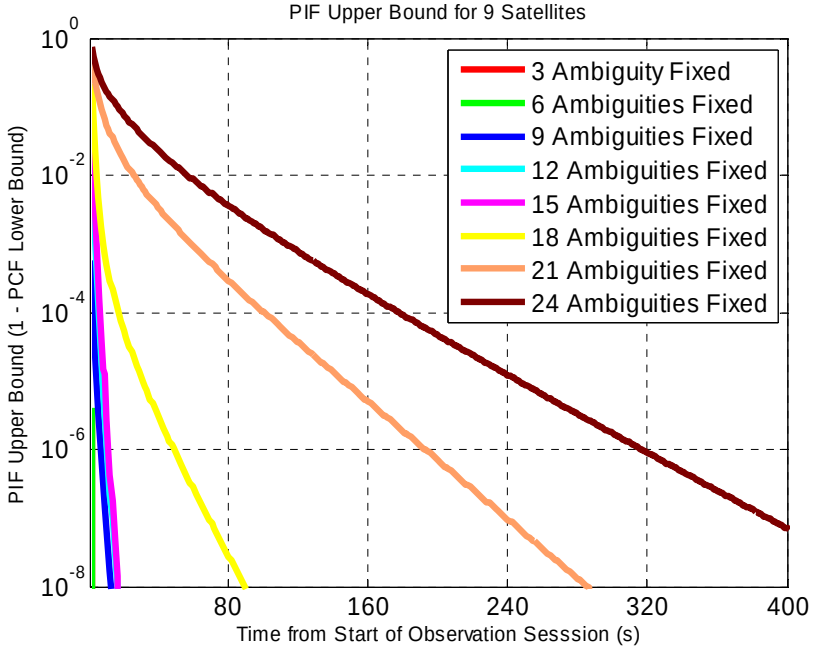

Figure A.5: PIF as a function of time with increasing number of ambiguities fixed of Scenario I (GPS L1, L2 and L5)

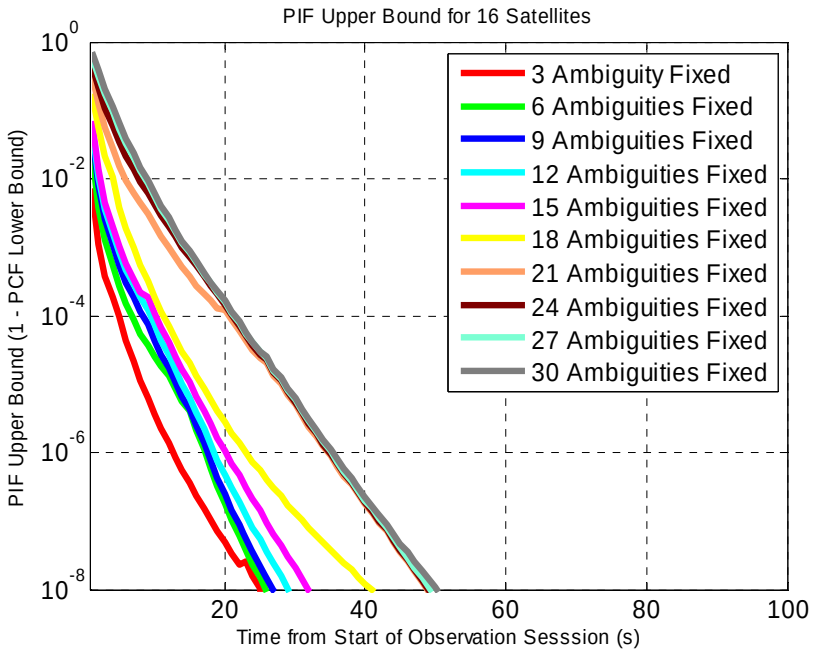

Figure A.6: PIF as a function of time with increasing number of ambiguities fixed of Scenario K (GPS L1, L5 and Galileo E1, E5a)

Scenarios M, N, O and P: Partial fixing over the long baseline

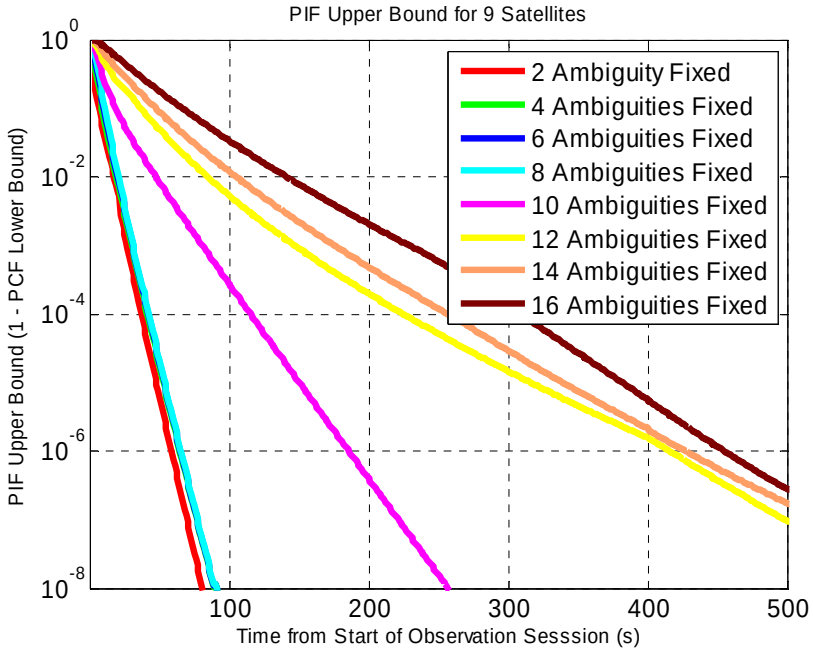

Figure A.7: PIF as a function of time with increasing number of ambiguities fixed of Scenario M (GPS L1 and L5)

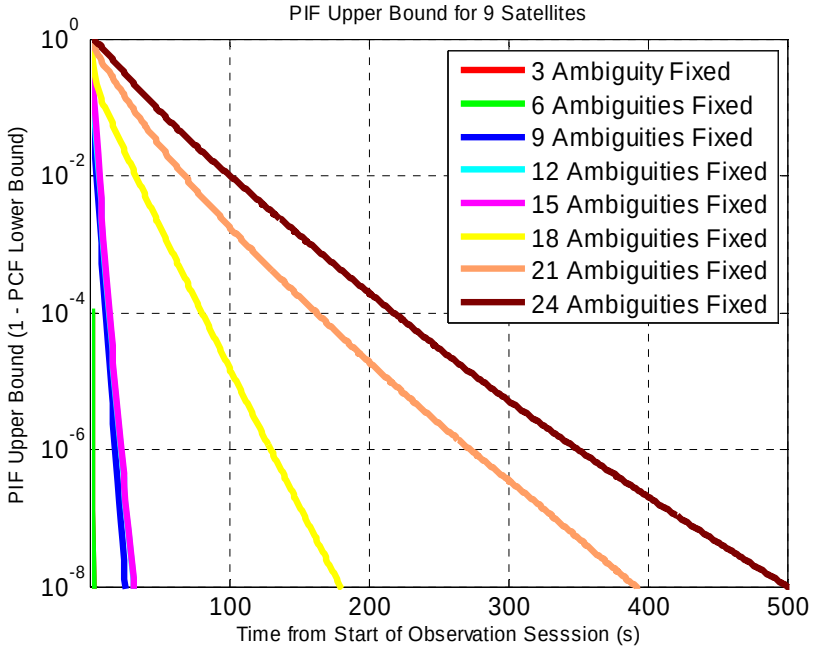

Figure A.8: PIF as a function of time with increasing number of ambiguities fixed of Scenario N (GPS L1, L2 and L5)

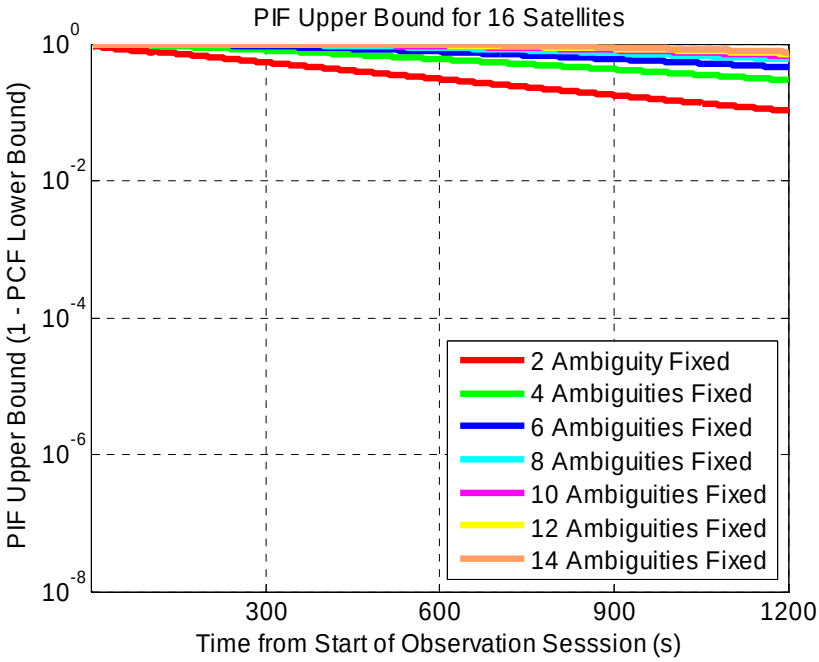

Figure A.9: PIF as a function of time with increasing number of ambiguities fixed of Scenario O (GPS L1 and Galileo E1)

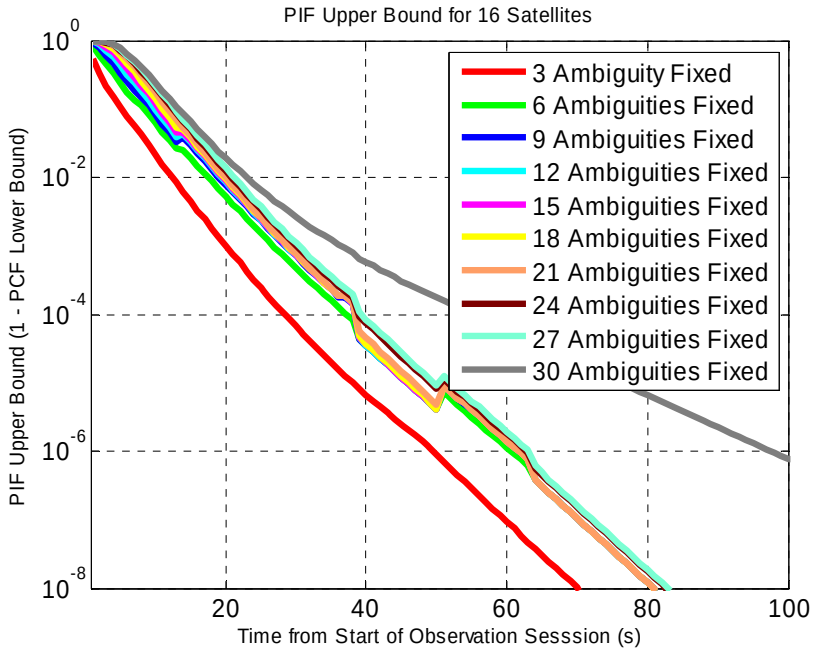

Figure A.10: PIF as a function of time with increasing number of ambiguities fixed of Scenario P (GPS L1, L5 and Galileo E1, E5a)